

AD A111147

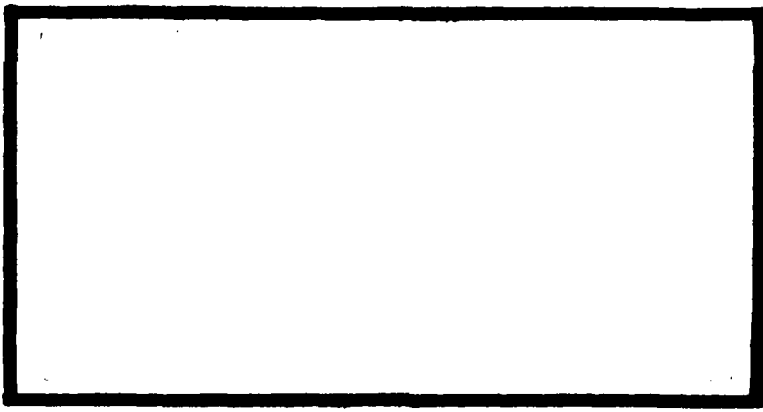
LEVEL II

①

110 H



DTIC
ELECTE
FEB 19 1982



DTIC FILE COPY

DEPARTMENT OF THE AIR FORCE
 AIR UNIVERSITY (ATC)
AIR FORCE INSTITUTE OF TECHNOLOGY

Wright-Patterson Air Force Base, Ohio

This document has been approved
 for public release and sale; its
 distribution is unlimited.

82 02 18 127

AFIT/GA/AA/81D-11

CLOSED-LOOP CONTROL OF A SATELLITE
IN AN UNSTABLE PERIODIC ORBIT
ABOUT L3

THESIS

AFIT/GA/AA/81D-11 Felicia C. Vass
2Lt USAF

Approved for public release; distribution unlimited

Acknowledgements

It is beyond my simple means to express the respect and admiration I have held for my advisor, Dr. William Wiesel, since I first walked into his classroom. I believe it rare for a man to hold so much knowledge and yet also exhibit such infinite patience toward one of so little talent or true understanding. Had I been able to take the opportunity, I could truly have learned a great deal more than I did. Without his guidance any achievement of mine would have been insignificant. I deeply appreciate everything he has done in my behalf.

I would also like to thank my family, classmates, and many friends without whose constant support, words of encouragement, and laughter I could never have survived the past few years.

Also, toward my co-workers, Dennis and Gerry, who helped defray much of the extreme frustration the computer could provide and who went out of their way to clarify many points, my gratitude is deep.

"It is given to any man to learn all he can during his lifetime, no limit set upon that learning. Only to refuse knowledge is our choice, and he who does so cuts himself off from much."

(André Norton) May those who seek to tread the Road behind me be sincere in their efforts and realize that naught, when once accomplished, has ever been in vain.

Acknowledgement For	
NO. _____	X
By _____	
Date _____	
Code _____	
Dist _____	
A	

Table of Contents

Acknowledgements	ii
List of Figures	iv
List of Tables	v
List of Symbols	vi
Abstract	ix
I. Introduction	1
Background	1
System	5
Coordinate Frame	5
Periodic Orbit	7
II. Floquet Theory	10
III. Modal Control	16
IV. Observer Theory	19
V. Controller/Observer Implementation	28
VI. Results, Conclusions, and Recommendations	31
Results	31
Conclusions	41
Recommendations	42
Bibliography	97
Vita	99

List of Figures

Figure		Page
1	Lagrangian Points in Earth-Moon System	2
2	Geometry of the Four-Body Problem	6
3	Orbit about L ₃	9
4	State Observability	21
5	Root Position vs Gain	32
6	Uncontrolled System with Observer	36
7	Modal Vector vs Time: Case A	43
8	Modal Vector vs Time: Case B	49
9	Modal Vector vs Time: Case C	55
10	Error vs Time: Case A	61
11	Error vs Time: Case B	62
12	Error vs Time: Case C	63
13	Phase Portraits: Case A	64
14	Phase Portraits: Case B	67
15	Phase Portraits: Case C	70
16	Effect of Large Observer Initial Conditions	73
17	Case of Figure 16 with Alternate Observer Gain Matrix	77
18	Additional Example of a Faster Observer	81
19	Behavior With Large Initial Conditions	85
20	Case of Figure 19 With Order of Magnitude Difference in Observer Initial Conditions	89
21	Case of Figure 20 With Order of Magnitude Difference in Orbit Initial Conditions	93

List of Tables

Table		Page
I	L3 Orbit Initial Conditions	8
II	Poincaré Exponents for the Uncontrolled System .	13
III	Observer Exponent-Gain Correlations	33
IV	Exponential Envelopes for Errors	40

List of Symbols

α	monodromy matrix eigenvalues
$A(t)$	system plant matrix
β	arbitrary gain matrix element
$B(t)$	distribution matrix
$C(t)$	system output matrix
$C'(t)$	modified system output matrix
∂	partial differentiation
e	exponentiation
$\bar{e}_o(t)$	physical observer reconstruction error
$\bar{e}_m(t)$	modal observer reconstruction error
$\bar{n}(t)$	modal vector of the four-body problem
$\hat{n}(t)$	modal vector estimate
$F(t)$	modified control matrix
G	constant controller gain
G_1	universal gravitational constant
γ_o	constant component of control term
H	Hamiltonian of the four-body system
I	identity matrix
J	Jordan form of the matrix of Poincaré exponents
$K(t)$	observer gain matrix
$K'(t)$	modified observer gain matrix
L_1-L_5	Lagrangian points in the four-body system
λ	Poincaré exponents of the four-body system
$\Lambda(t)$	matrix of eigenvectors

m_1	mass of Earth
m_2	mass of the Moon
m_3	mass of the Sun
M	monodromy matrix
M_0	sum of the masses of the Earth, Moon and Sun
v	element of system state transition matrix
$\dot{\omega}$	angular velocity of rotating reference frame
ω	imaginary component of a complex Poincaré exponent
P_x, P_y, P_z	momenta of the satellite
θ	arbitrary gain matrix element
$\phi(t)$	fundamental matrix
$\phi(t, t_0)$	state transition matrix
$\phi^S(t)$	system state transition matrix
ψ	element of system state transition matrix
$Q(t)$	periodic matrix
$\bar{r}(t)$	range vector
$\dot{\bar{r}}(t)$	range-rate vector
$\bar{r}_m(t)$	vector from the Earth to the Moon
$\bar{R}(t)$	vector from the Earth-Moon center of mass to the satellite
$\bar{\rho}(t)$	vector from the Earth-Moon center of mass to the Sun
$\dot{\bar{\rho}}(t)$	time derivative of $\bar{\rho}(t)$ taken with respect to the rotating reference frame
σ	real component of a complex Poincaré exponent
t	time

t_0	initial time
τ	period of the orbit about L3
$\bar{u}(t)$	control vector
$\bar{x}(t)$	state vector of four-body system
$\delta\bar{x}(t)$	variational state vector
$\hat{x}(t)$	state vector estimate
$\bar{x}_p(t)$	state vector for the periodic orbit
$\xi(t)$	element of the modified system output matrix
$\bar{y}(t)$	system output vector
ζ	element of system state transition matrix

Abstract

A stable Luenberger Observer was developed to reconstruct the error states in modal coordinates for a satellite in a periodic orbit about the Earth-Moon Lagrangian point, L3. Observer pole placement for the third root was found to be linear with applied gain. Convergence of the observer estimate to the true state vector was rapid in all cases, but depended upon the initial conditions considered. The addition of the observer did not impede the long-term behavior of the controller in stabilizing the orbit.

CLOSED-LOOP CONTROL OF A SATELLITE

IN AN

UNSTABLE PERIODIC ORBIT

ABOUT L3

I. Introduction

Background

The n-body problem came into existence when celestial mechanics began studying the solar system with an eye toward evaluating the equations of motion of the various gravitationally-attracted bodies found therein. The motion of two bodies in a circular orbit about each other and affecting each other only through their mutual forces of gravitation is now readily understood, and when a third body, infinitesimal and massless in comparison to the others is added to the system, the restricted three-body problem is established. The discovery of the Trojan group of satellites in the Sun-Jupiter system (1906) confirmed Comte Joseph Louis Lagrange's 1772 mathematical depiction of such a configuration. His work developed the existence of equilibrium solutions to the equations of motion where the gravitational forces on the infinitesimal third body as exerted by the other two would exactly balance, thereby rendering it motionless with respect to a rotating coordinate reference frame. These five equilibrium positions, L1 through L5, called alternately Lagrangian or libration points, also exist for the Earth-Moon system and are shown in Figure 1. For a rotating coordinate frame of reference

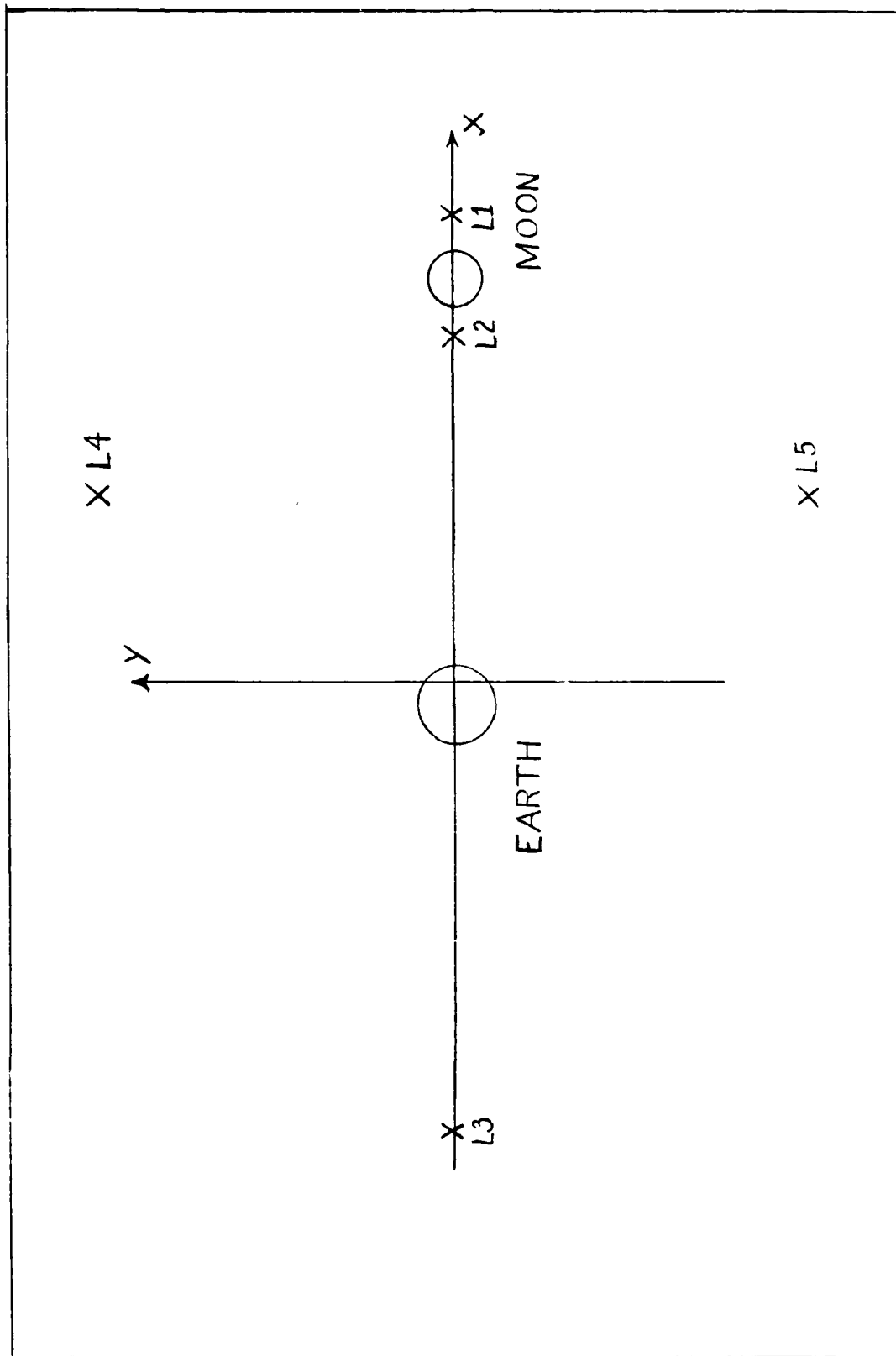


Figure 1. Lagrangian Points in Earth-Moon System (ref 20:5)

centered at the Earth-Moon center of mass, the Lagrangian points are five fixed points at which a third mass would be stationary if placed with zero velocity relative to the frame. Through infinitesimal analysis (Ref 17:427) it can be shown that motion in the neighborhood of the collinear points (L1, L2, and L3) is inherently unstable since a positive real eigenvalue exists in each case. Similar evaluation yields motion in the vicinity of L4 and L5 to be infinitesimally stable. In 1907, Charlier (Ref 22) analyzed two classes of periodic orbits around these triangular points, long and short, depending on the period or mass ratio of the two large masses. The desirability of placing satellites at any or all of these Lagrangian points coupled with the related instabilities has justified the vast amount of research which has surfaced in the past two decades dealing with the orbital control of this system.

The major asset attained by satellites placed at the Lagrangian points is that they remain in a motionless configuration with respect to the Earth and the Moon at all times. Many uses for which such positioning would be ideal have been proposed. One is in the development of a communications link between the Earth and semipermanent bases on the far side of the Moon. Relay satellites placed at L1 and L2 could provide uninterrupted communications to the Earth as well as to far-reaching lunar exploration vehicles. Communication with interplanetary probes would be similarly facilitated since the Earth as a noise source could thus be virtually eliminated. Instead of a lunar parking orbit, a station at L2 would provide an infinite launch window for lunar activities since it is stationary with respect to the surface. Telescopes of all types would be free from the

restricting layers of the Earth's atmosphere, or, depending on position, be entirely blocked from Earth interference by the Moon. Situated outside of the magnetosphere, satellites to study solar plasma, cosmic rays, and other cosmic phenomena would find ideal settings, similar to the ISEE-3 research satellite already in use. L4 or L5 satellites could provide long-term solar flare observations, early warning programs, and secure the previously unaccomplished task of performing simultaneous measurements at different locations within cislunar space, thus separating temporal from spatial variations for the first time (Refs 5, 6, 8). Militarily, a defense satellite network placed in orbit around L3, L4, and L5 would provide continual global coverage, especially vital in today's potentially explosive environment. Synchronous satellites are not totally efficient in such instances since they exist in equatorial orbits, leaving the polar regions essentially hidden. For the Lagrangian system, this restriction does not apply, since these points lie in the Earth-Moon plane rather than equatorial (Ref 26). Also, they are distant enough that the lead time for any interceptor is sufficient for adequate evasive maneuvers to be implemented. Prior work by Captain Tilton (Ref 23) established the existence of appropriate stable orbits about L4 and L5 in which reconnaissance satellites could be placed with relatively little cost and remain for up to fifty years. Only the lack of a similarly stable orbit about L3 prevents the completion of the triad for total coverage and is the subject of this and other research endeavors.

System

The restricted four-body problem is a more realistic extension of the three-body problem for evaluation since the large perturbative effects of the Sun are no longer neglected. However, in this case, the Hamiltonian becomes an explicit function of time and there is no longer a constant of the motion. It has been shown, however, that families of periodic orbits still exist about the five Lagrangian points.

The modelling assumptions used in previous research were maintained here. The Earth is taken to be moving in a circular orbit about the Sun with a period of 365.256365 days. The Moon's motion is approximated as a periodic orbit about the Earth as developed by Professor Wiesel in his work (Ref 25), which is more realistic than a circular one. All bodies are considered to lie in a plane, so that perturbations due to inclination and eccentricity effects have been neglected. The importance of these are described in Reference 4. In later cases, where greater stability characteristics were sought for the nonplanar (z) mode, inclination and eccentricity had to be included. Effects due to the presence of other solar system bodies and the Sun's radiative pressure may be considered negligible and have been disregarded.

Coordinate Frame

Even though there is no longer a constant of the motion, which instigated the use of a rotating reference frame with respect to the restricted three-body problem, that configuration is maintained here. The rectangular reference frame, depicted in Figure 2, has its origin at the Earth-Moon center of mass and one axis coinciding with the line

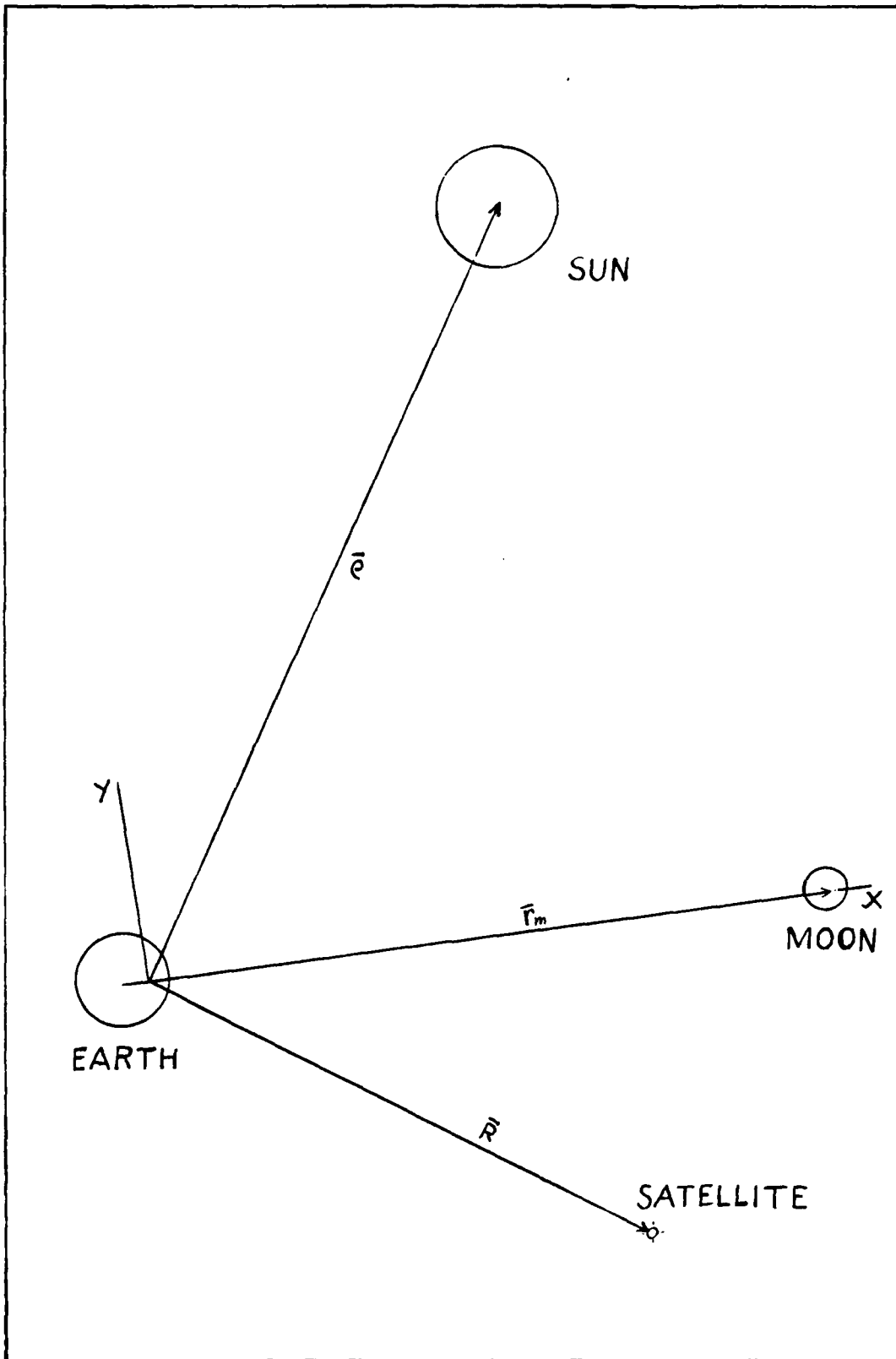


Figure 2. Geometry of the Four-Body Problem (Ref 20:11)

connecting the Earth and the Moon. This system rotates at the average angular velocity of the Moon about the Earth, with the Lagrangian points maintaining their relative positions within the frame at all times.

Periodic Orbit

With the satellite assumed massless for the sake of calculation and the attracting bodies having their respective masses, the Hamiltonian for the system was derived by Captain Shelton to be

$$\begin{aligned}
 H = & \frac{1}{2}(P_x^2 + P_y^2 + P_z^2) + \tilde{\omega}(P_x R_y - P_y R_x) \\
 & + \frac{m_3}{M_0} (\dot{r}_{\rho x} - \tilde{\omega}_0 y) P_x + (\dot{r}_{\rho y} + \tilde{\omega}_0 x) P_y \\
 & - \frac{G_1 m_3}{|\bar{R} - \bar{\rho}|} - \frac{G_1 m_1}{\left| \frac{m_2}{m_1 + m_2} \bar{r} + \bar{R} \right|} - \frac{G_1 m_2}{\left| \bar{R} - \frac{m_1}{m_1 + m_2} \bar{r} \right|}
 \end{aligned} \tag{1}$$

where $M_0 = m_1 + m_2 + m_3$ is the sum of the masses of the Earth, Moon, and Sun respectively, the scale factor $\frac{m_3}{M_0}$ locates the inertial point of the system, $\tilde{\omega}$ is the angular velocity of the rotating frame, \bar{R} , $\bar{\rho}$, and \bar{r}_m are the position vectors from the origin to the satellite, Sun, and Moon respectively, with subscripts x, y, and z denoting the components in those directions, the superscript r represents differentiation in the rotating frame, G_1 is the gravitational constant, and P_x , P_y , and P_z denote the momenta of the Hamiltonian (Ref 20:14).

Using the equations of motion as derived from the Hamiltonian and the theory described in Chapter II of Captain Shelton's work, he was able to construct a viable periodic orbit about L3. This orbit is shown in Figure 3 and the initial conditions incorporated in its implementation are given in Table I. Since such an orbit was previously

shown to be inherently unstable, some form of control law is necessary if a satellite is to remain in the vicinity of L3 for any considerable length of time.

State variable feedback control designs rely on the availability of the system's state vector through direct measurement or derivation from the output. In this case, where only two of the six state vector elements are accessible through range and range-rate measurements, a Luenberger Observer is introduced to reconstruct the missing states. This approximate state vector can then be substituted into the control law. Rapid convergence to the true states is assured by placing the observer poles to the left of those of the system. Conceivably, approximately instantaneous convergence could be attained if the poles were specified at negative infinity, but this tends to make the observer behave like a differentiator, (Ref 15), greatly influenced by noise, an undesirable characteristic. These two constraints limit effective observer pole placement.

Table I. L3 Orbit Initial Conditions (Ref 20:20)

x position (km)	-383,537.27
y position (km)	0.0
z position (km)	0.0
x momentum (km/sec)	0.0
y momentum (km/sec)	-30.825537
z momentum (km/sec)	0.0

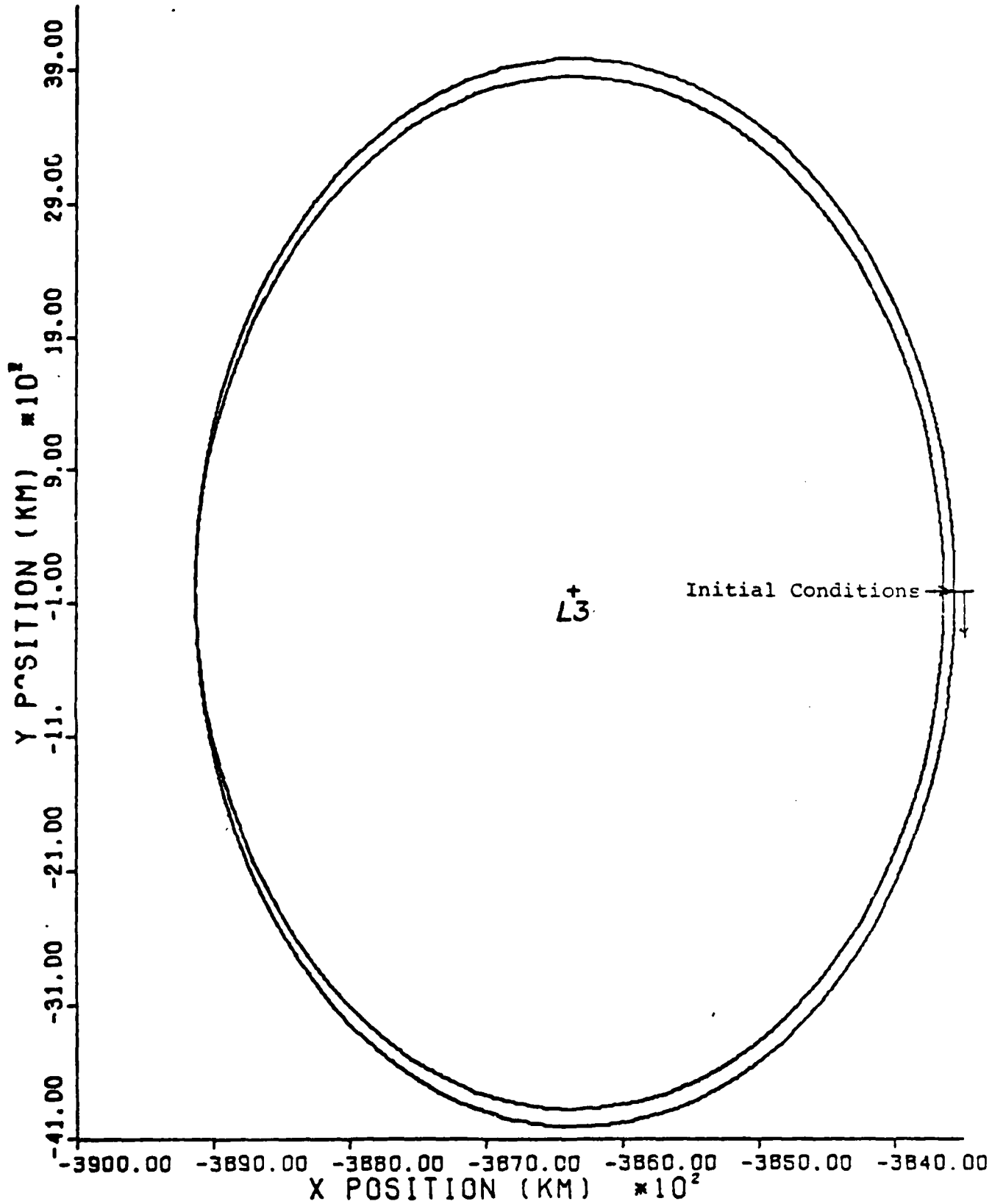


Figure 3. Orbit About L3 (Ref 20:21)

II. Floquet Theory

The equations of motion for the restricted four-body problem as derived from the Hamiltonian (1) are time-varying and exhibit some periodic solutions. This means that the motion repeats itself predictably so that only one orbital period need be examined to determine characteristic behavior. In general form the equations of motion may be written:

$$\dot{\bar{x}}(t) = \bar{f}[\bar{x}(t), t] \quad (2)$$

where $\bar{x}(t)$ is the state vector composed of the coordinates and momenta of the system. Allowing $\delta\bar{x}(t)$ to be a small displacement from the previously determined periodic orbit taken as a reference,

$$\delta\bar{x}(t) = \bar{x}(t) - \bar{x}_p(t) \quad (3)$$

the state vector considered throughout this study actually becomes

$$\bar{x}(t) = \left[\delta x(t) \quad \delta P_x(t) \quad \delta y(t) \quad \delta P_y(t) \quad \delta z(t) \quad \delta P_z(t) \right]^T \quad (4)$$

Substituting (3) into (2), expanding in a Taylor series about the reference, and then linearizing (Ref 20:15-17) results in the equations of motion written as:

$$\delta\dot{\bar{x}}(t) = A(t)\delta\bar{x}(t) \quad (5)$$

where $A(t) = \left. \frac{\partial \bar{f}}{\partial \bar{x}(t)} \right|_{\bar{x}_p(t)}$ is termed the system plant matrix. The

elements of $A(t)$, $A_{ij}(t)$, are continuous periodic functions of time with period $\tau = 29.530589$ days, so that

$$A(t + \tau) = A(t) \quad (6)$$

defines the periodicity. The n linearly independent solutions to (5), $\delta\bar{x}_i(t)$ ($i = 1, 2, \dots, n$), may be collected to form an $n \times n$ matrix,

$$\Phi(t) = \left[\begin{array}{cccc} \delta\bar{x}_1(t) & \vdots & \delta\bar{x}_2(t) & \vdots & \dots & \vdots & \delta\bar{x}_n(t) \end{array} \right] \quad (7)$$

called a fundamental matrix.

A specialized case of this fundamental matrix, satisfying

$$\delta\bar{x}(t) = \Phi(t, t_0) \delta\bar{x}(t_0) \quad (8)$$

where

$$\Phi(t, t_0) = \frac{\partial \bar{x}(t)}{\partial \bar{x}(t_0)} \bigg|_{\bar{x}_p(t)}$$

is necessary to solve a Floquet problem in general. $\Phi(t, t_0)$ is called the state transition matrix, is evaluated along a known reference solution, in this case the periodic orbit, and is a function of only the initial and final times under consideration. In addition, it has the following properties:

$$\Phi(t, t_0) = \Phi(t, t_1) \Phi(t_1, t_0) \quad (9)$$

$$\Phi(t_0, t_0) = I$$

where I is the standard $n \times n$ identity matrix.

With $\Phi(t)$ defined as in (7), (8) becomes

$$\Phi(t) = \Phi(t, t_0) \Phi(t_0) \quad (10)$$

Over one period (10) yields

$$\Phi(\tau) = \Phi(\tau, 0) \Phi(0) \quad (11)$$

A general fundamental matrix satisfies

$$\dot{\Phi}(t) = A(t) \Phi(t) \quad (12)$$

from (5) and at the end of one period this equation becomes

$$\dot{\Phi}(t + \tau) = A(t + \tau) \Phi(t + \tau) \quad (13)$$

Inserting (6) into (13) results in

$$\dot{\Phi}(t + \tau) = A(t) \Phi(t + \tau) \quad (14)$$

from which it is seen that $\Phi(t + \tau)$ is also a fundamental matrix. These two solutions, $\Phi(t)$ and $\Phi(t + \tau)$, may be correlated through the existence of a constant matrix M , called the monodromy matrix of the fundamental matrix $\Phi(t)$, such that

$$\Phi(t + \tau) = M\Phi(t) \quad (15)$$

From this equation at $t=0$ and recalling (11), it is seen that the monodromy matrix is actually equivalent to the state transition matrix from $t=0$ to $t=\tau$.

The eigenvalues of M (or $\Phi(\tau,0)$), α_i ($i=1,2,\dots,n$), are termed the characteristic multipliers of $A(t)$. There also exists a set of λ_i ($i=1,2,\dots,n$), related to the characteristic multipliers by

$$\lambda_i = \frac{1}{\tau} \ln(\alpha_i)$$

These are called Poincaré exponents and may have real or complex values. Since previous work established a multiplicity of 1 for the λ_i , they may be arranged in the following Jordan canonical form

(Ref 17:267):

$$J = \begin{bmatrix} \lambda_1 & & & 0 \\ & \lambda_2 & & \\ & & \ddots & \\ & & & \lambda_n \\ 0 & & & & \end{bmatrix}$$

For complex conjugate values, this format becomes unwieldy since imaginary vectors would then be involved in computations. To avoid this inconvenience, the form shown in (16) may be used instead. Here, each complex conjugate pair forms an off-diagonal 2×2 submatrix within the basically diagonal structure.

$$J = \begin{bmatrix} \sigma_1 & -\omega_1 & & & & 0 \\ \omega_1 & \sigma_1 & & & & \\ & & \sigma_2 & -\omega_2 & & \\ & & \omega_2 & \sigma_2 & & \\ & & & & \ddots & \\ & & & & & \sigma_n & -\omega_n \\ & & & & & \omega_n & \sigma_n \\ 0 & & & & & & \end{bmatrix} \quad (16)$$

where σ_i ($i = 1,2,\dots,n$) are the real components and ω_i are the imaginary components of the λ_i .

For purposes of stability, all Poincaré exponents must lie on the negative real axis of the s -plane, or, if complex, have a negative real part. The imaginary component yields oscillation in that particular related state.

The Poincaré exponents for the uncontrolled periodic orbit about L3 are listed in Table II. These determine three modes of oscillation, two planar and one nonplanar, of which one is real and the other two consist of complex conjugate pairs. As can be seen, the third value has a positive real part, thus rendering the entire system unstable. This, then, is the element which must be controlled in order to make this a useful and predictable system.

To determine the actual solution to (12), the fundamental matrix may be expressed as

$$\phi(t) = Q(t)e^{Jt} \quad (17)$$

where $Q(t)$ is a periodic matrix satisfying

$$Q(t + \tau) = Q(t)$$

and J is the Jordan canonical form associated with $A(t)$ as defined above. Substituting (17) into (12),

$$\frac{d}{dt} [Q(t)e^{Jt}] = A(t) Q(t)e^{Jt}$$

differentiating,

$$\dot{Q}(t)e^{Jt} + Q(t)Je^{Jt} = A(t) Q(t)e^{Jt}$$

and cancelling the e^{Jt} terms since they can never be zero, produces

Table II. Poincaré Exponents for the Uncontrolled System

Planar Mode (x)	0.0 - 1.0392i
	0.0 + 1.0392i
Planar Mode (y)	2.3921 + 0.0i
	-2.3921 + 0.0i
Nonplanar Mode (z)	0.0 - 1.1247i
	0.0 + 1.1247i

$$\dot{Q}(t) + Q(t)J = A(t)Q(t)$$

Defining $\Lambda(t)$ as the $Q(t)$ matrix partitioned into columns

$$\Lambda(t) = \left[\begin{array}{c|c|c|c} \bar{O}_1(t) & \bar{O}_2(t) & \dots & \bar{O}_n(t) \end{array} \right] \quad (18)$$

results in a simple, analytical equation for J :

$$J = \Lambda^{-1}(t) \left[A(t)\Lambda(t) - \dot{\Lambda}(t) \right] \quad (19)$$

Now, substituting $\phi(t, t_0)$ into (12) gives the result

$$\dot{\phi}(t, t_0) = A(t)\phi(t, t_0)$$

This may be integrated numerically with the initial conditions described by (9) to yield information regarding a particular solution's local variation with initial conditions.

Picking $\delta\bar{x}_i(t)$ as an arbitrary solution to (5) and extracting this from (17) results in

$$\delta\bar{x}_i(t) = \bar{O}_i(t)e^{\lambda_i t} \quad (20)$$

From (8) at $t_0 = 0$, it is seen that

$$\delta\bar{x}_i(t) = \phi(t, 0)\delta\bar{x}_i(0) \quad (21)$$

Equating (20) and (21),

$$\delta\bar{x}_i(t) = \bar{O}_i(t)e^{\lambda_i t} = \phi(t, 0)\delta\bar{x}_i(0)$$

and substituting $\bar{O}_i(0)$ for $\delta\bar{x}_i(0)$ from (20) evaluated at $t=0$ gives

$$\delta\bar{x}_i(t) = \bar{O}_i(t)e^{\lambda_i t} = \phi(t, 0)\bar{O}_i(0) \quad (22)$$

Because $Q(t)$ is periodic, $\bar{O}_i(\tau) = \bar{O}_i(0)$,

$$\delta\bar{x}_i(\tau) = \bar{O}_i(\tau)e^{\lambda_i \tau} = \bar{O}_i(0)e^{\lambda_i \tau} = \phi(\tau, 0)\bar{O}_i(0) \quad (23)$$

when (20) and (22) are equated at the end of one period.

Incorporating $M = \phi(\tau, 0)$ in the latter part of (23) and simplifying yields the eigenvalue/eigenvector problem,

$$\left[M - e^{\lambda_i \tau} I \right] \bar{O}_i(0) = \bar{0} \quad (24)$$

where $e^{\lambda_i \tau}$ are the eigenvalues and the $\bar{O}_i(0)$ the respective eigenvectors of the monodromy matrix.

For the complete solution, the $\bar{O}_i(t)$ must be computed over an entire period. Equation (19) is essentially an ordinary differential equation for $\Lambda(t)$, the partitioned $O(t)$ matrix, having as initial conditions the eigenvectors of M .

III. Modal Control

Due to the system's unstable characteristics, some form of control is necessary. Rate and position feedback laws were unsuccessful since all modes, the stable as well as the unstable, were excited (Ref 21) with appreciable control costs. In order to avoid this, Captain Shelton implemented a modal controller which resulted in moving only the third root, leaving the other modes and the conjugate root of the unstable mode unchanged. Although this method is not the only alternative available, it is commensurate with present knowledge in the control of periodic systems.

So that a controller may be added to the system, the state equations, (5), must be augmented with a control term

$$B(t)\bar{u}(t) \quad (25)$$

where $\bar{u}(t)$ is the control vector and $B(t)$ is the distribution matrix which determines to which states control is applied.

$$\dot{\delta\bar{x}}(t) = A(t)\delta\bar{x}(t) + B(t)\bar{u}(t) \quad (26)$$

For Captain Shelton's work $B(t)$ was taken as $\begin{bmatrix} 0 & 1 & 0 & 1 & 0 & 0 \end{bmatrix}^T$ signifying changes in momenta in the x and y directions due to thrust application.

So that only the desired mode is affected by the controller, the system must be converted to a set of diagonal equations. Implementing the transformation,

$$\delta\bar{x}(t) = \Lambda(t)\bar{\eta}(t) \quad (27)$$

where $\bar{\eta}(t)$ is the modal vector and $\Lambda(t)$ is as defined in (18), and its derivative,

$$\dot{\delta\bar{x}}(t) = \dot{\Lambda}(t)\bar{\eta}(t) + \Lambda(t)\dot{\bar{\eta}}(t) \quad (28)$$

the modal state equations become

$$\dot{\Lambda}(t)\bar{\eta}(t) + \Lambda(t)\dot{\bar{\eta}}(t) = A(t)\Lambda(t)\bar{\eta}(t) + B(t)\bar{u}(t) \quad (29)$$

Rearranging (29) produces

$$\dot{\bar{\eta}}(t) = \Lambda^{-1}(t) [A(t)\Lambda(t) - \dot{\Lambda}(t)] \bar{\eta}(t) + \Lambda^{-1}(t) B(t) \bar{u}(t) \quad (30)$$

Recalling (19)

$$J = \Lambda^{-1}(t) [A(t)\Lambda(t) - \dot{\Lambda}(t)] \quad (19)$$

where J is the diagonal matrix of Poincaré exponents defined previously, the differential equations of motion in modal variables are:

$$\dot{\bar{\eta}}(t) = J\bar{\eta}(t) + \Lambda^{-1}(t) B(t) \bar{u}(t) \quad (31)$$

which can be expanded into the six equations representing the modal system.

Previous work maintained a scalar control law for simplicity. So that the only unstable component of the modal vector (η_3) would be influenced, the control law was defined as

$$u = G\eta_3(t) \quad (32)$$

where G is the constant gain term. Transforming this back to physical variables through the inverse of (27) gives

$$u = G\Lambda_3^{-1}(t) \delta\bar{x}(t) \quad (33)$$

where $\Lambda_3^{-1}(t)$ is defined as the third row of the $\Lambda^{-1}(t)$ matrix.

Expanding (31) fully and substituting for $\bar{u}(t)$ results in a linear, first-order, time-varying differential equation for $\eta_3(t)$:

$$\dot{\eta}_3(t) = \left[\lambda_3 + (\Lambda_{32}^{-1}(t) + \Lambda_{34}^{-1}(t)) G \right] \eta_3(t) \quad (34)$$

where the subscripts refer to the rows and columns respectively of $\Lambda^{-1}(t)$. Solving this equation with an integrating factor and separating $\Lambda_{32}^{-1}(t)$ and $\Lambda_{34}^{-1}(t)$ into their respective Fourier series for analysis resulted in constant and periodic components of each term. This gave rise to a linear relationship between the actual and desired pole locations,

$$\lambda_3' = \lambda_3 + G\gamma_0 \quad (35)$$

where λ_3 is the present third Poincaré exponent, λ_3' is its desired position, and γ_0 is the constant component yielded by the Fourier analysis (See Ref 20: 31-33, for detailed derivation). Thus, this procedure reduces to a pole placement technique.

By varying the gain, Captain Shelton was able to determine that a value of $G = .259$ was just adequate to bring the third Poincaré exponent into the left-half plane, thereby resulting in a controlled stable system. Other gains simply vary its position linearly in accordance with the above law.

IV. Observer Theory

The observability of a state vector is fundamental to state estimation since if a particular state is unobservable, its value cannot be derived from the output. Alternatively, a combination of states may be observable, thus rendering the individual states indistinguishable from each other. Therefore, for many feedback control systems it is assumed that the entire state vector is available through measurements. Often, however, one or more of the states cannot be observed directly with only the measured data, and an approximate state vector must be substituted, with control applied to the estimate instead.

In 1963, David G. Luenberger derived a dynamic device which would generate estimates of the inaccessible plant states of a deterministic linear system from exact measurements of the output (Ref 14, 15). A control law can then be implemented utilizing the resulting full state vector. Again, this may be looked upon as a pole placement technique, and as long as the noise component is tiny the only restriction on the arbitrarily-placed observer poles is that they have faster response characteristics than those of the plant matrix, e.g., further to the left in the s-plane, for rapid convergence to the true state.

For the system under consideration, it is extremely difficult to determine a satellite's position in the orbit through conventional triangularization. Only line-of-sight data for range and range-rate can be determined to any great degree of accuracy due to the alignment of the Earth, Moon, and L3 point and the size of the orbit (see Figure 4). However, from transponder and Doppler shift data, accuracies for these radial measurements are quite impressive, on the order of three meters for range when averaging the round trip time of radio signals or down

to a few centimeters for laser pulses (Ref 18). The standard deviation for range-rate is .02 meters per second (Ref 5:66). This defines the noise in range and range-rate measurements to be on the order of 10^{-9} , so that double precision arithmetic would be necessary to accurately simulate the effects. Truncation errors due to computerized numerical integration are large enough to completely obliterate any noise from the observations themselves. Therefore, this may be considered a strictly deterministic system.

With the distances involved, range measurements vary little with nonradial displacements. For example, if the satellite is at its maximum y position, there is a mere .7% variation in the range. This renders the plant states for the y and z directions essentially unobservable and estimates must be constructed using a Luenberger Observer.

Repeating the state equations and presenting the output equations for the first time results in the complete system to be considered:

$$\begin{aligned}\dot{\bar{x}}(t) &= A(t)\bar{x}(t) + B(t)\bar{u}(t) \\ \bar{y}(t) &= C(t)\bar{x}(t)\end{aligned}\quad (36)$$

The output or measurement vector, $\bar{y}(t)$, is shown in component variational form in (37). The general range and range-rate equations are:

$$\begin{aligned}\text{Range: } \bar{r}(t) &= \sqrt{x(t)^2 + y(t)^2 + z(t)^2} \\ \text{Range Rate: } \dot{\bar{r}}(t) &= \bar{v}(t) \cdot \frac{\bar{r}(t)}{|\bar{r}(t)|}\end{aligned}$$

$$\bar{y}(t) = \begin{bmatrix} \delta\bar{r}(t) \\ \delta\dot{\bar{r}}(t) \end{bmatrix} = \begin{bmatrix} [\delta x(t)^2 + \delta y(t)^2 + \delta z(t)^2]^{\frac{1}{2}} \\ [\delta\dot{x}(t)\delta x(t) + \delta\dot{y}(t)\delta y(t) + \delta\dot{z}(t)\delta z(t)] / \delta\bar{r}(t) \end{bmatrix}\quad (37)$$

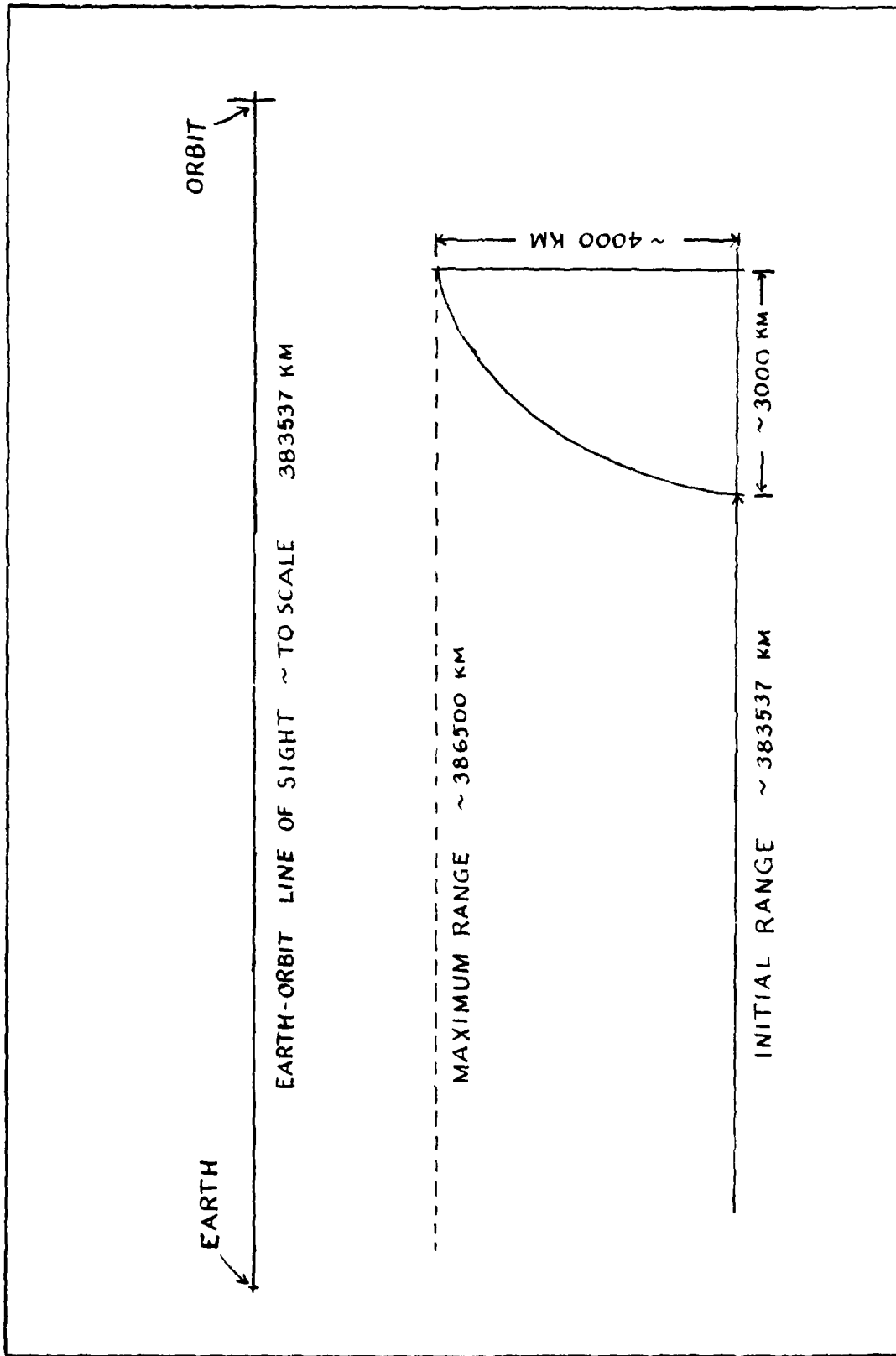


Figure 4. State Observability

This generates an output matrix, $C(t)$, of the following form:

$$C(t) = \begin{bmatrix} \frac{\partial \delta \bar{r}(t)}{\partial \delta x(t)} & \frac{\partial \delta \bar{r}(t)}{\partial \delta P_x(t)} & \frac{\partial \delta \bar{r}(t)}{\partial \delta y(t)} & \frac{\partial \delta \bar{r}(t)}{\partial \delta P_y(t)} & \frac{\partial \delta \bar{r}(t)}{\partial \delta z(t)} & \frac{\partial \delta \bar{r}(t)}{\partial \delta P_z(t)} \\ \frac{\partial \dot{\delta \bar{r}}(t)}{\partial \delta x(t)} & \frac{\partial \dot{\delta \bar{r}}(t)}{\partial \delta P_x(t)} & \frac{\partial \dot{\delta \bar{r}}(t)}{\partial \delta y(t)} & \frac{\partial \dot{\delta \bar{r}}(t)}{\partial \delta P_y(t)} & \frac{\partial \dot{\delta \bar{r}}(t)}{\partial \delta z(t)} & \frac{\partial \dot{\delta \bar{r}}(t)}{\partial \delta P_z(t)} \end{bmatrix} \quad (38)$$

The individual $C(t)$ matrix elements were verified using the definition of the derivative. For example,

$$C_{11} = \frac{\partial \delta \bar{r}}{\partial \delta x} = \frac{[\delta \bar{r}(\delta x = 2.001) - \delta \bar{r}(\delta x = 2)]}{.001}$$

The ranges and range-rates were examined for the entire orbit and were consistent with the respective data.

Since the $C(t)$ matrix is a 2×6 matrix rather than a full 6×6 matrix, a reduced order observer will need to be considered. The observer state and output equations are

$$\begin{aligned} \dot{\hat{x}}(t) &= A(t)\hat{x}(t) + B(t)\bar{u}(t) + K(t)[\bar{y}(t) - \hat{y}(t)] \\ \hat{y}(t) &= C(t)\hat{x}(t) \end{aligned} \quad (39)$$

where the caret represents the estimate of the respective vectors.

Allowing the observer reconstruction error to be defined as

$$\bar{e}_o(t) = \bar{x}(t) - \hat{x}(t) \quad (40)$$

gives

$$\begin{aligned} \dot{\bar{e}}_o(t) &= A(t)\bar{x}(t) + B(t)\bar{u}(t) - A(t)\hat{x}(t) - B(t)\bar{u}(t) \\ &\quad - K(t)[\bar{y}(t) - \hat{y}(t)] \end{aligned} \quad (41)$$

when (36) and (39) are substituted into (40).

Simplifying,

$$\dot{\bar{e}}_o(t) = [A(t) - K(t)C(t)]\bar{e}_o(t) \quad (42)$$

$K(t)$ is termed the observer gain matrix, the dimensions of which must be 6×2 . Elements of this matrix can be chosen so that the eigenvalues of

$$[A(t) - K(t)C(t)]$$

will all lie in the left-half plane, thus allowing the steady state value of $\bar{e}(t)$ for any initial conditions to approach zero as t approaches infinity.

Since only one of the three system modes is unstable, modal control theory may be used to move the one positive pole into the other plane, following the same derivational steps as for the controller.

Through the modal transformation (27) and its time derivative (28) the system equations (36) become

$$\begin{aligned} \dot{\bar{\eta}}(t) &= \Lambda^{-1}(t)[A(t)\Lambda(t) - \dot{\Lambda}(t)]\bar{\eta}(t) + \Lambda^{-1}(t)B(t)\bar{u}(t) \\ \bar{y}(t) &= C(t)\Lambda(t)\bar{\eta}(t) \end{aligned} \quad (43)$$

These reduce to

$$\begin{aligned} \dot{\bar{\eta}}(t) &= J\bar{\eta}(t) + \Lambda^{-1}(t)B(t)\bar{u}(t) \\ \bar{y}(t) &= C(t)\Lambda(t)\bar{\eta}(t) \end{aligned} \quad (44)$$

when (19) is used.

Substituting the equivalent transformation into the observer

(39) results in

$$\begin{aligned} \Lambda(t)\dot{\hat{\eta}}(t) &= [A(t)\Lambda(t) - \dot{\Lambda}(t)]\hat{\eta}(t) + B(t)\bar{u}(t) \\ &\quad + K(t)C(t)\Lambda(t)[\bar{\eta}(t) - \hat{\eta}(t)] \end{aligned} \quad (45)$$

which, when multiplied by $\Lambda^{-1}(t)$, becomes

$$\begin{aligned} \dot{\hat{n}}(t) &= J\hat{n}(t) + \Lambda^{-1}(t)B(t)\bar{u}(t) \\ &+ \Lambda^{-1}(t)K(t)C(t)\Lambda(t)\left[\bar{n}(t) - \hat{n}(t)\right] \end{aligned} \quad (46)$$

Defining the modal reconstruction error as

$$\bar{e}_m(t) = \bar{n}(t) - \hat{n}(t) \quad (47)$$

gives

$$\dot{\bar{e}}_m(t) = \dot{\bar{n}}(t) - \dot{\hat{n}}(t) \quad (48)$$

Substituting (43), (45), and (47) into (48) results in an equation for the error.

$$\begin{aligned} \dot{\bar{e}}_m(t) &= J\bar{n}(t) + \Lambda^{-1}(t)B(t)\bar{u}(t) - J\hat{n}(t) - \Lambda^{-1}(t)B(t)\bar{u}(t) \\ &\quad - \Lambda^{-1}(t)K(t)C(t)\Lambda(t)\left[\bar{n}(t) - \hat{n}(t)\right] \\ \dot{\bar{e}}_m(t) &= \left[J - \Lambda^{-1}(t)K(t)C(t)\Lambda(t) \right] \bar{e}_m(t) \end{aligned} \quad (49)$$

When the elements of the observer gain matrix are chosen so that

$$\left[J - \Lambda^{-1}(t)K(t)C(t)\Lambda(t) \right]$$

has Poincaré exponents with only negative real parts, the observer is stable. This will give identical Poincaré exponents when transformed back to the physical system.

In order to choose the elements of the gain matrix easily, the following transformations are made:

$$\begin{aligned} K'(t) &= \Lambda^{-1}(t)K(t) \\ C'(t) &= C(t)\Lambda(t) \end{aligned} \quad (50)$$

This is justified since the observer introduces an additional set of time periodic coefficients and Floquet Theory may be used for its analysis. Now (49) becomes

$$\dot{\bar{e}}_m(t) = \left[J - K'(t)C'(t) \right] \bar{e}_m(t) \quad (51)$$

If $K'(t)$ is defined as

$$\begin{bmatrix} 0 & 0 & \emptyset & 0 & 0 & 0 \\ 0 & 0 & \beta & 0 & 0 & 0 \end{bmatrix}^T \quad (52)$$

where \emptyset and β are arbitrary constants, then only one row is added to J . Thus, by appropriate choices of \emptyset and β the third root can be relocated in the left-half plane as desired. Since there is no analytical method to conveniently choose gains corresponding to desired pole placement, various values, both constant and time-varying, were implemented and the resulting Poincaré exponents examined. After the appropriate gain has been determined, the $K(t)$ matrix necessary to stabilize the system in the physical variables can thus be easily derived from $K'(t)$ using the definition.

Expanding (51) for the full six-dimensional error vector shows the addition of only one row to influence J .

$$\begin{bmatrix} \dot{e}_{m_1}(t) \\ \dot{e}_{m_2}(t) \\ \dot{e}_{m_3}(t) \\ \dot{e}_{m_4}(t) \\ \dot{e}_{m_5}(t) \\ \dot{e}_{m_6}(t) \end{bmatrix} = \begin{bmatrix} 0 & \omega_1 & 0 & 0 & 0 & 0 \\ \omega_2 & 0 & 0 & 0 & 0 & 0 \\ N_1 & N_2 & N_3 & N_4 & N_5 & N_6 \\ 0 & 0 & 0 & \lambda_4 & 0 & 0 \\ 0 & 0 & 0 & 0 & 0 & \omega_5 \\ 0 & 0 & 0 & 0 & \omega_6 & 0 \end{bmatrix} \begin{bmatrix} e_{m_1}(t) \\ e_{m_2}(t) \\ e_{m_3}(t) \\ e_{m_4}(t) \\ e_{m_5}(t) \\ e_{m_6}(t) \end{bmatrix} \quad (53)$$

where

$$\begin{aligned} N_1 &= -[\emptyset C'_{11}(t) + \beta C'_{21}(t)] \\ N_2 &= -[\emptyset C'_{12}(t) + \beta C'_{22}(t)] \\ N_3 &= \lambda_3 - [\emptyset C'_{13}(t) + \beta C'_{23}(t)] \\ N_4 &= -[\emptyset C'_{14}(t) + \beta C'_{24}(t)] \\ N_5 &= -[\emptyset C'_{15}(t) + \beta C'_{25}(t)] \\ N_6 &= -[\emptyset C'_{16}(t) + \beta C'_{26}(t)] \end{aligned}$$

Now an explicit equation for $\dot{e}_{m_3}(t)$ may be formulated.

$$\begin{aligned} \dot{e}_{m_3}(t) = & - \left[\theta C_{11}'(t) + \beta C_{21}'(t) \right] e_{m_1}(t) - \left[\theta C_{12}'(t) + \beta C_{22}'(t) \right] e_{m_2}(t) \\ & + \left\{ \lambda_3 - \left[\theta C_{13}'(t) + \beta C_{23}'(t) \right] \right\} e_{m_3}(t) - \left[\theta C_{14}'(t) + \beta C_{24}'(t) \right] e_{m_4}(t) \quad (54) \\ & - \left[\theta C_{15}'(t) + \beta C_{25}'(t) \right] e_{m_5}(t) - \left[\theta C_{16}'(t) + \beta C_{26}'(t) \right] e_{m_6}(t) \end{aligned}$$

Even though (54) involves the entire error vector, this may be simplified to

$$\dot{e}_{m_3}(t) = \left\{ \lambda_3 - \left[\theta C_{13}'(t) + \beta C_{23}'(t) \right] \right\} e_{m_3}(t)$$

since the remaining terms exhibit known time periodic behavior from (53) and so may be combined as a time-varying particular solution.

Substituting $\xi_1(t)$ for $C_{13}'(t)$ and $\xi_2(t)$ for $C_{23}'(t)$ renders the differential equation to be solved as

$$\dot{e}_{m_3}(t) - \left\{ \lambda_3 - \left[\theta \xi_1(t) + \beta \xi_2(t) \right] \right\} e_{m_3}(t) = 0 \quad (55)$$

Multiplying both sides by the integrating factor

$$e^{-\int \left\{ \lambda_3 - \left[\theta \xi_1(t) + \beta \xi_2(t) \right] \right\} dt}$$

gives

$$\begin{aligned} e^{-\int \left\{ \lambda_3 - \left[\theta \xi_1(t) + \beta \xi_2(t) \right] \right\} dt} \dot{e}_{m_3}(t) = \\ \left\{ \lambda_3 - \left[\theta \xi_1(t) + \beta \xi_2(t) \right] \right\} e^{-\int \left\{ \lambda_3 - \left[\theta \xi_1(t) + \beta \xi_2(t) \right] \right\} dt} e_{m_3}(t) \end{aligned}$$

The solution to this exact differential equation is

$$e_{m_3}(t) e^{-\int \left\{ \lambda_3 - \left[\theta \xi_1(t) + \beta \xi_2(t) \right] \right\} dt} = c \quad (56)$$

where c is the constant of integration.

Fourier analysis of the $C(t)$ matrix reveals that each element is made up of a constant and periodic terms. This allows $\xi_1(t)$ and $\xi_2(t)$ to be expanded into

$$\xi_1(t) = \xi_{10} + \xi_{1p}(t)$$

$$\xi_2(t) = \xi_{20} + \xi_{2p}(t)$$

where the o signifies constant and the p periodic terms.

Solving for $e_{m_3}(t)$ and substituting for $\xi_1(t)$ and $\xi_2(t)$ gives

$$\begin{aligned} e_{m_3}(t) &= ce^{\int [\lambda_3 - \theta \xi_{10} - \theta \xi_{1p}(t) - \beta \xi_{20} - \beta \xi_{2p}(t)] dt} \\ &= ce^{\int [\lambda_3 - \theta \xi_{10} - \beta \xi_{20}] dt} e^{-\int [\theta \xi_{1p}(t) + \beta \xi_{2p}(t)] dt} \\ &= ce^{[\lambda_3 - \theta \xi_{10} - \beta \xi_{20}] t} e^{-\int [\theta \xi_{1p}(t) + \beta \xi_{2p}(t)] dt} \quad (57) \end{aligned}$$

The periodic terms oscillate so that the stability characteristics are dominated by the

$$e^{[\lambda_3 - \theta \xi_{10} - \beta \xi_{20}] t}$$

term. Therefore, the Poincaré exponent is placed by

$$\lambda'_3 = \lambda_3 - \theta \xi_{10} - \beta \xi_{20} \quad (58)$$

a linear form. Here λ_3 is the present position and λ'_3 is the desired position of the Poincaré exponent.

V. Controller/Observer Implementation

The purpose of designing a Luenberger Observer is to be able to feed the resulting state estimate into the controller which would then act to stabilize the system. If the observer poles are to the left of those of the system, keeping in mind the noise component restrictions mentioned earlier, convergence to the actual state vector is rapid and the controller is furnished with excellent state values. It should not, however, deteriorate the performance of the controller.

It can be shown that observer and controller eigenvalues can be assigned independently, thereby creating a composite and yet uncoupled set. The former control law, (33), modified to utilize the state estimate, $\hat{x}(t)$, becomes

$$\bar{u}(t) = -F(t)\hat{x}(t) \quad \text{if} \quad F(t) = -GA_3^{-1}(t)$$

Inserting this into (36) results in

$$\dot{\bar{x}}(t) = A(t)\bar{x}(t) - B(t)F(t)\hat{x}(t) \quad (59)$$

$$\bar{y}(t) = C(t)\bar{x}(t)$$

Recalling the reconstruction error in physical variables,

$$\bar{e}_o(t) = \bar{x}(t) - \hat{x}(t) \quad (40)$$

and substituting into (59) above yields

$$\dot{\bar{x}}(t) = [A(t) - B(t)F(t)]\bar{x}(t) + B(t)F(t)\bar{e}_o(t) \quad (60)$$

This can be presented in partitioned form in conjunction with the observer reconstruction error equation (42) as

$$\begin{bmatrix} \dot{\bar{x}}(t) \\ \dot{\bar{e}}_o(t) \end{bmatrix} = \begin{bmatrix} A(t) - B(t)F(t) & B(t)F(t) \\ 0 & A(t) - K(t)C(t) \end{bmatrix} \begin{bmatrix} \bar{x}(t) \\ \bar{e}_o(t) \end{bmatrix} \quad (61)$$

Now defining a system state transition matrix as

$$\phi^S(t) = \begin{bmatrix} \phi^S_{11}(t) & \phi^S_{12}(t) \\ \phi^S_{21}(t) & \phi^S_{22}(t) \end{bmatrix} = \begin{bmatrix} \dot{x}(t) & 0 \\ 0 & \dot{e}_o(t) \end{bmatrix}$$

(61) becomes

$$\dot{\phi}^S(t) = \begin{bmatrix} \psi & \zeta \\ 0 & \nu \end{bmatrix} \phi^S(t) \quad (62)$$

where

$$\psi = A(t) - B(t)F(t)$$

$$\zeta = B(t)F(t)$$

$$\nu = A(t) - K(t)C(t)$$

Expanding the partitioned equations yields

$$\dot{\phi}^S_{11}(t) = \psi \phi^S_{11}(t) + \zeta \phi^S_{21}(t) \quad (63a)$$

$$\dot{\phi}^S_{12}(t) = \psi \phi^S_{12}(t) + \zeta \phi^S_{22}(t) \quad (63b)$$

$$\dot{\phi}^S_{21}(t) = \nu \phi^S_{21}(t) \quad (63c)$$

$$\dot{\phi}^S_{22}(t) = \nu \phi^S_{22}(t) \quad (63d)$$

As in any state transition matrix, the initial conditions are

$$\phi^S(0) = I$$

This sets the initial conditions for the submatrices defined by the partitions as well:

$$\dot{\phi}^S_{11}(0) = I \quad (64a)$$

$$\dot{\phi}^S_{12}(0) = [0] \quad (64b)$$

$$\dot{\phi}^S_{21}(0) = [0] \quad (64c)$$

$$\dot{\phi}^S_{22}(0) = I \quad (64d)$$

(63c) implies that $\phi^S_{21} = 0$ for all time, so (63a) and (63d) become

$$\dot{\phi}^S_{11}(t) = \psi \phi^S_{11}(t) \quad \text{and} \quad \dot{\phi}^S_{22}(t) = \nu \phi^S_{22}(t)$$

After one period has elapsed

$$\phi^S(\tau) = \begin{bmatrix} \phi_{11}^S(\tau) & \phi_{12}^S(\tau) \\ 0 & \phi_{22}^S(\tau) \end{bmatrix} \quad (65)$$

Forming the characteristic equation of this time-varying composite system gives

$$\left[\lambda_{\text{plant}}^I - \phi_{11}^S(t) \right] \left[\lambda_{\text{observer}}^I - \phi_{22}^S(t) \right] = \bar{0}$$

where λ_{plant} are the n eigenvalues of the system and $\lambda_{\text{observer}}$ are those for the Luenberger Observer. This separation demonstrates that placing an observer in a feedback system does not affect its eigenvalues. The two sets merely produce a composite formation.

VI. Results, Conclusions, and Recommendations

Results. Since all of the system's states cannot be measured directly, a suitable approximation, which could be substituted into the control law developed by Captain Shelton, was sought. Therefore, a logical extension to his work was the implementation of a Luenberger Observer which would reconstruct the entire state vector. As developed in Chapter IV, the observer moves the unstable component linearly with gain, similar to the case of the controller. Appropriate elements of the modified observer gain matrix were found using a systematic search technique and are depicted in Figure 5. For example, a value of $\delta = 2000.0$ and $\beta = 0.0$ in (58), moves the root from 2.392121 to -14.92828, obviously far enough into the left half-plane to render the system stable. The slope was calculated as -0.00866.

When other elements of the modified observer gain matrix were filled in order to try to bring the oscillating components into negative real configuration, the linear correlation is destroyed. All the states except the fourth couple and it becomes virtually impossible to predict the effect of various $K'(t)$ values. Some examples of exponent-gain correlation are presented in Table III. It was eventually possible to bring the oscillating planar mode into negative real form through appropriate application of gains, but to date, the same has not been accomplished for the nonplanar mode. The best has been to move the real part slightly farther into the left-half plane, e.g. -0.045 ± 1.2321 .

With no nonplanar motion considered, a gain matrix producing a set of Poincaré exponents which fulfills the stabilization criteria

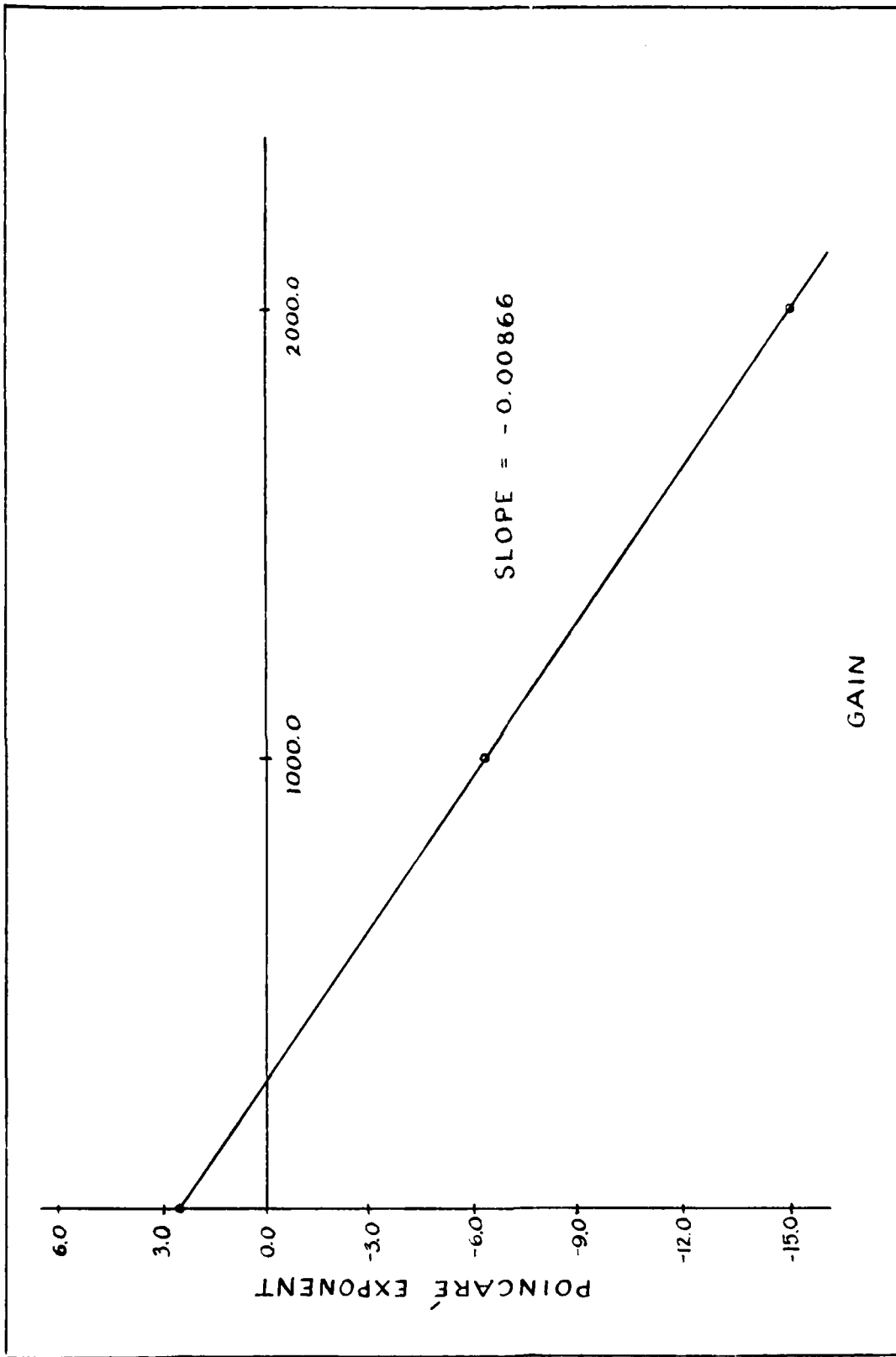


Figure 5. Root Position vs. Gain

Table III. Observer Exponent-Gain Correlations

$K'_{12} = 10.0$	$K'_{12} = 3.0$	$K'_{12} = 3.0$	$K'_{12} = 3.0$
$K'_{31} = 1000.0$	$K'_{31} = 1500.0$	$K'_{31} = 1500.0$	$K'_{61} = -100000.0$
-6.42	-2.214	-2.59	0.01
-10.86	-6.05	-4.53	0.01
-19.43	-11.47	-8.77	0.01
-2.39	-2.39	-2.39	0.01
0.0	0.0	-0.05	1.231
0.0	0.0	-0.05	-1.231

$K'_{12} = 3.0$	$K'_{12} = 1.0$	$K'_{12} = 1.0$	$K'_{12} = 1.0$
$K'_{31} = 6000.0$	$K'_{31} = 1500.0$	$K'_{31} = 1500.0$	$K'_{52} = -1.7 \times 10^{-5}$
$K'_{52} = 1000.0$	$K'_{52} = 100.0$	$K'_{52} = -1.7 \times 10^{-5}$	
0.002	$-.43 \times 10^{-4}$	-3.96	0.01
0.002	$-.43 \times 10^{-4}$	-.47	4.471
-0.96	-1.19	-.47	-4.471
-32.9	-13.09	-1.18	2.971
-24.83	-18.41	-1.18	-2.971
-2.39	-2.39	-2.39	0.01

without experiencing adverse noise effects is

$$\begin{bmatrix} 0 & 0 & 1500.0 & 0 & 0 & 0 \\ 3.0 & 0 & 0 & 0 & 0 & 0 \end{bmatrix}^T$$

The corresponding Poincaré exponents are -2.214, -6.047, -11.47, -2.39, $0.0 \pm 1.125i$, with -2.214 dominating the system's behavior since the rest are further in the left-half plane.

Examining this observer's performance by evaluating the data retention time reveals that this system is being implemented correctly. The fastest root, -11.47, exhibits a time constant of approximately .1719 periods or 5.07 days, which is quite sufficient since an update is taken every few seconds. The model under consideration is strictly deterministic with observational inaccuracies inconsequential when compared to those imposed by numerical integration. It is even difficult to distinguish noise in the double precision mode. Therefore, this observer is not in any danger of approaching the undesirable behavior characteristics of a differentiator, and is the basic one used in various test cases.

When the controller and observer were implemented in conjunction, the estimates of the states converged rapidly to the true ones. Three basic cases were chosen to demonstrate the widest range of performance characteristics. The first (Case A) is a very accurate observer, assuming a 14.9 m accuracy for the line-of-sight direction and a 14.9 km accuracy in the y, with orbit initial conditions beyond the range of the controller's ability to achieve convergence. The second (Case B) was chosen as very close to the periodic orbit so that controller behavior could be checked and incorporated an observer having realistic

properties, e.g., extremely accurate data in the line-of-sight direction and almost no knowledge of cross track capability. The third case (Case C) is the former with the out-of-plane mode included for comparison.

To note the behavior of the observer alone, the case of no control on orbit initial conditions (implying exact positioning on the periodic orbit) was run (Figure 6). This showed the observer converging fairly rapidly, matching the true states exactly by at least the end of the fifth orbit.

The next series of figures (7-9) depict the characteristic time evaluation of the modal states. With the extremely accurate observer, convergence to the true state is so rapid that the difference between the two is not discernible even though this case is unstable. The other two cases depict almost total convergence by the end of the third orbit. In addition, appropriate long-term controller behavior is demonstrated for η_1 and η_3 in that these elements of the modal state vector approach zero with time. To check this behavior for the other two elements would only necessitate a longer time interval, but similar tendencies appear to be present. The z mode, when affected (See Figure 9), depicts the expected oscillatory behavior.

Figures 10, 11, and 12 are the errors between the modal and true states with time. These show convergence to zero, but may be somewhat misleading due to the scale. Approximate exponential envelopes may be constructed to define the convergence rate more closely (Table IV). These reveal that the errors are dominated by the largest negative real Poincaré exponent of the observer.

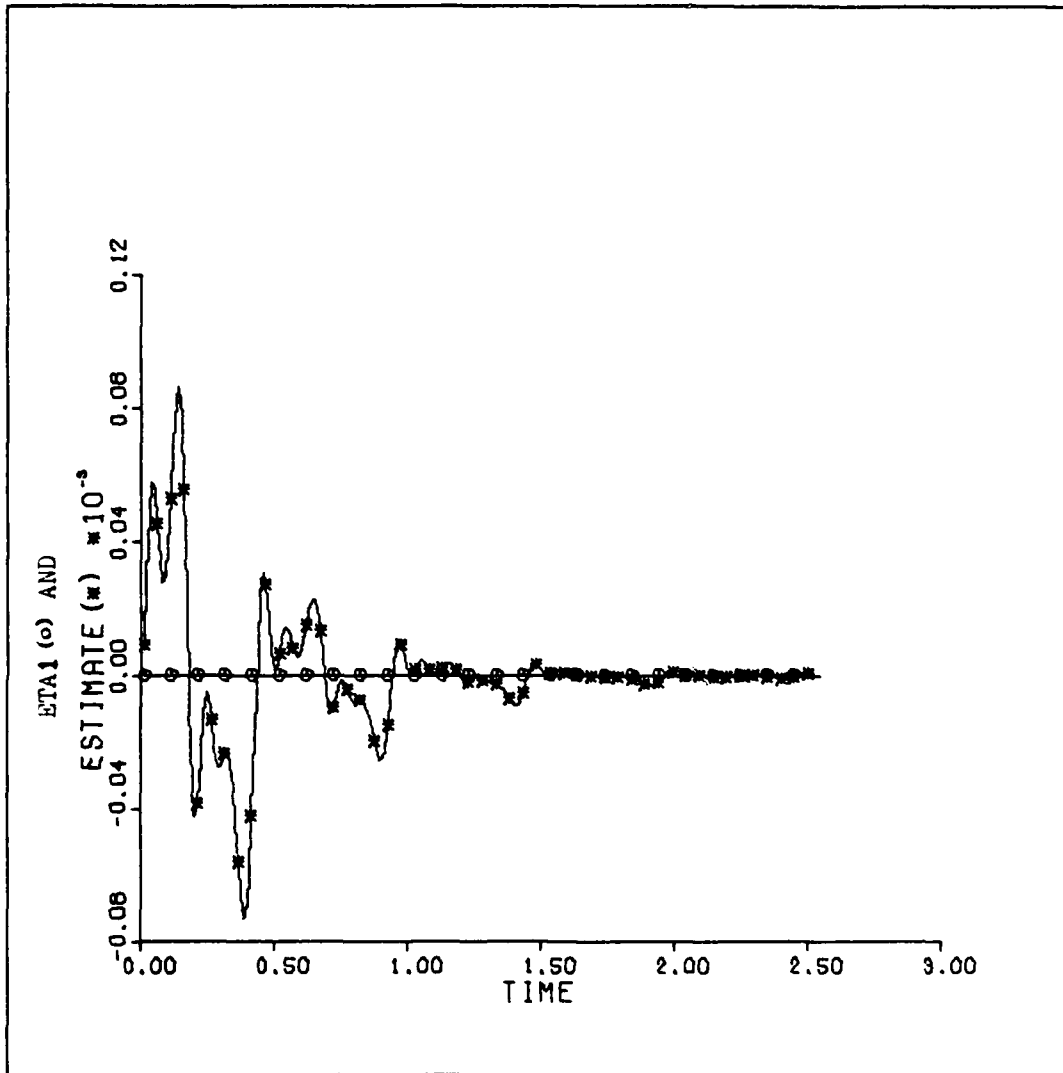


Figure 6a. Uncontrolled System with Observer

Controller gain 0.0
 Orbit initial conditions
 $x = 0.0$ km
 $\dot{x} = 0.0$ km/sec
 $y = 0.0$ km
 $\dot{y} = 0.0$ km/sec
 $z = 0.0$ km
 $\dot{z} = 0.0$ km/sec

Five orbits

Observer initial conditions
 $e_{m1} = 14.96$ m
 $e_{m2} = 14.96$ m/sec
 $e_{m3} = 14959.97$ km
 $e_{m4} = 14959.97$ km/sec
 $e_{m5} = 0.0$ km
 $e_{m6} = 0.0$ km/sec

Observer gain elements
 $K_{12} = 3.0$
 $K_{j1} = 1500.0$

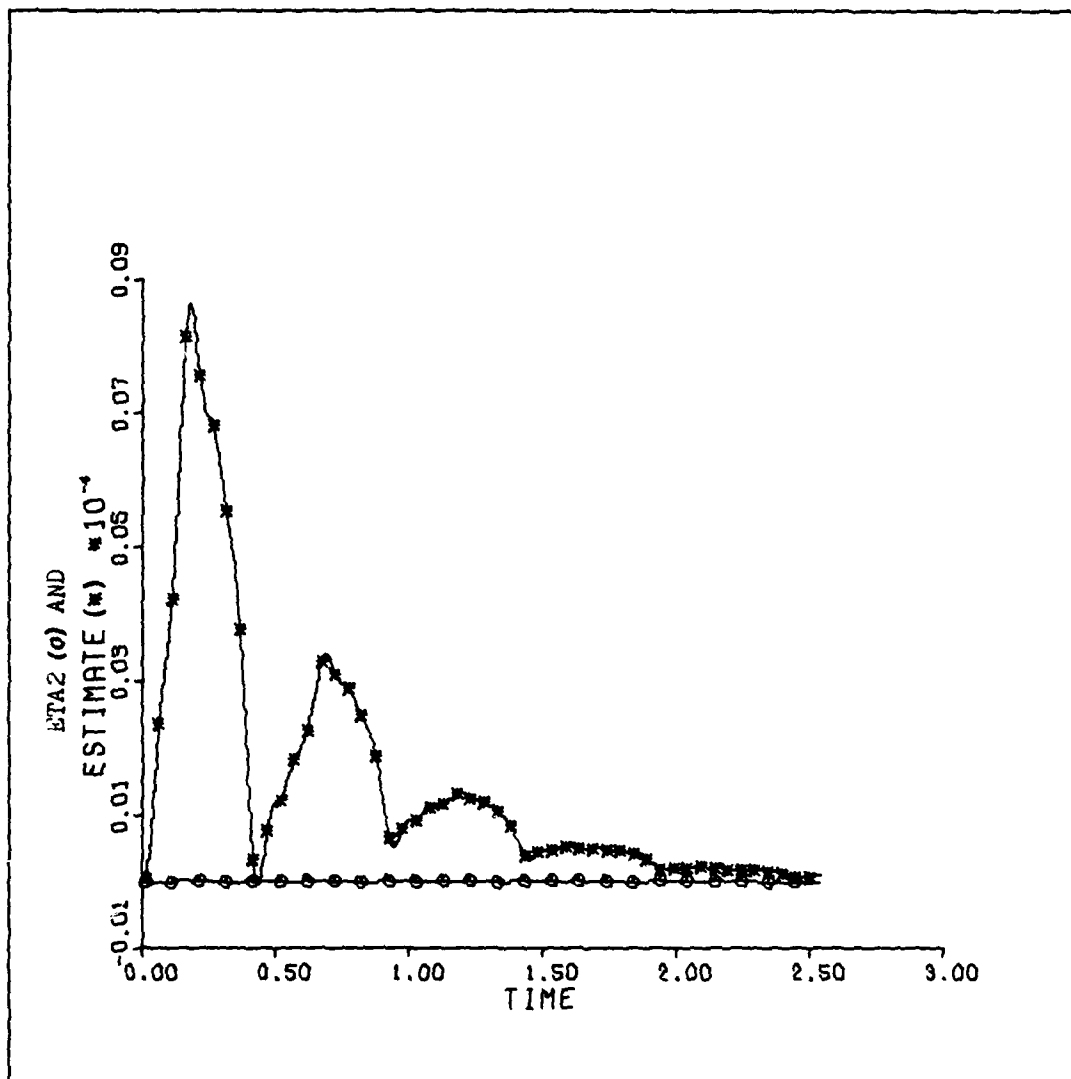


Figure 6b. Second State

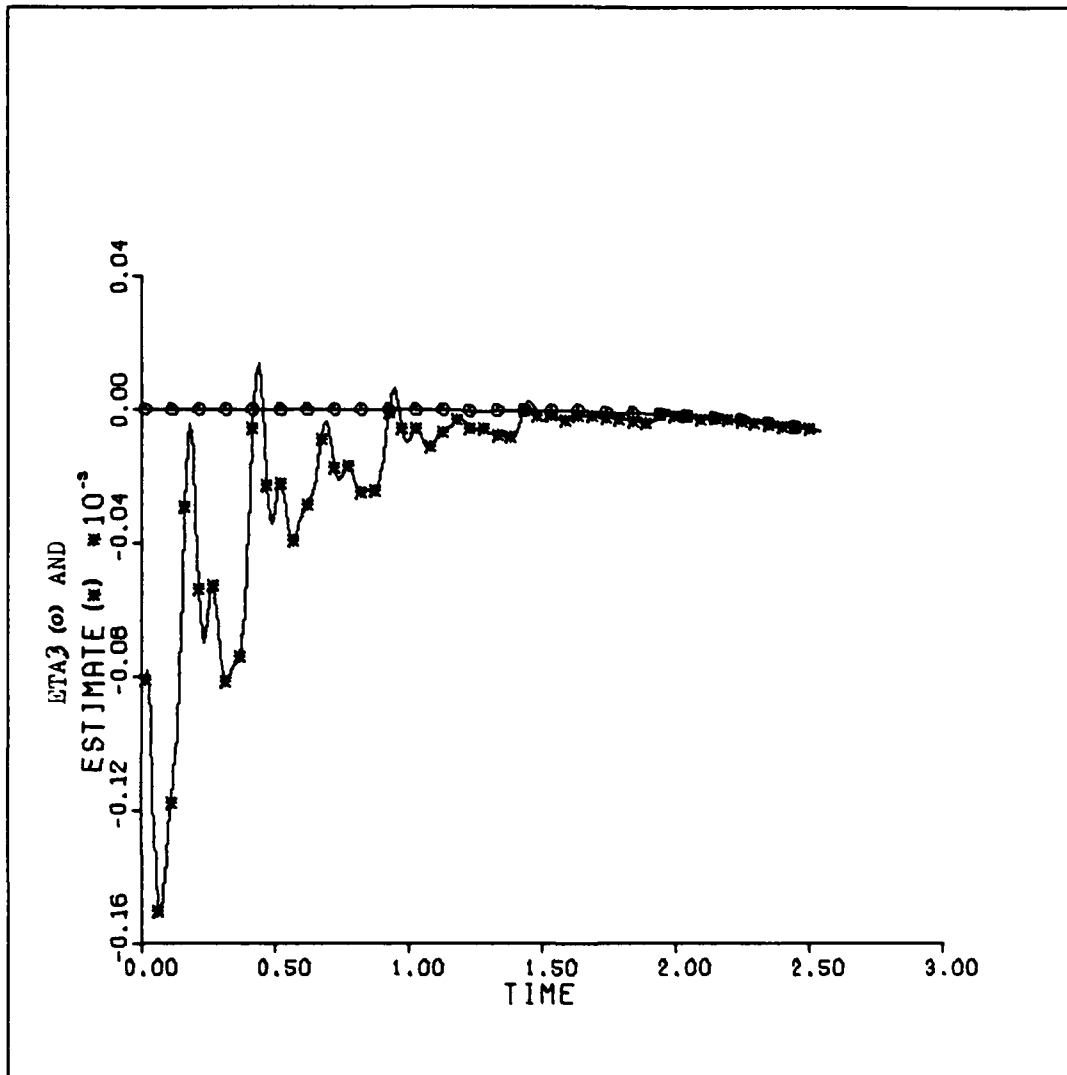


Figure 6c. Third State

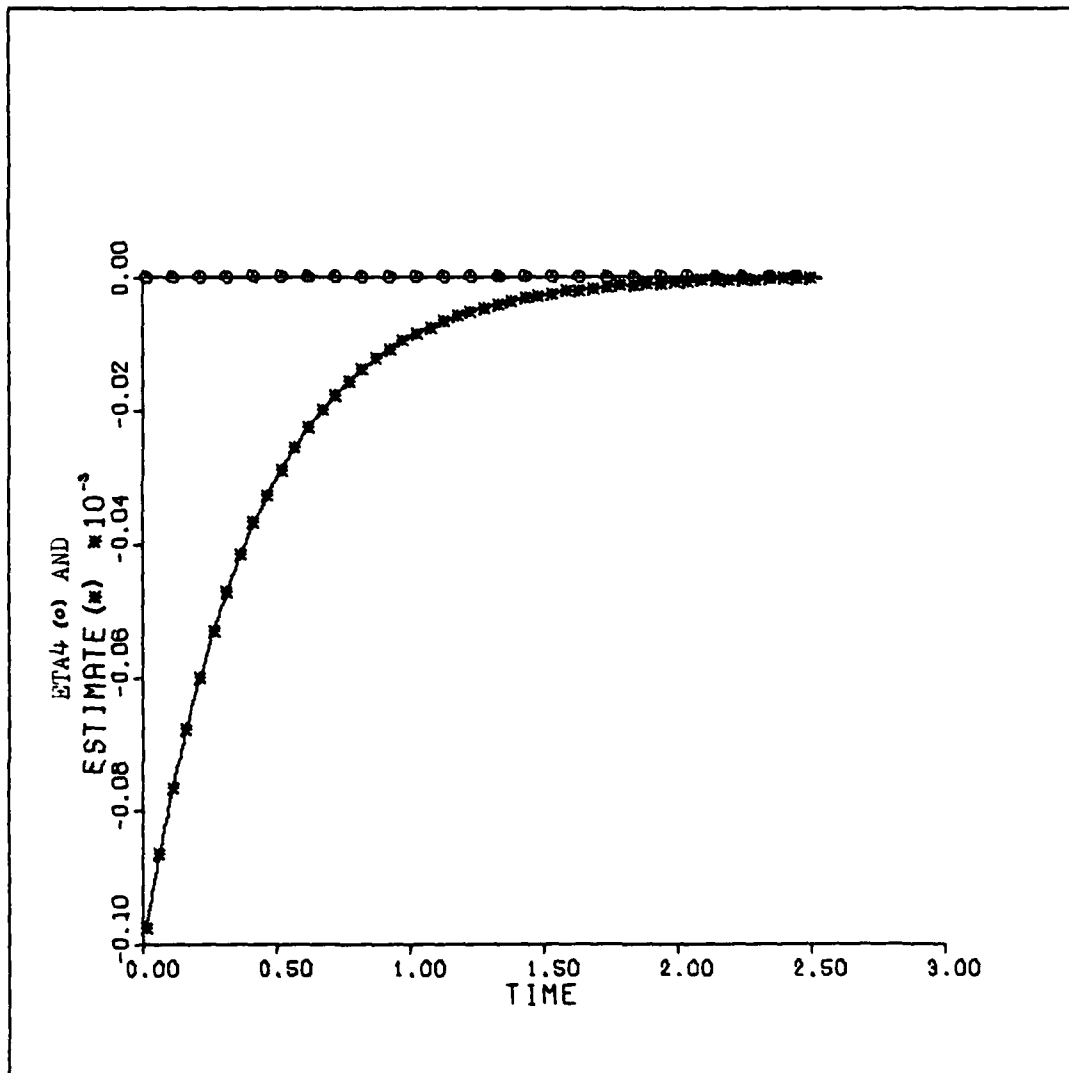


Figure 6d. Fourth State

Examining the phase portraits for the individual modes in each test case (Figures 13, 14, and 15) reveals that once again the accurate observer of Case A has already caused the estimate to match the true state vector identically even though the system is inherently unstable. From the figures it is somewhat difficult to determine the point of convergence for the other two cases, but the listing of the data reveals convergence to the sixth decimal by the third orbit in Case B (nonplanar mode unchanged) and similarly for Case C.

Figure 14b. is especially interesting since it demonstrates the suppression of an unrealistically large initial transient. The observer and controller have widely disparate starting positions and for the first four points (approximately one-half orbit) the controller actually diverges from the state estimate. Later, the trend returns to convergence and joint motion toward zero.

Figure 16 depicts a large orbit initial condition and almost unrealistic lack of knowledge in the y-direction observer states. This example was chosen to demonstrate the system's behavior as the

Table IV. Exponential Envelopes for Errors

Case A:	upper envelope = $1.835 \times 10^{-7} e^{-2.214t}$
	lower envelope = $-1.183 \times 10^{-7} e^{-2.214t}$
Case B:	upper envelope = $1.845 \times 10^{-4} e^{-2.214t}$
	lower envelope = $-1.179 \times 10^{-4} e^{-2.214t}$
Case C:	upper envelope = $1.728 \times 10^{-4} e^{-2.214t}$
	lower envelope = $-1.185 \times 10^{-4} e^{-2.214t}$

observer converges. Even with such a massive uncertainty, the observer behaves well. Figure 17 was included to exhibit the observer's characteristic of converging faster with increased negative positioning of the Poincaré exponent. However, the data reveals that the convergence is actually slower in this case. This occurs because with the gain combinations utilized, the dominant negative root now becomes -1.01 .

Figures 18-21 describe other interesting cases, comparing effects of variations in observer and orbit initial conditions. Even with generally large initial conditions, trends toward state convergence are evident after only one orbit (Figure 19) and more so with an order of magnitude difference in the third and fourth observer error states (Figure 20). However, in this instance, as with an order of magnitude improvement in its initial conditions (Figure 21), the controller no longer appears effective unless numerous orbits are necessary for convergence to occur.

Conclusions

These various cases exhibit all the points this study was meant to investigate: the existence of a stable Luenberger Observer for the restricted four-body problem in question, the observer pole-placement behavior, which proved to be linear as in the case of Captain Shelton's controller, the rapidity of convergence to the true states, and the long-term observer and controller behavior which does not impede controller performance.

Recommendations

The number of cases which could be tested for system behavior evaluation is practically unlimited, and almost all would be valuable if resources and time would allow. One should be able to determine a combination of gains which result in a totally negative real system, including the nonplanar mode, which would then be evaluated for comparative performance. Hopefully, the long-term oscillatory behavior could then be reduced or eliminated.

One should also seek analytical alternatives to arbitrary pole placement. It has been suggested that an examination of Butterworth patterns (Ref 12) would be a possible route.

An extensive evaluation of noise effects on observer and observer/controller behavior is appropriate as well. Even though, operationally, this is a deterministic system almost impervious to noise, it is essential to establish the left-half plane boundary for the positioning of the observer poles in order to avoid undesirable differentiator properties.

Another interesting characteristic which may reveal some useful system properties is the presence of the large frequency component, 6.18, evident in numerous trial and error gain calculations. These may occur with either positive or negative real parts of dissimilar values and the same imaginary part, instead of the expected complex conjugate pairs. Perhaps they indicate the maximum extent of a stable observer performance region, a boundary to be avoided, or perhaps the damping characteristics of such a root would render such a situation favorable.

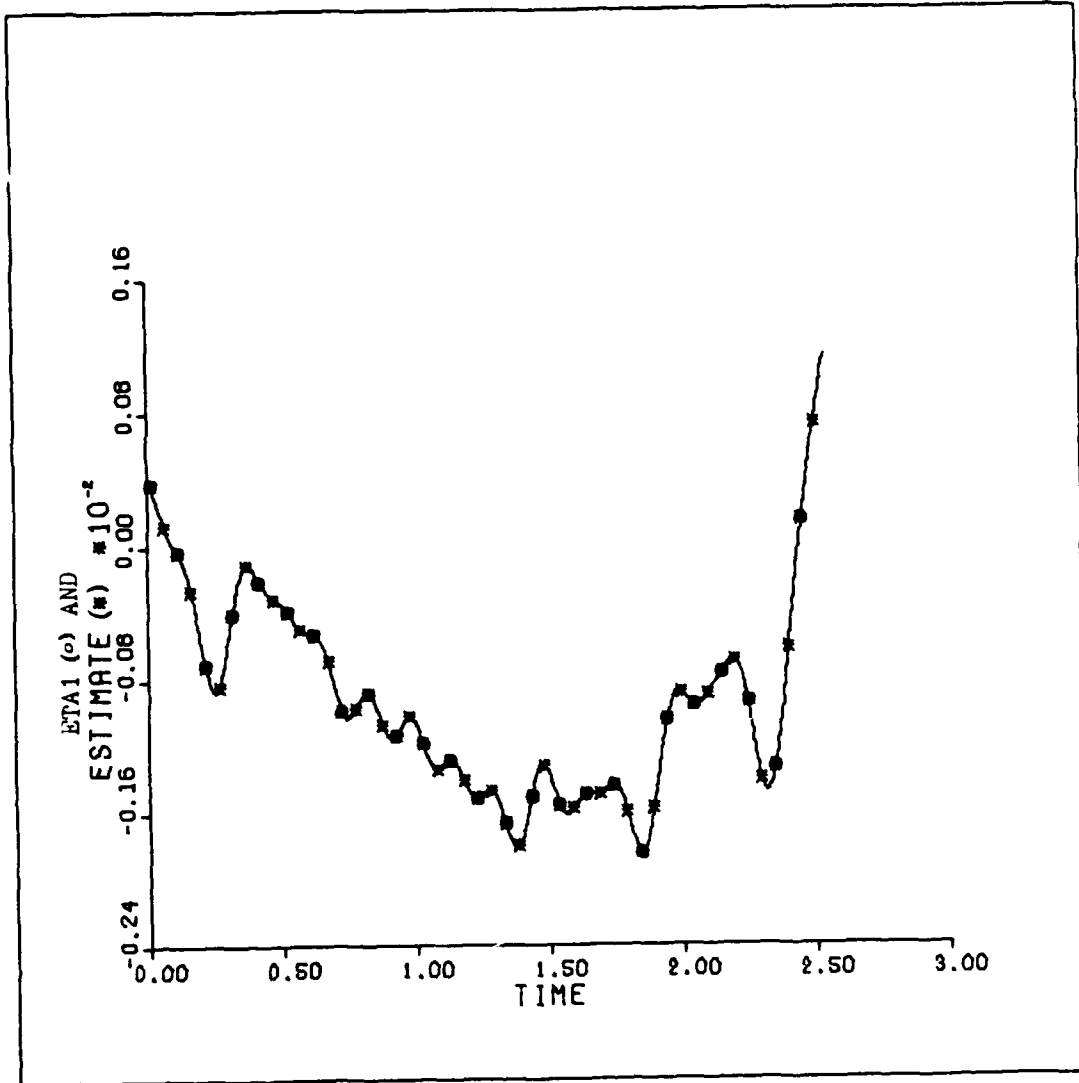


Figure 7a. Modal Vector vs. Time: Case A

Controller gain 0.5
 Orbit initial conditions
 $x = 4488 \text{ km}$
 $P_x = 4488 \text{ km/sec}$
 $y = 4488 \text{ km}$
 $P_y = 4488 \text{ km/sec}$
 $z = 0.0 \text{ km}$
 $P_z = 0.0 \text{ km/sec}$

Five orbits

Observer initial conditions
 $e_{m1} = 14.96 \text{ m}$
 $e_{m2} = 14.96 \text{ m/sec}$
 $e_{m3} = 14.96 \text{ km}$
 $e_{m4} = 14.96 \text{ km/sec}$
 $e_{m5} = 0.0 \text{ km}$
 $e_{m6} = 0.0 \text{ km/sec}$

Observer initial gain
 $K'_{12} = 3.0$
 $K'_{31} = 1500.0$

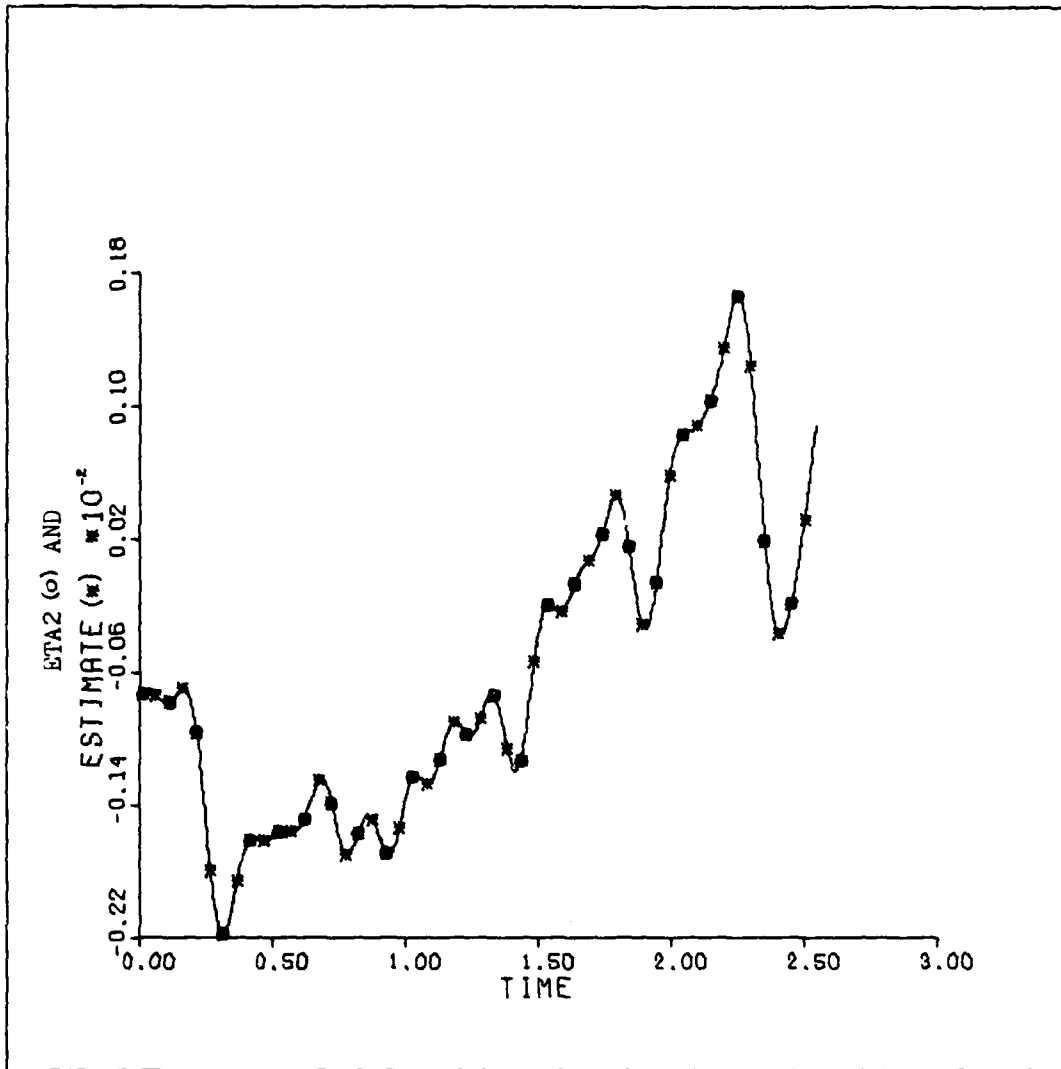


Figure 7b. Second State

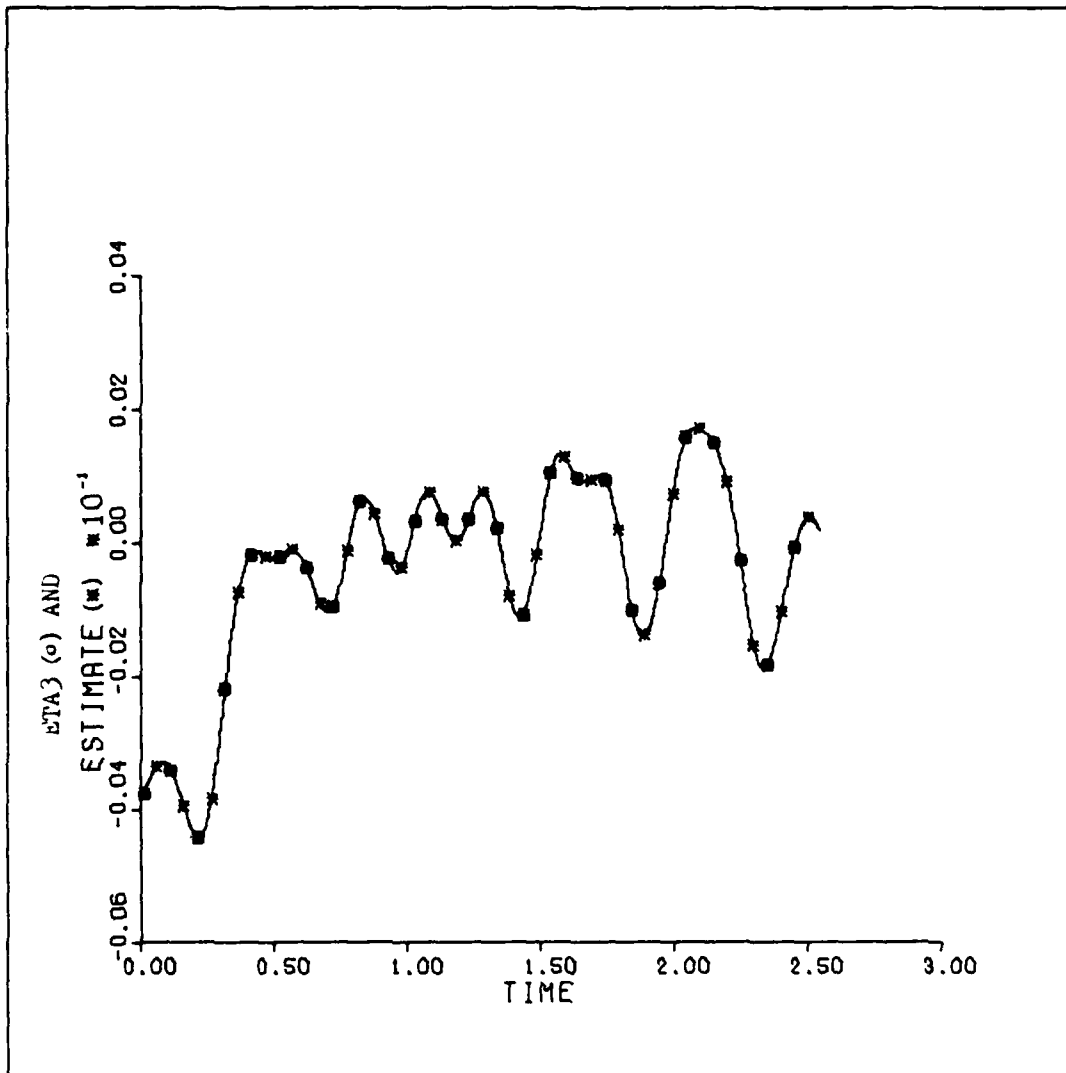


Figure 7c. Third State

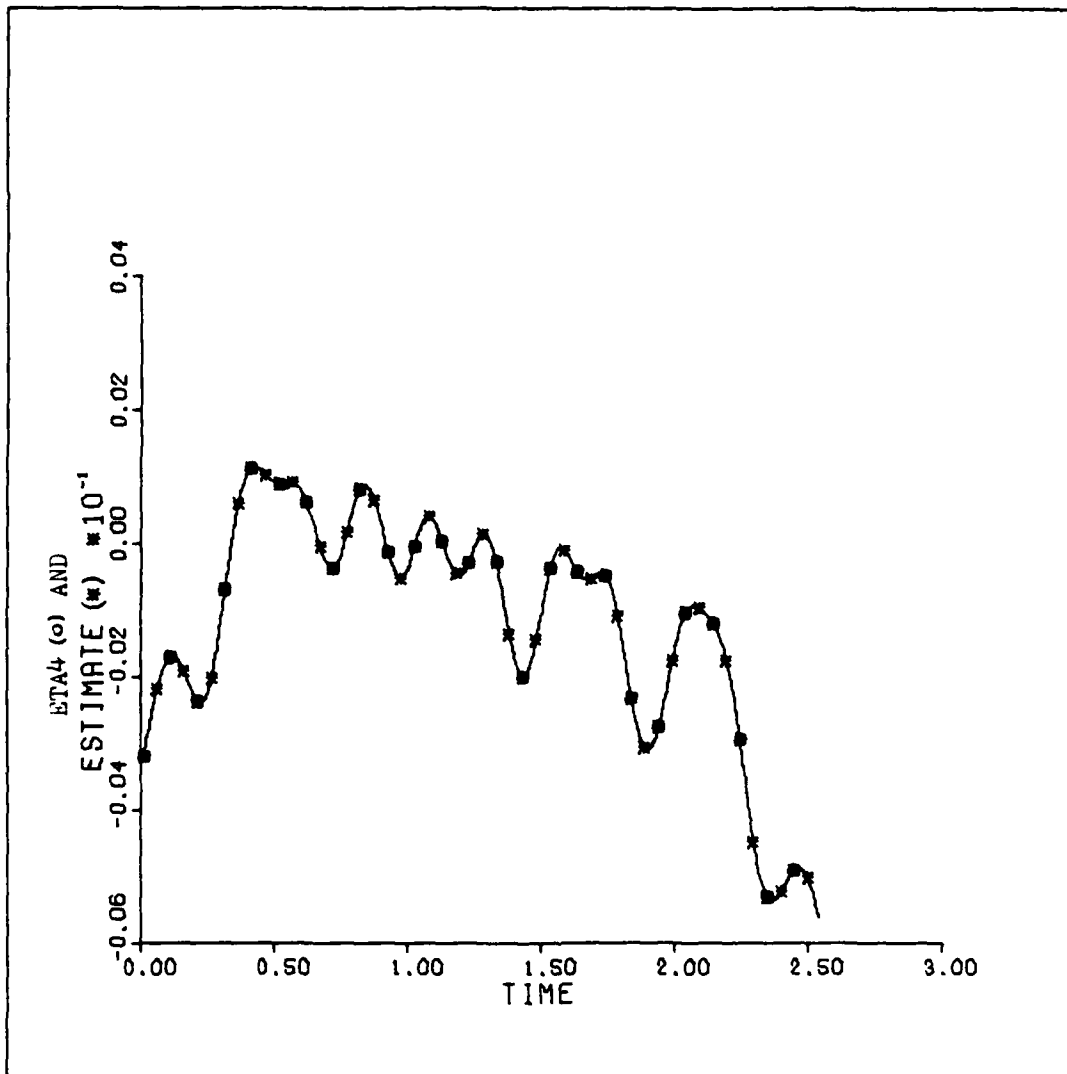


Figure 7d. Fourth State

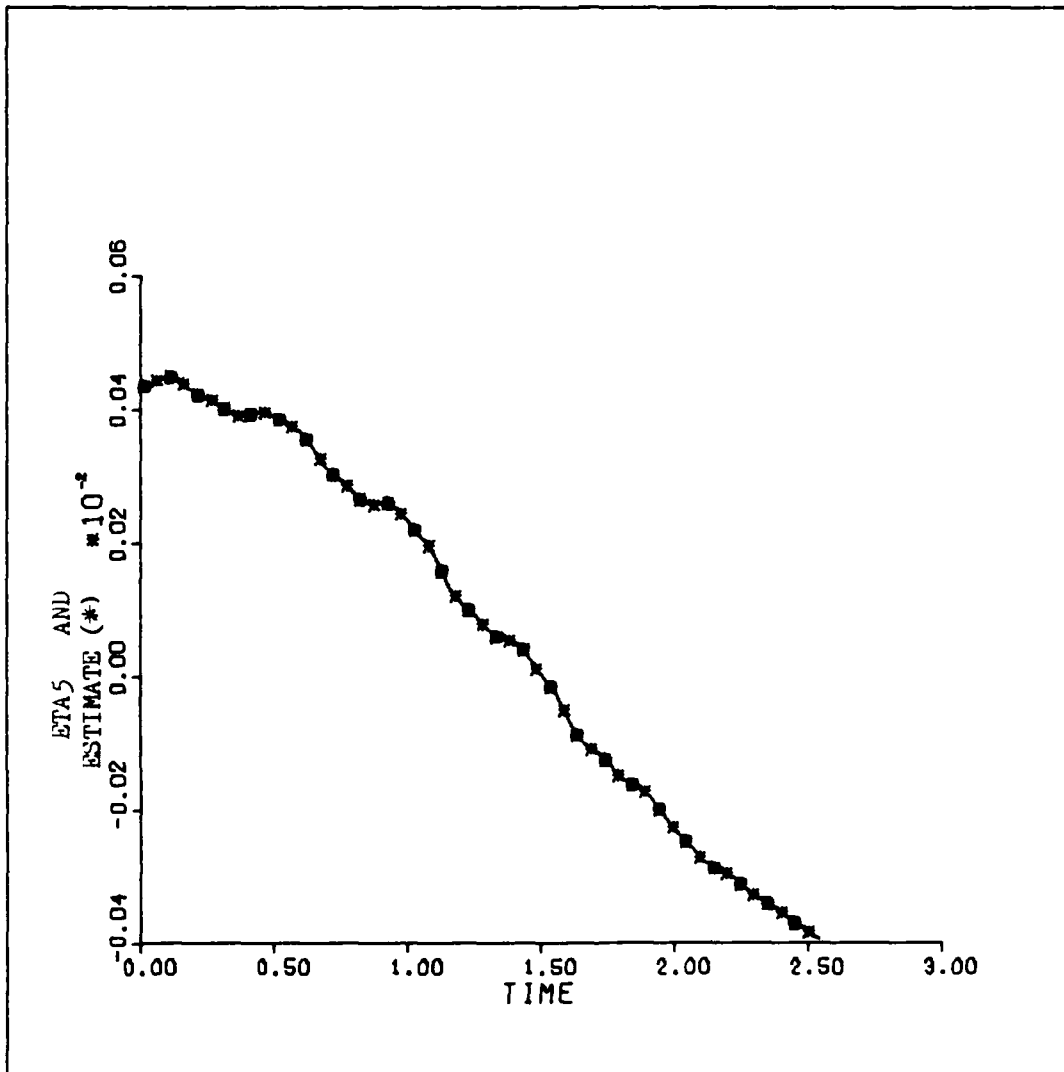


Figure 7e. Fifth State

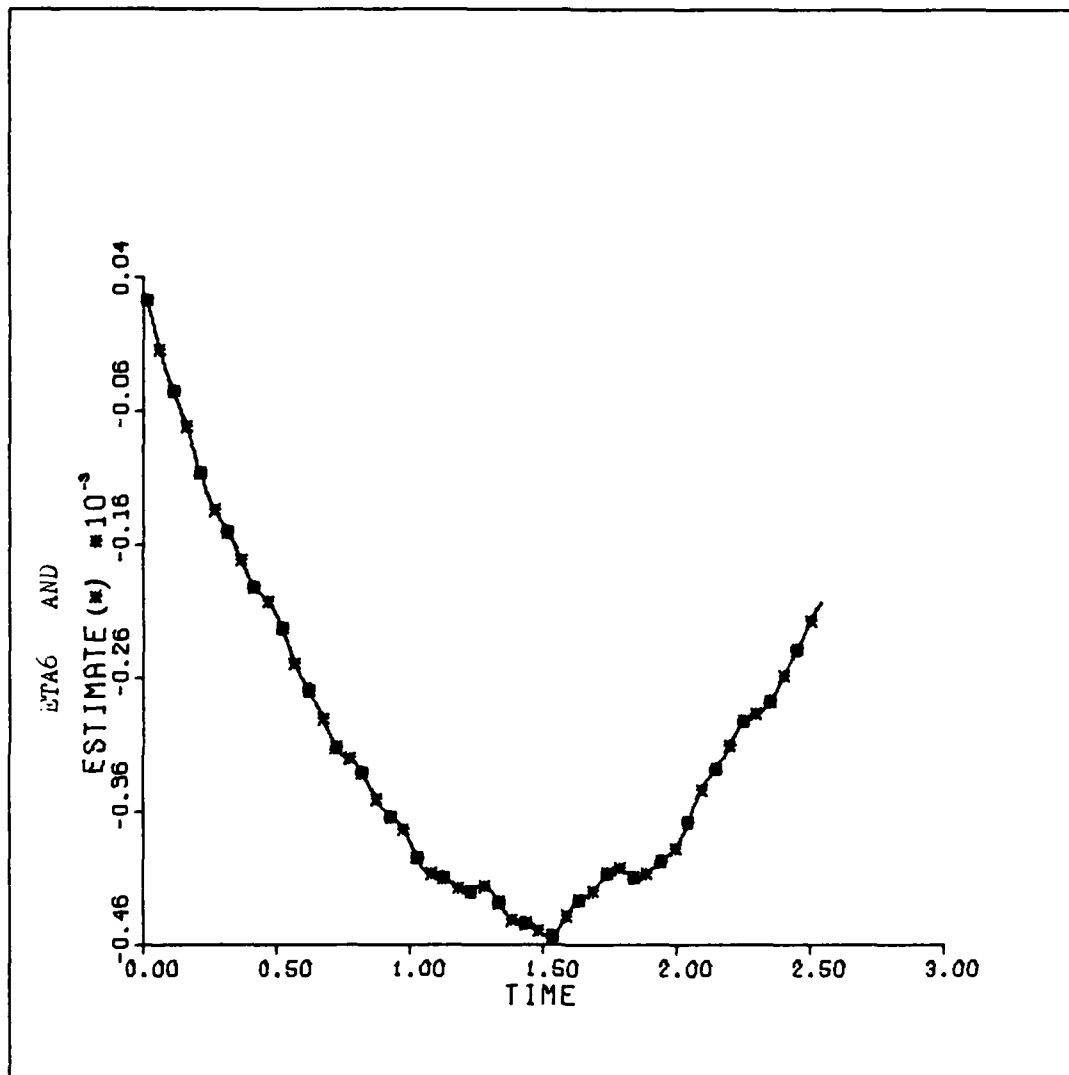


Figure 7f. Sixth State

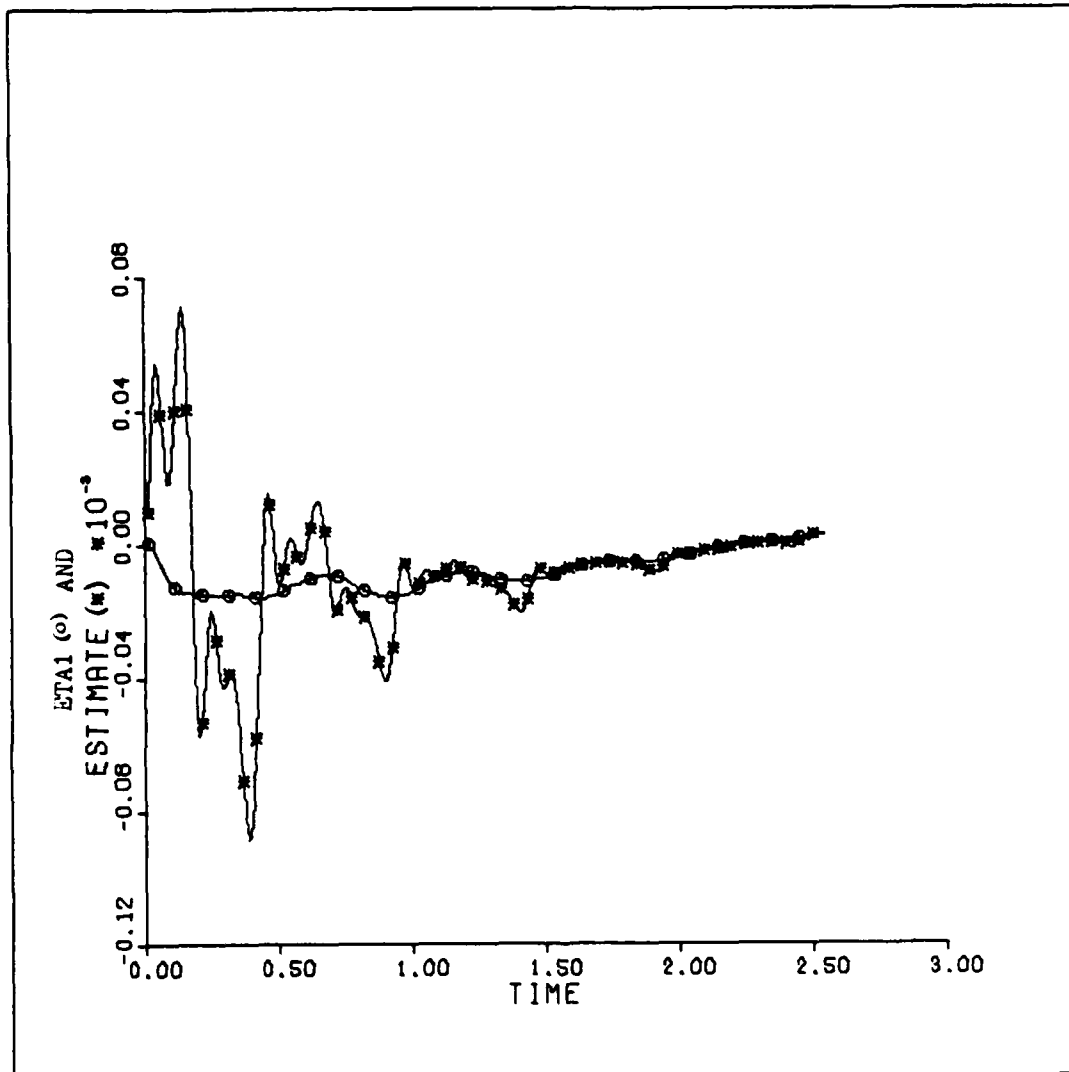


Figure 8a. Modal Vector vs. Time: Case B

Controller gain 0.5

Orbit initial conditions

$x = 14.96$ km

$P_x = 14.96$ km/sec

$y = 14.96$ km

$P_y = 14.96$ km/sec

$z = 0.0$ km

$P_z = 0.0$ km/sec

Observer initial conditions

$e_{m1} = 14.96$ m

$e_{m2} = 14.96$ m/sec

$e_{m3} = 14959.97$ km

$e_{m4} = 14959.97$ km/sec

$e_{m5} = 0.0$ km

$e_{m6} = 0.0$ km/sec

Five orbits

Observer gain elements

$K'_{12} = 3.0$

$K'_{31} = 1500.0$

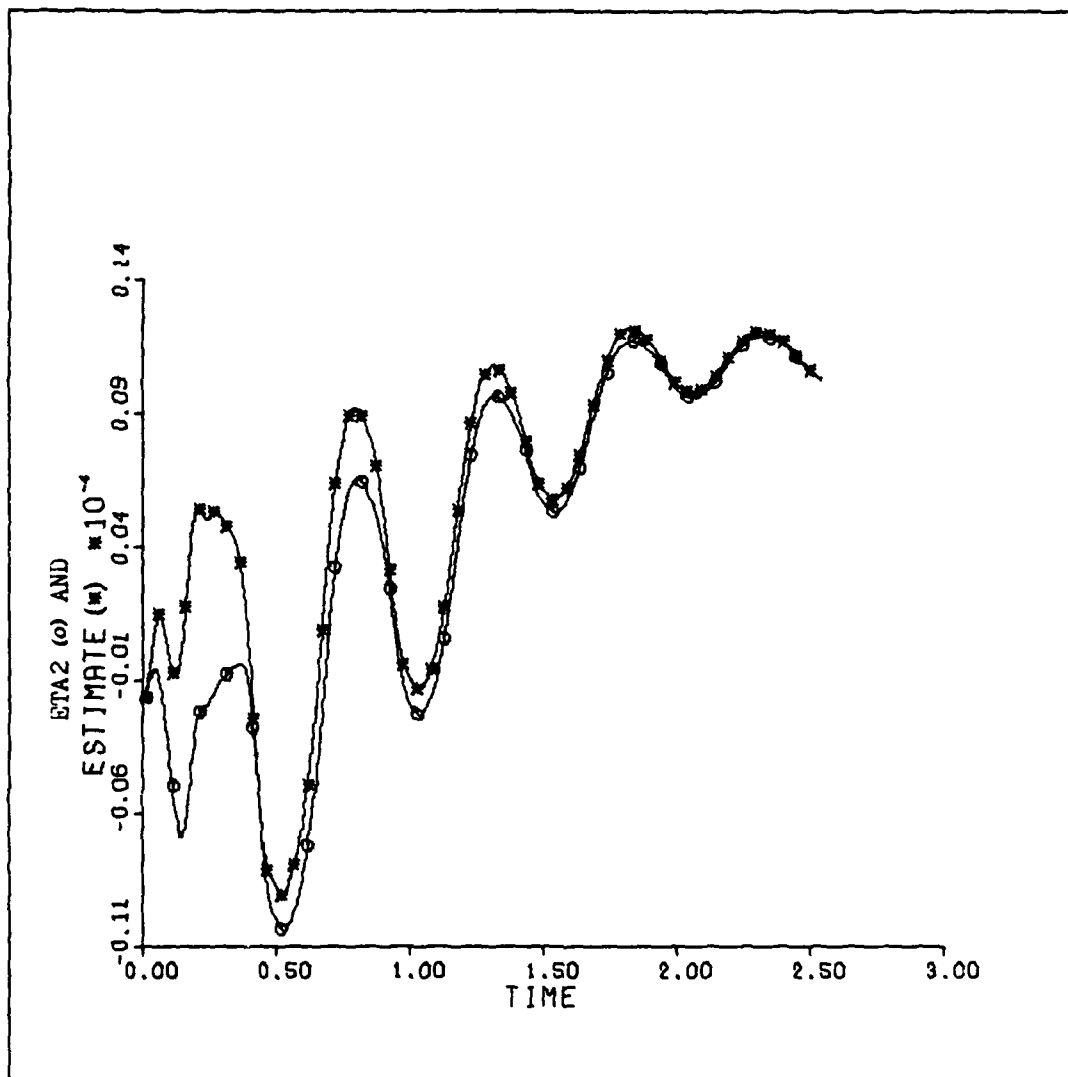


Figure 8b. Second State

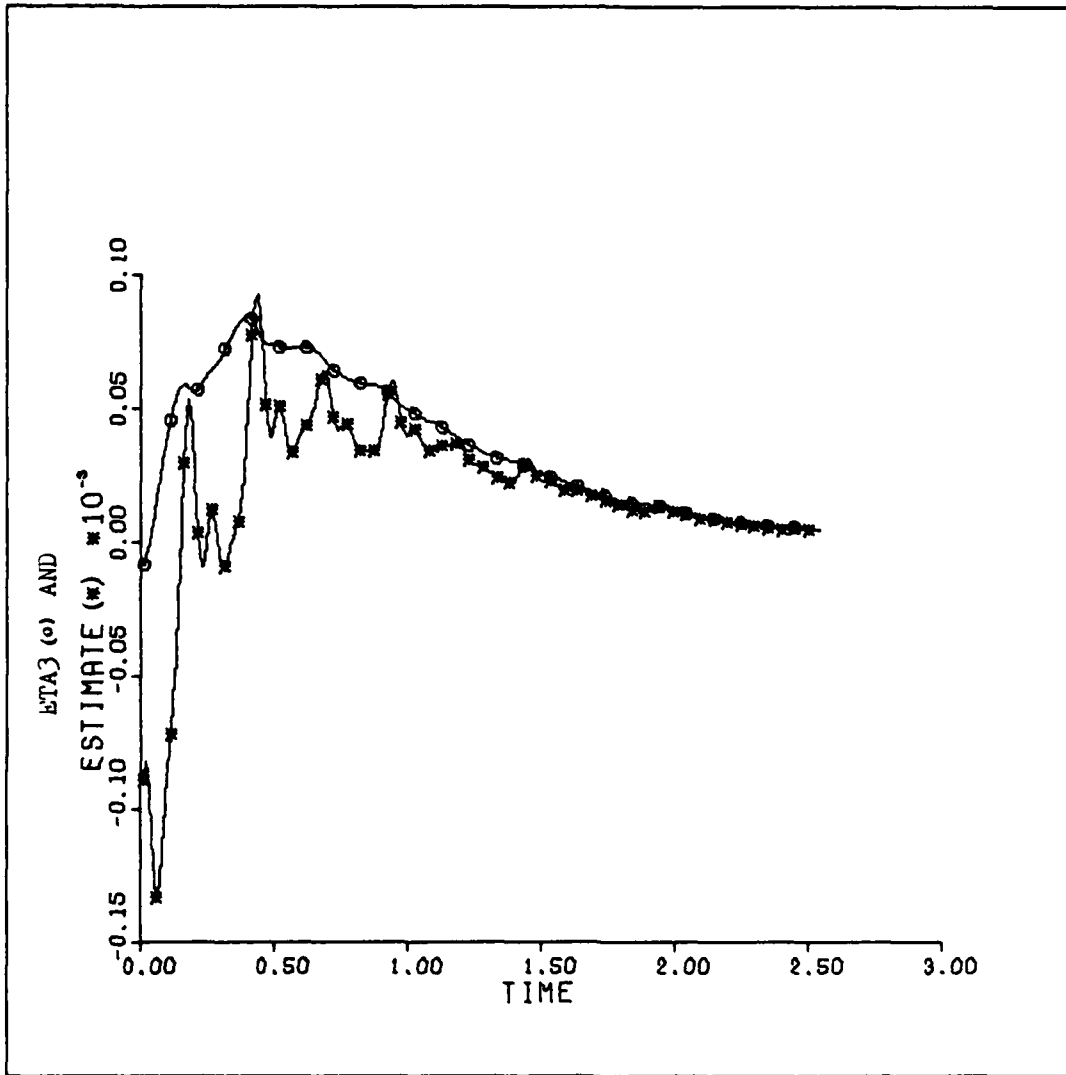


Figure 8c. Third State

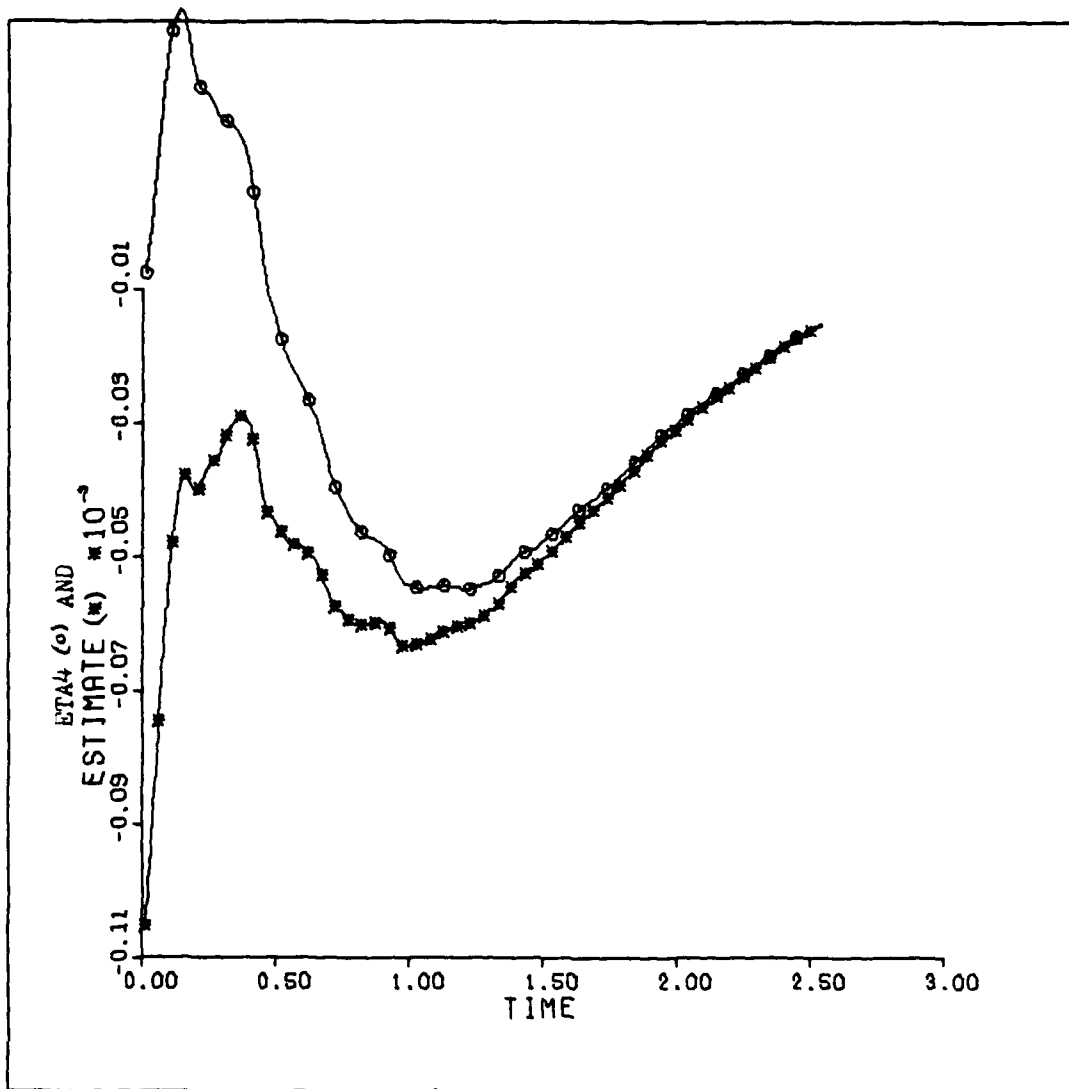


Figure 8d. Fourth State

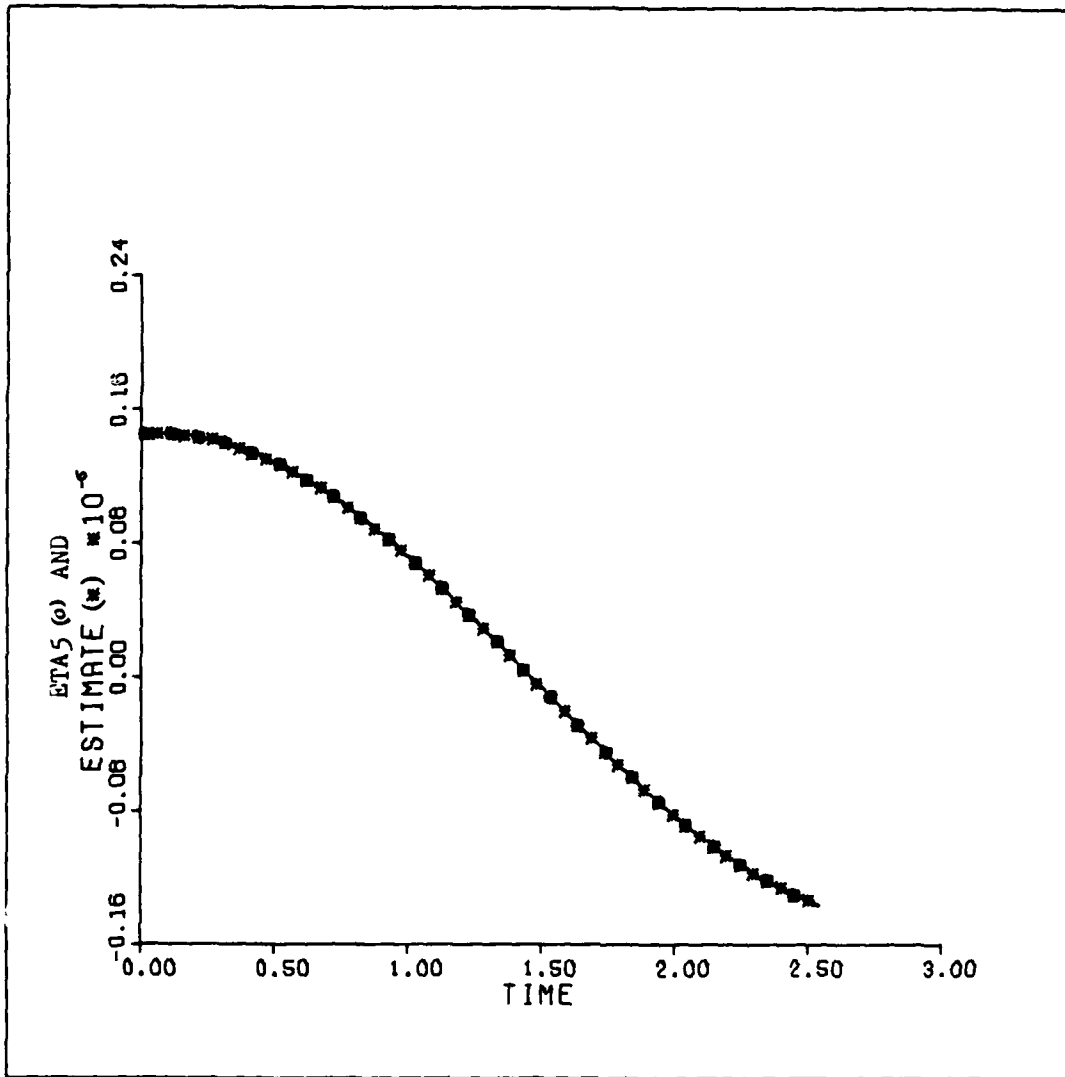


Figure 8e. Fifth State

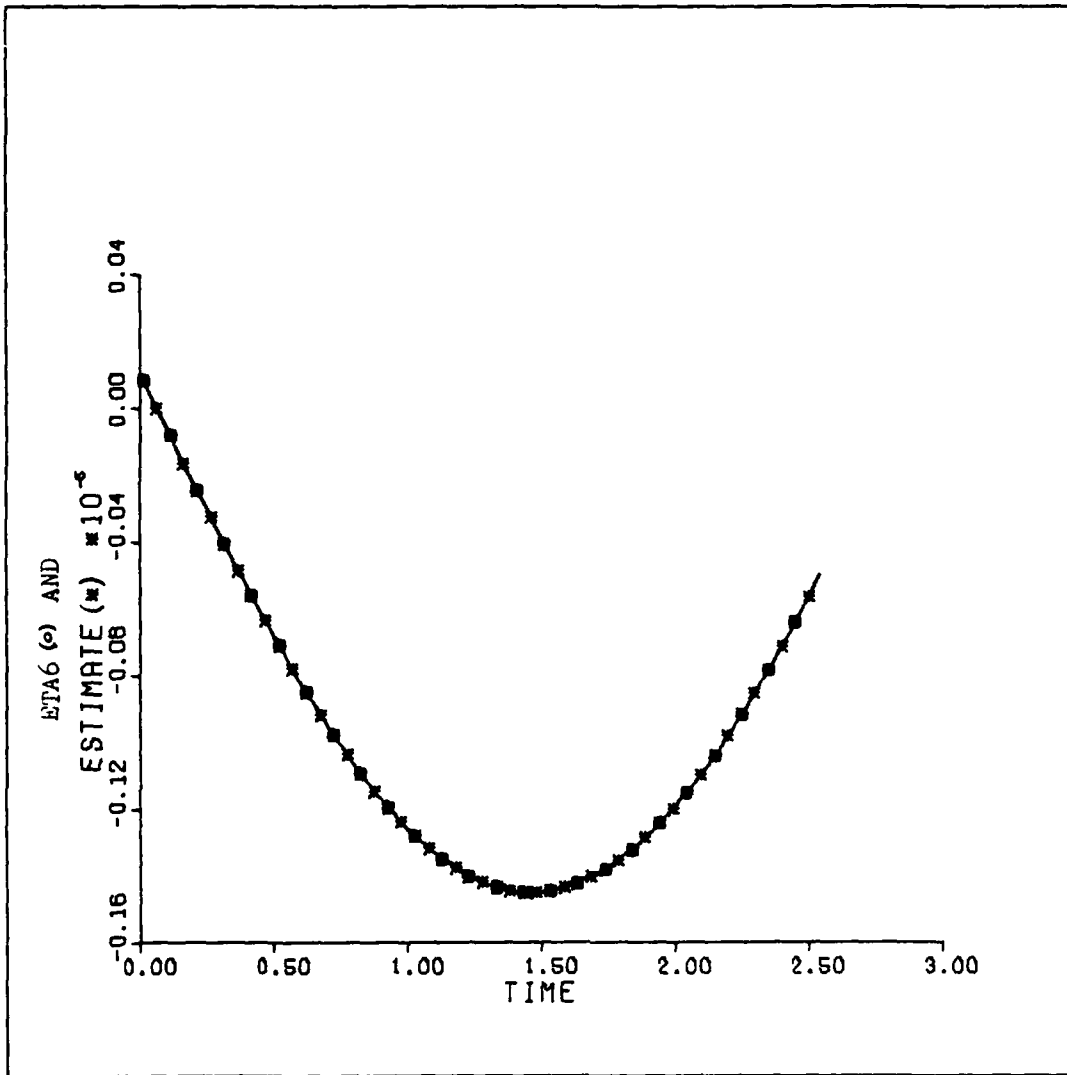


Figure 8f. Sixth State

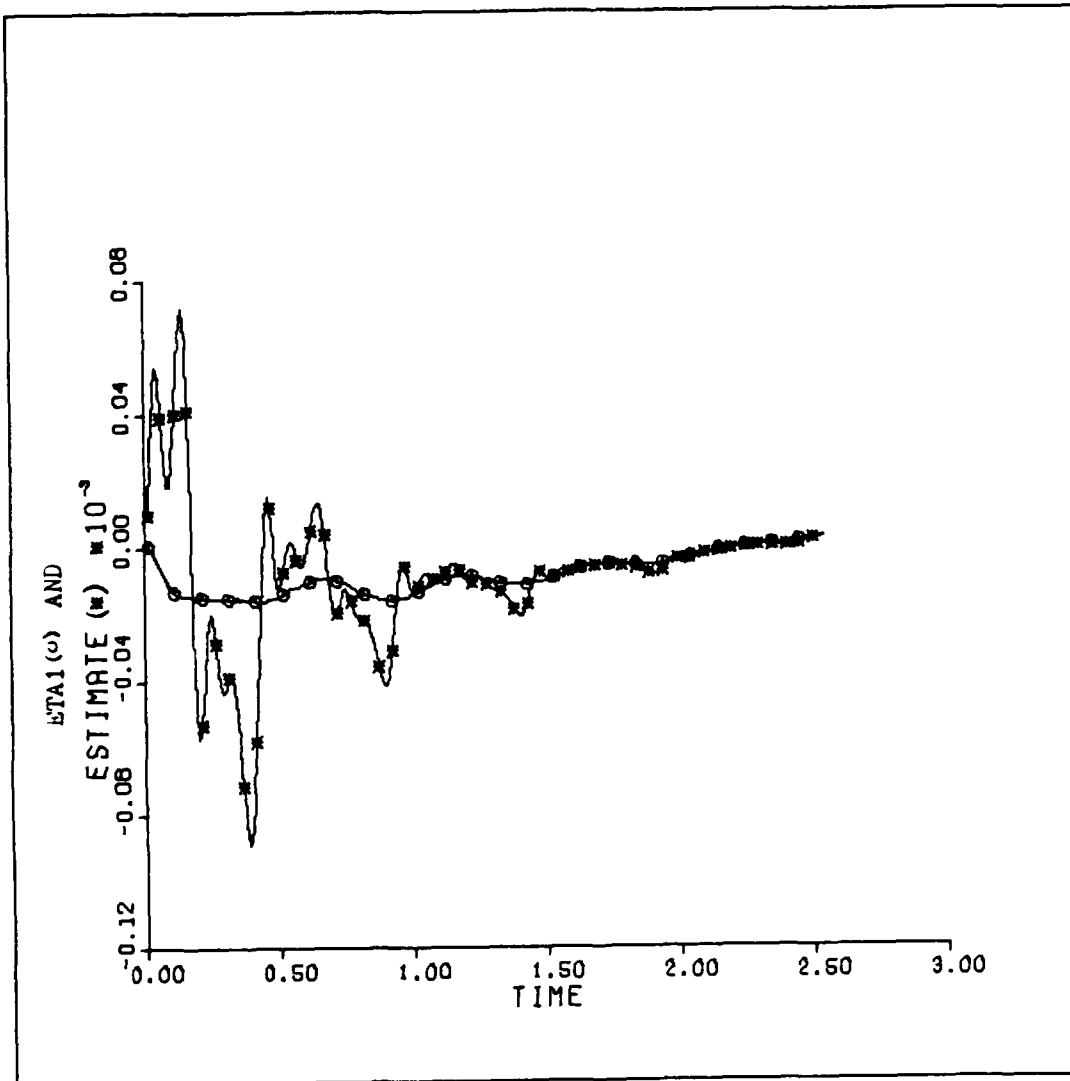


Figure 9a, Modal Vector vs. Time: Case C

Controller gain	0.5	Observer initial conditions
Orbit initial conditions		$e_{m1} = 14.96$ m
$x = 14.96$ km		$e_{m2} = 14.96$ m/sec
$P_x = 14.96$ km/sec		$e_{m3} = 14959.97$ km
$y = 14.96$ km		$e_{m4} = 14959.97$ km/sec
$P_y = 14.96$ km/sec		$e_{m5} = 14959.97$ km
$z = 14.96$ km		$e_{m6} = 14959.97$ km/sec
$P_z = 14.96$ km/sec		

Five orbits

Observer gain elements
 $K'_{12} = 3.0$
 $K'_{31} = 1500.0$

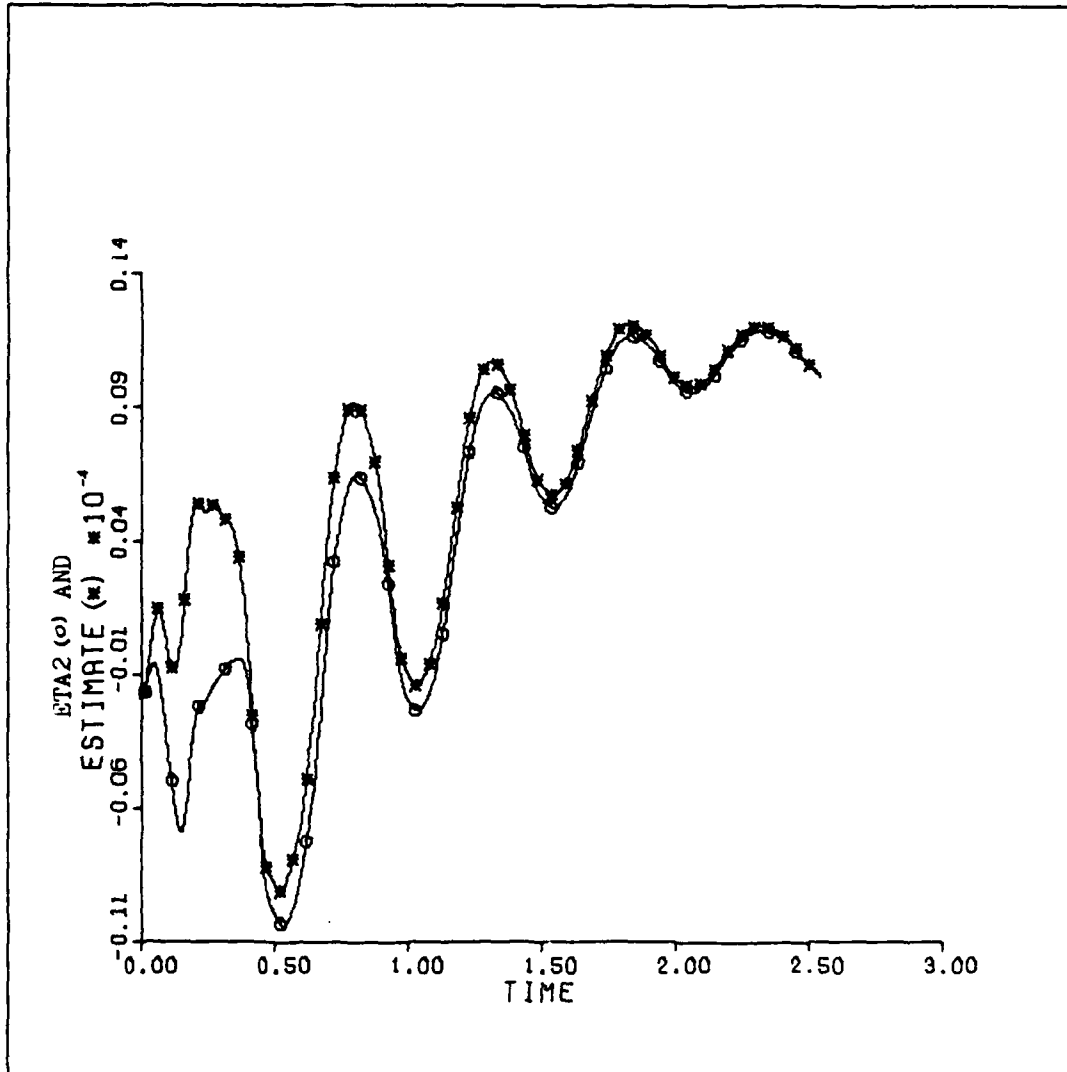


Figure 9b. Second State

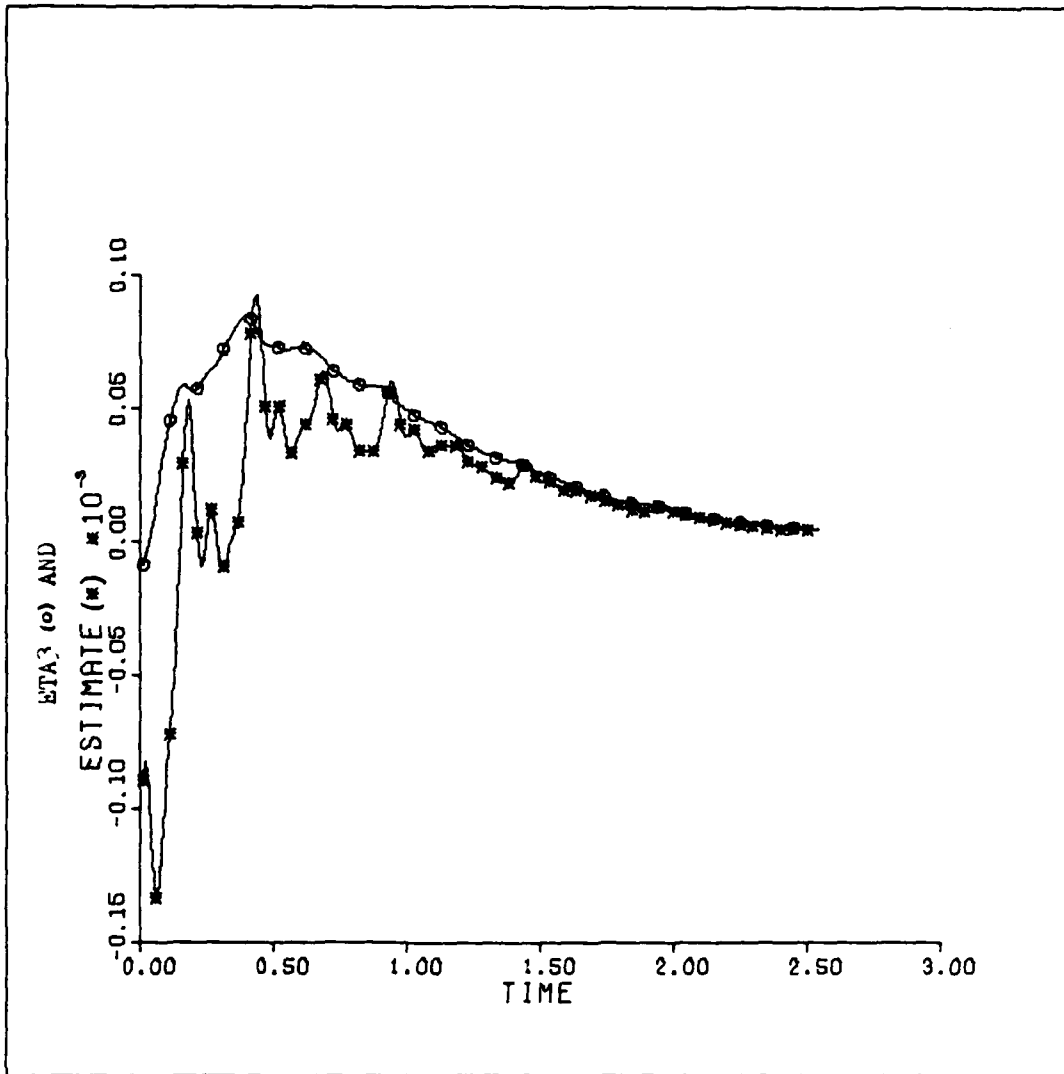


Figure 9c. Third State

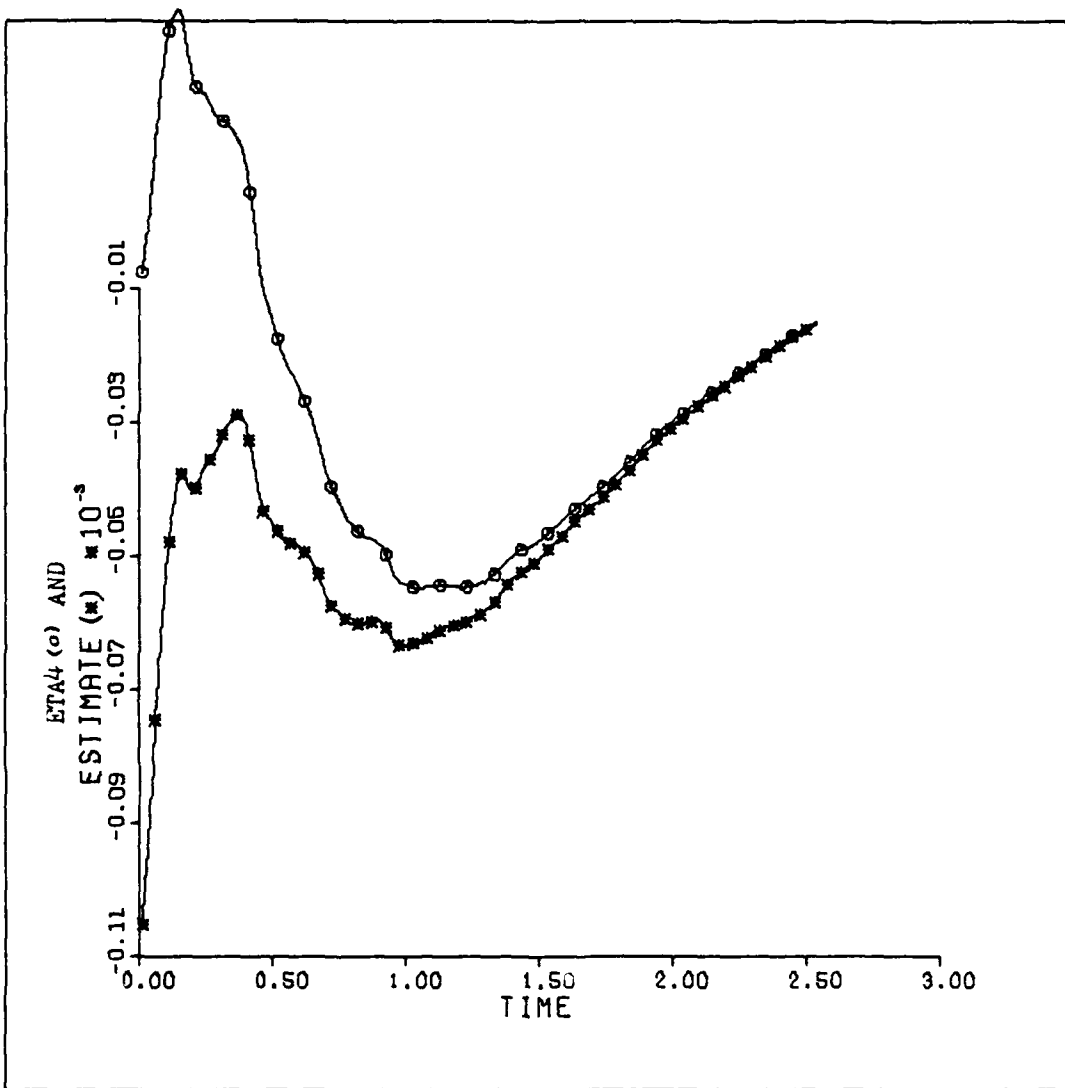


Figure 9d. Fourth State

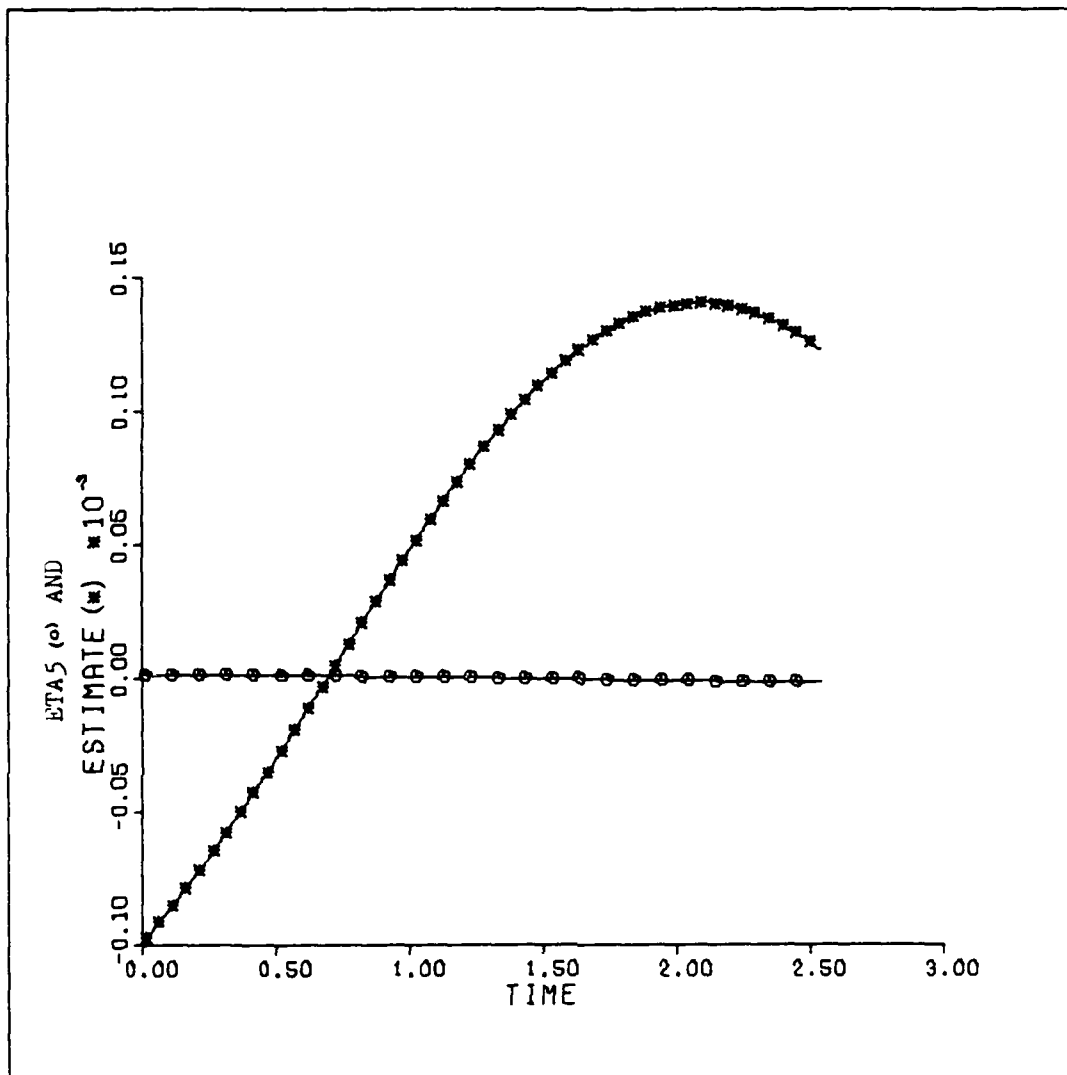


Figure 9e. Fifth State

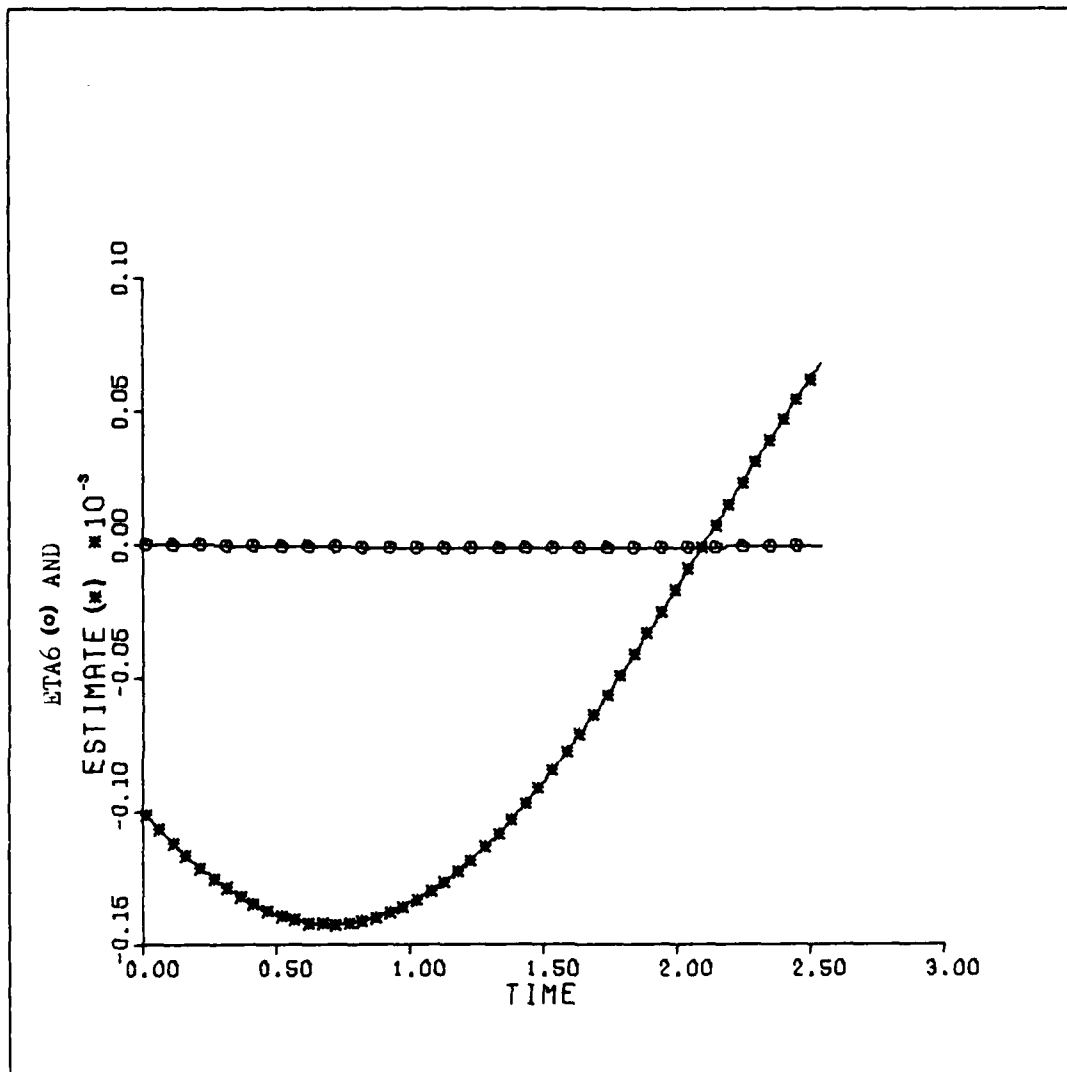


Figure 9f. Sixth State

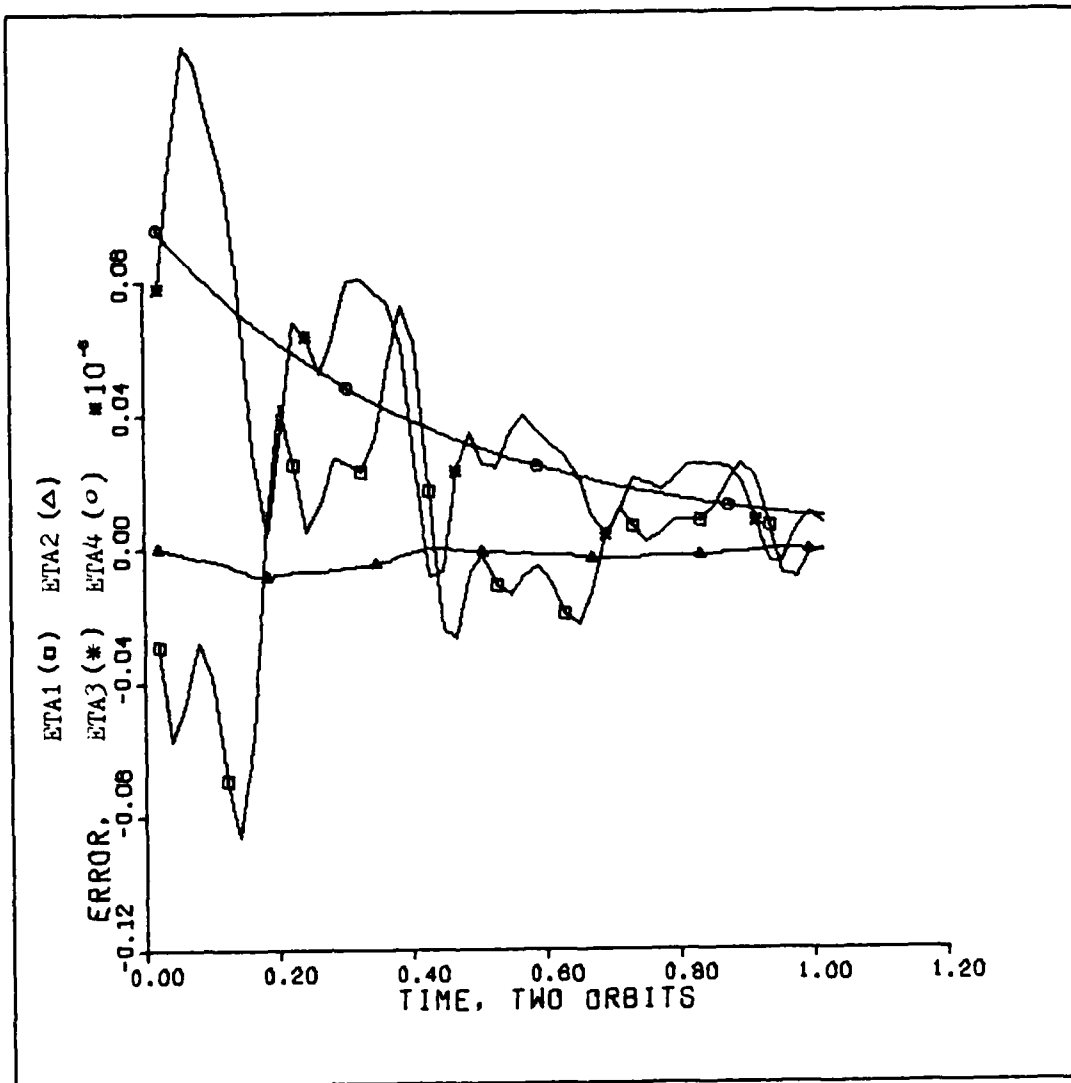


Figure 10. Error vs. Time: Case A

Controller gain 0.5
 Orbit initial conditions
 $x = 4488$ km
 $P_x = 4488$ km/sec
 $y = 4488$ km
 $P_y = 4488$ km/sec
 $z = 0.0$ km
 $P_z = 0.0$ km/sec

Observer initial conditions
 $e_{m1} = 14.96$ m
 $e_{m2} = 14.96$ m/sec
 $e_{m3} = 14.96$ km
 $e_{m4} = 14.96$ km/sec
 $e_{m5} = 0.0$ km
 $e_{m6} = 0.0$ km/sec

Two orbits

Observer gain elements
 $K'_{12} = 3.0$
 $K'_{31} = 1500.0$

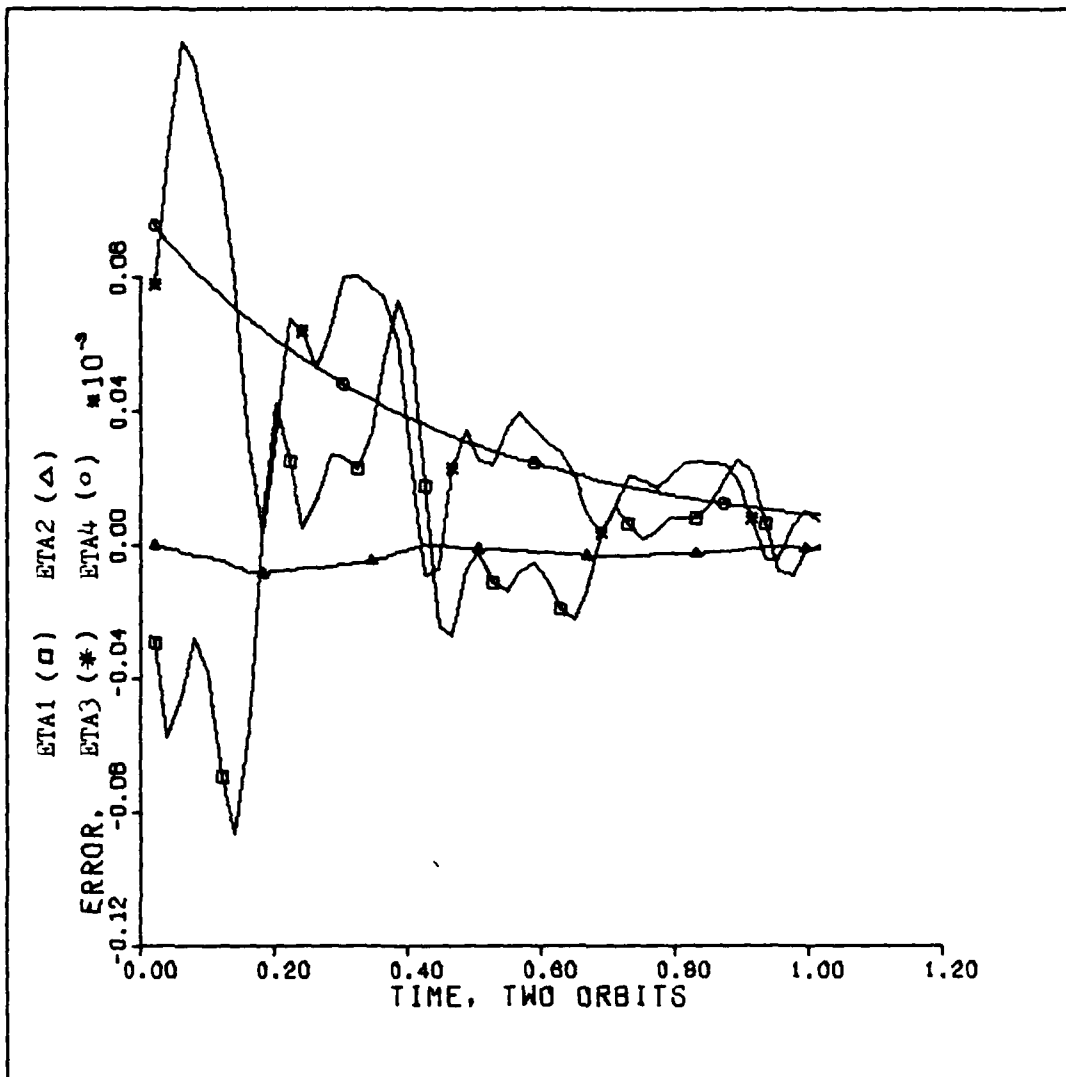


Figure 11. Error vs. Time: Case B

Controller gain 0.5
 Orbit initial conditions
 $x = 14.96$ km
 $P_x = 14.96$ km/sec
 $y = 14.96$ km
 $P_y = 14.96$ km/sec
 $z = 0.0$ km
 $P_z = 0.0$ km/sec

Observer initial conditions
 $e_{m1} = 14.96$ m
 $e_{m2} = 14.96$ m/sec
 $e_{m3} = 14959.97$ km
 $e_{m4} = 14959.97$ km/sec
 $e_{m5} = 0.0$ km
 $e_{m6} = 0.0$ km/sec

Two orbits

Observer gain elements
 $K'_{12} = 3.0$
 $K'_{31} = 1500.0$

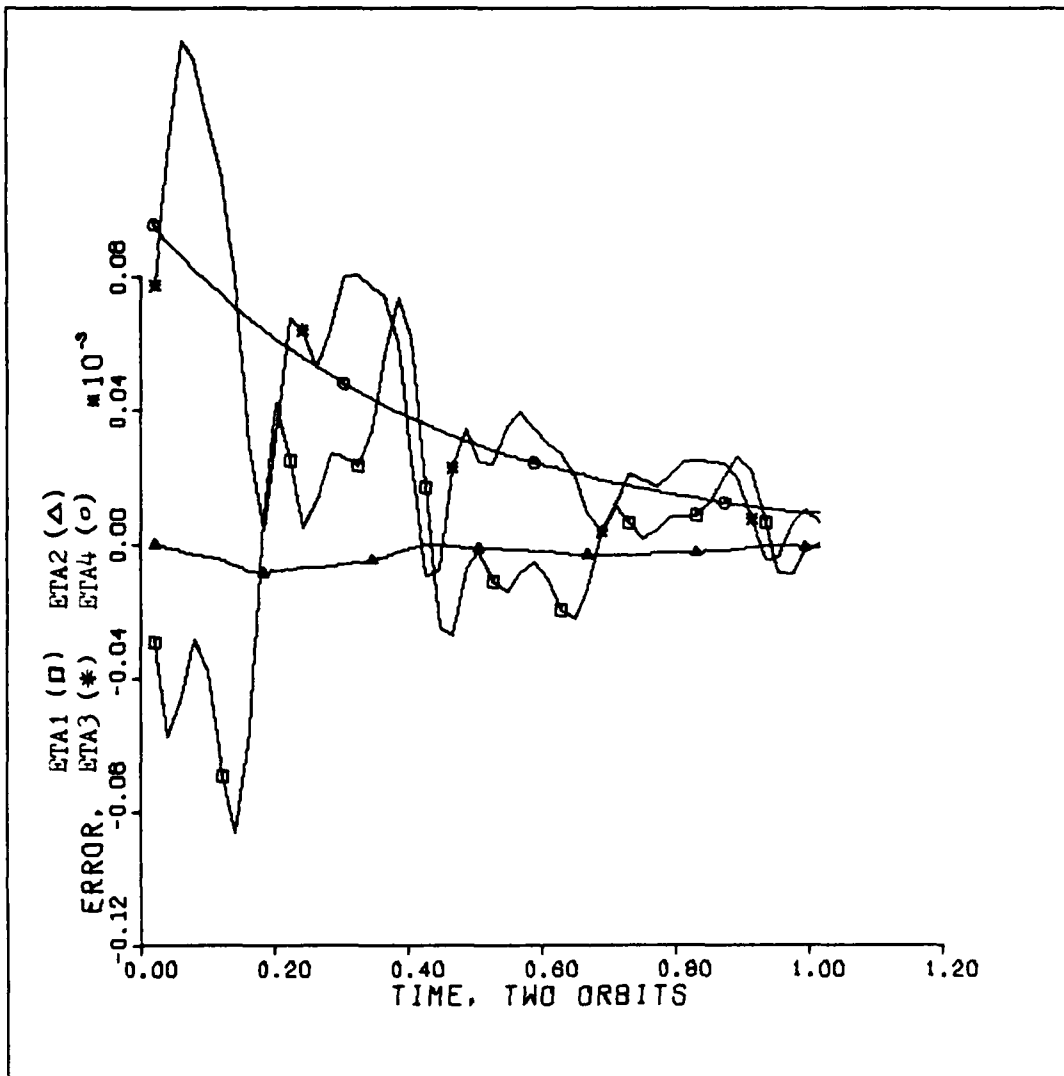


Figure 12. Error vs. Time: Case C

Controller gain 0.5
 Orbit initial conditions
 $x = 14.96 \text{ km}$
 $P_x = 14.96 \text{ km/sec}$
 $y = 14.96 \text{ km}$
 $P_y = 14.96 \text{ km/sec}$
 $z = 14.96 \text{ km}$
 $P_z = 14.96 \text{ km/sec}$

Observer initial conditions
 $e_{m1} = 14.96 \text{ m}$
 $e_{m2} = 14.96 \text{ m/sec}$
 $e_{m3} = 14959.97 \text{ km}$
 $e_{m4} = 14959.97 \text{ km/sec}$
 $e_{m5} = 14959.97 \text{ km}$
 $e_{m6} = 14959.97 \text{ km/sec}$

Two orbits

Observer gain elements
 $K'_{12} = 3.0$
 $K'_{31} = 1500.0$

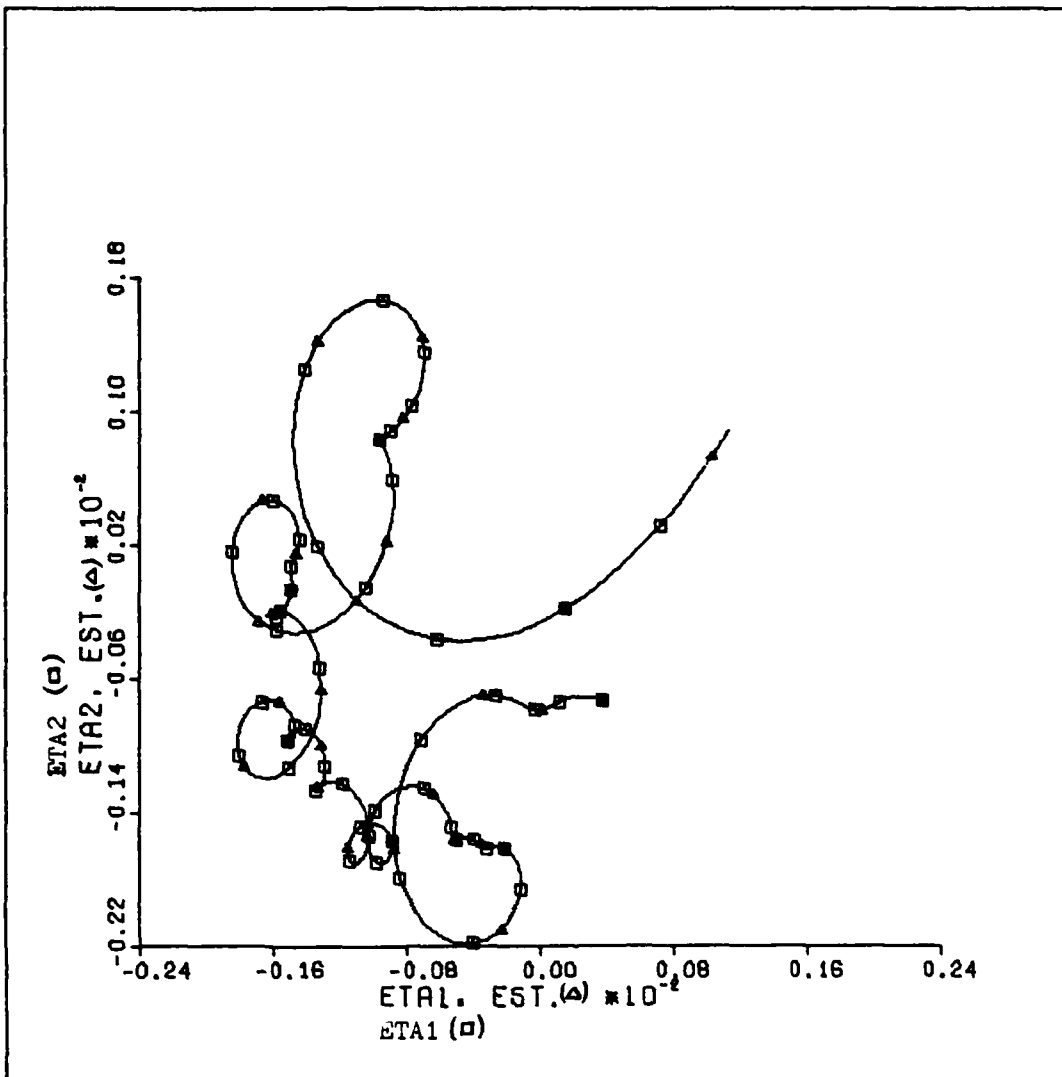


Figure 13a. Phase Portraits: Case A

Controller gain 0.5
 Orbit initial conditions
 $x = 4488$ km
 $P_x = 4488$ km/sec
 $y = 4488$ km
 $P_y = 4488$ km/sec
 $z = 0.0$ km
 $P_z = 0.0$ km/sec

Observer initial conditions
 $e_{m1} = 14.96$ m
 $e_{m2} = 14.96$ m/sec
 $e_{m3} = 14.96$ km
 $e_{m4} = 14.96$ km/sec
 $e_{m5} = 0.0$ km
 $e_{m6} = 0.0$ km/sec

Five orbits

Observer gain elements

$K'_{12} = 3.0$
 $K'_{31} = 1500.0$

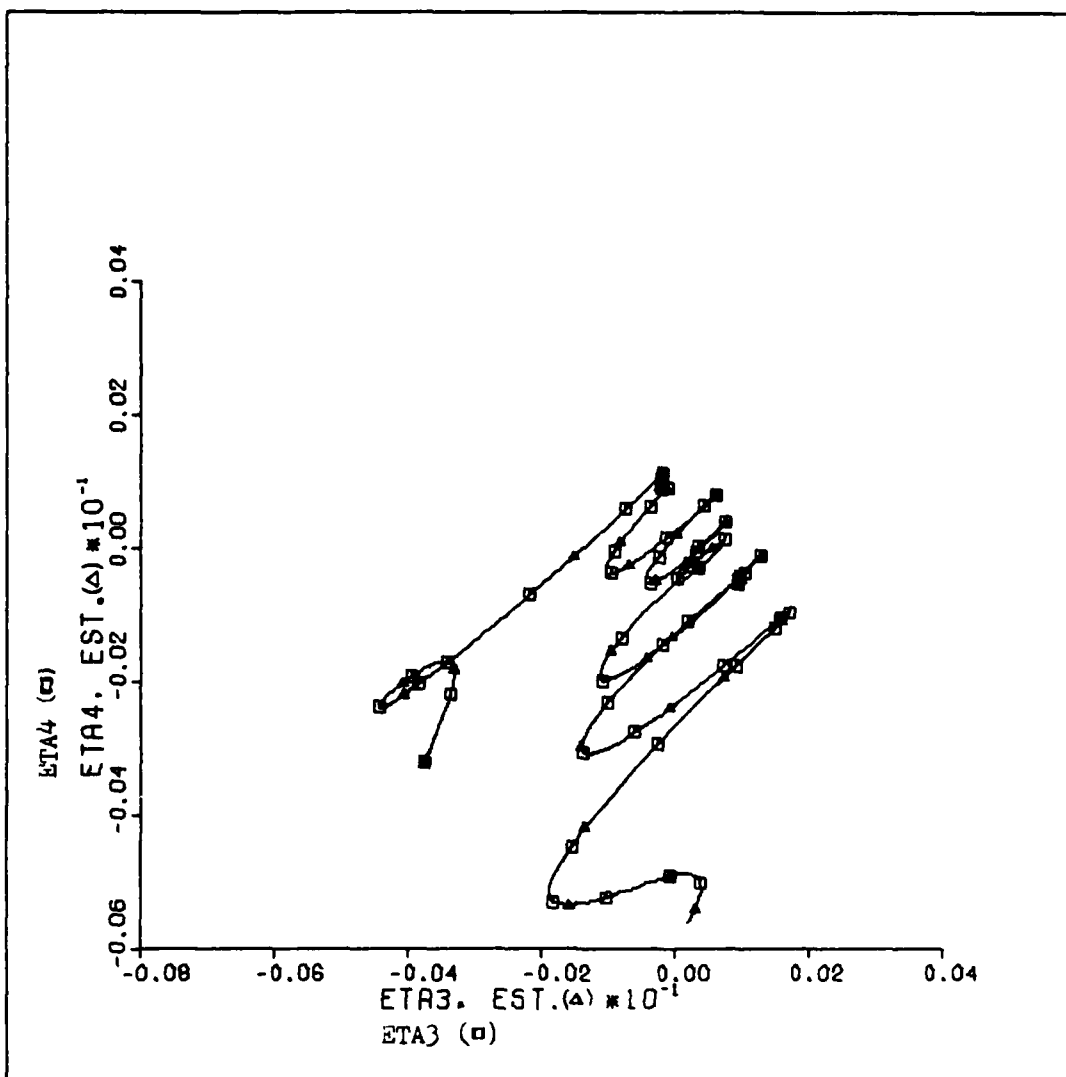


Figure 13b. Third and Fourth States

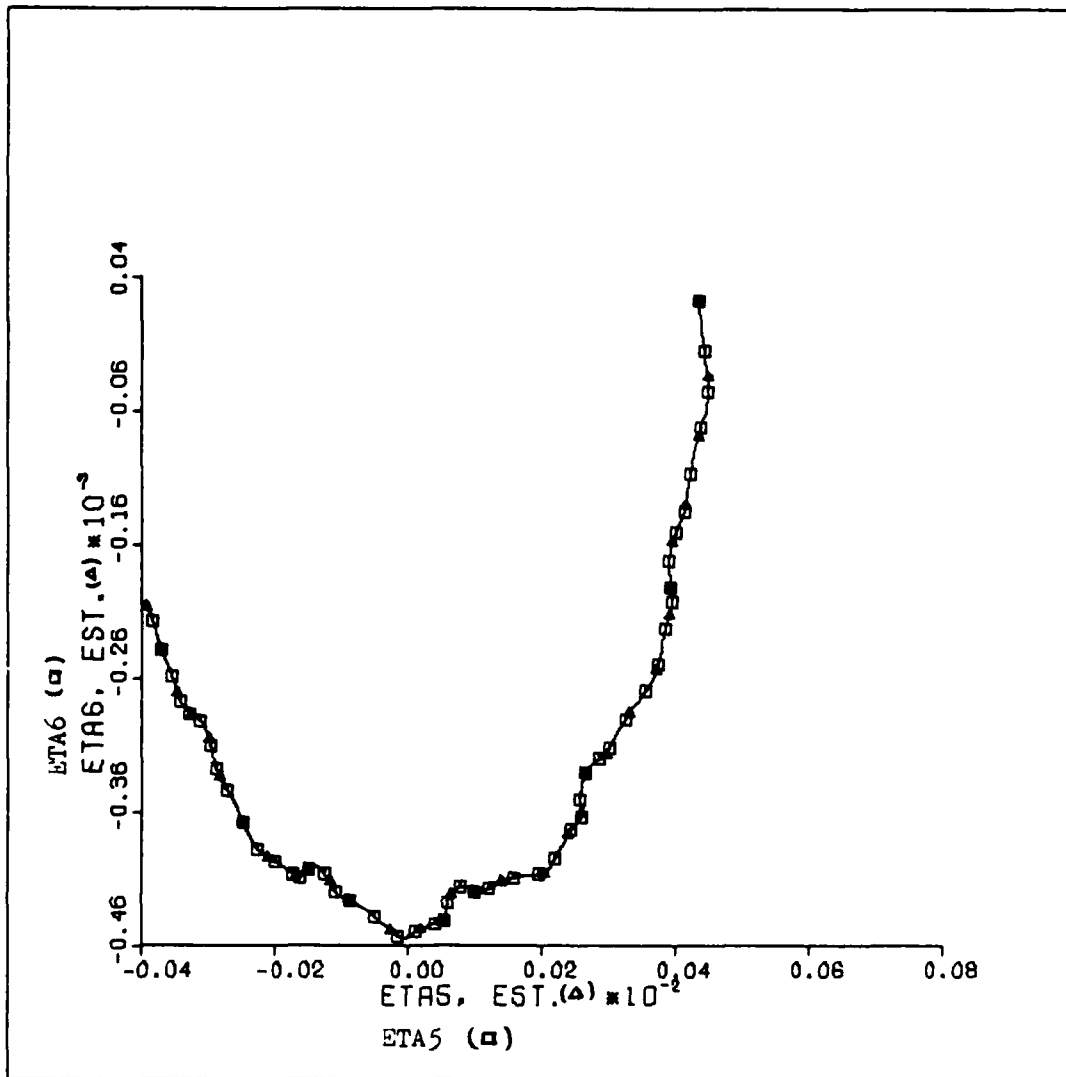


Figure 13c. Fifth and Sixth States

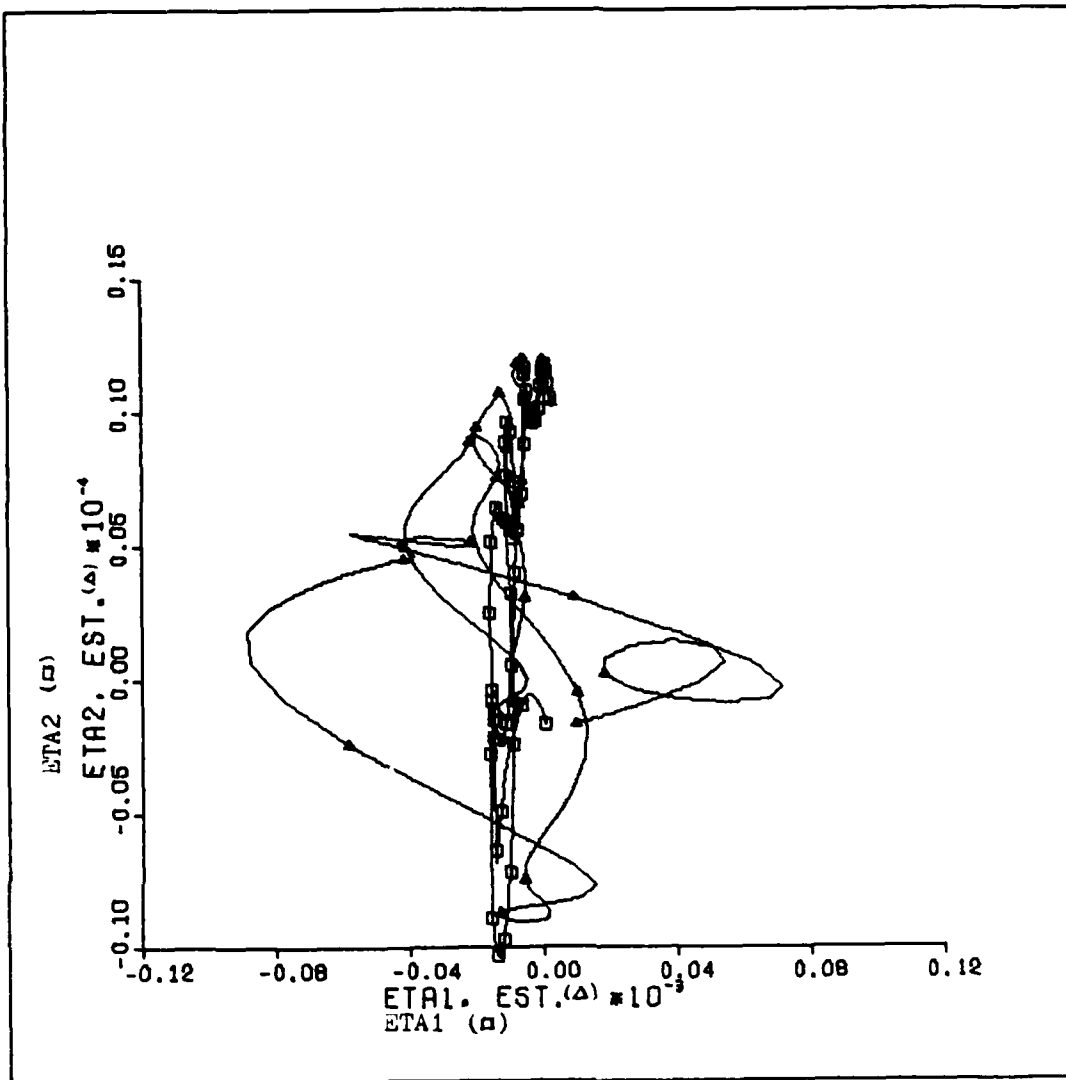


Figure 14a. Phase Portraits: Case B

Controller gain 0.5

Orbit initial conditions

x = 14.96 km
 $P_x = 14.96$ km/sec
 y = 14.96 km
 $P_y = 14.96$ km/sec
 z = 0.0 km
 $P_z = 0.0$ km/sec

Observer initial conditions

$e_{m1} = 14.96$ m
 $e_{m2} = 14.96$ m/sec
 $e_{m3} = 14959.97$ km
 $e_{m4} = 14959.97$ km/sec
 $e_{m5} = 0.0$ km
 $e_{m6} = 0.0$ km/sec

Five orbits

Observer gain elements

$K'_{12} = 3.0$
 $K'_{31} = 1500.0$

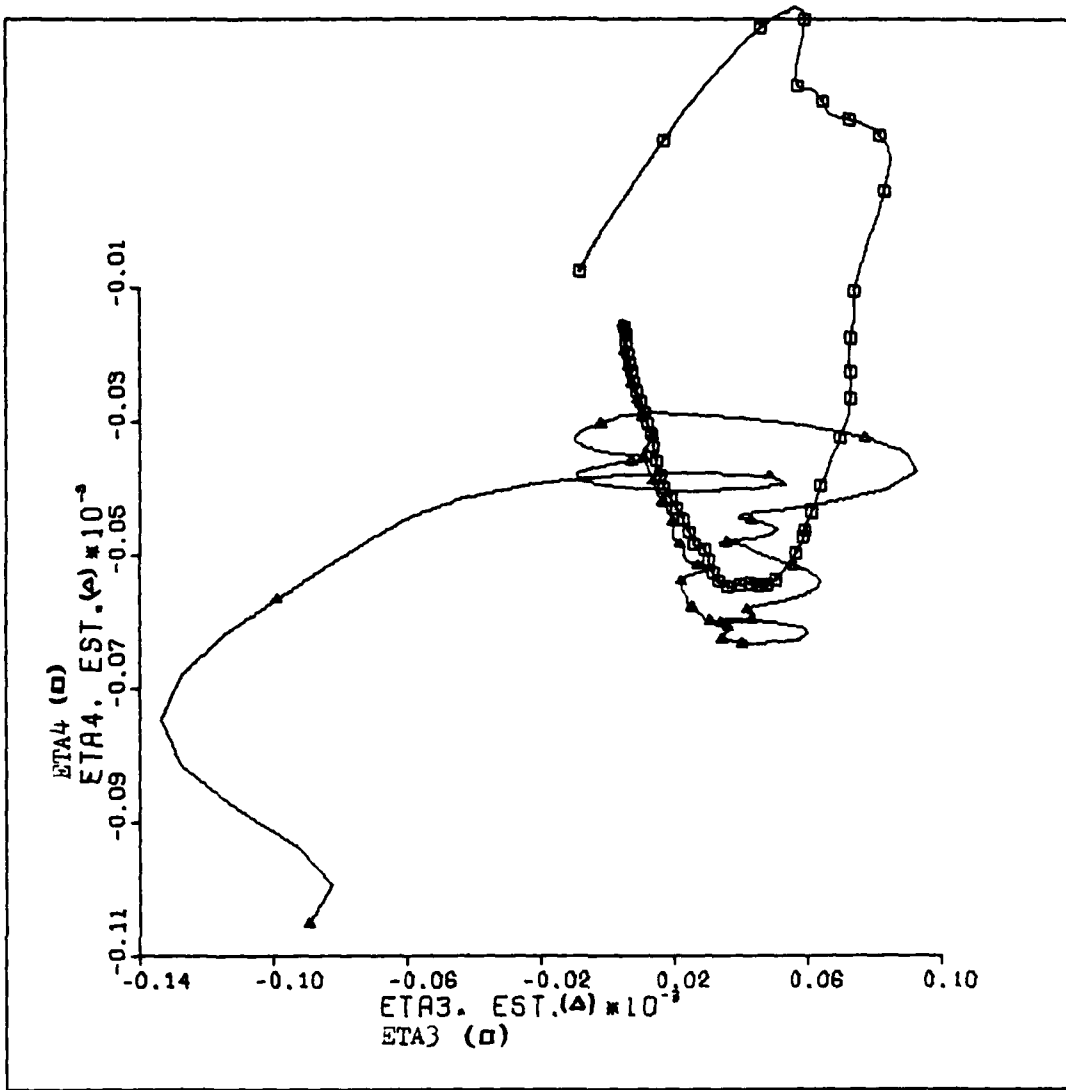


Figure 14b. Third and Fourth States

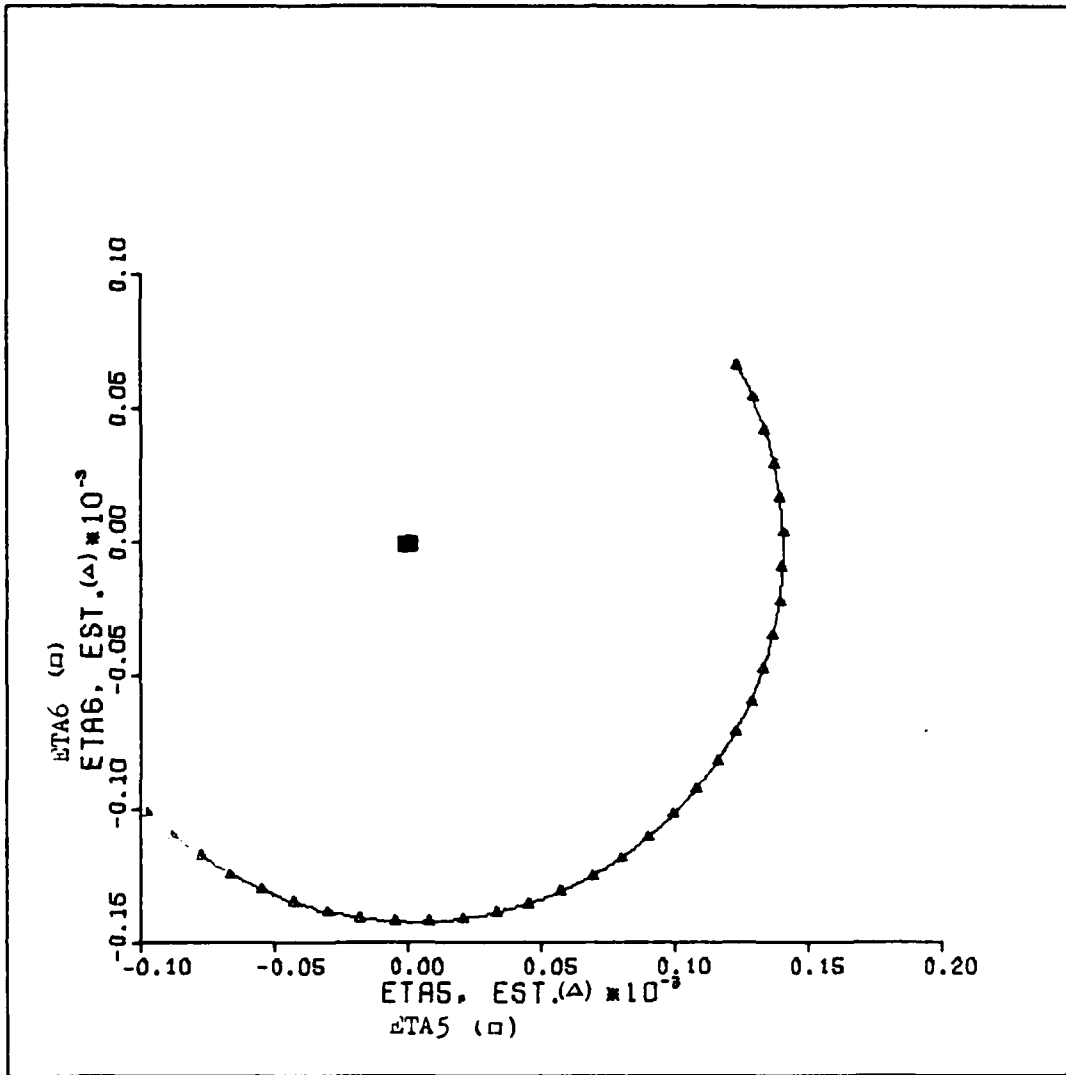


Figure 14c. Fifth and Sixth States

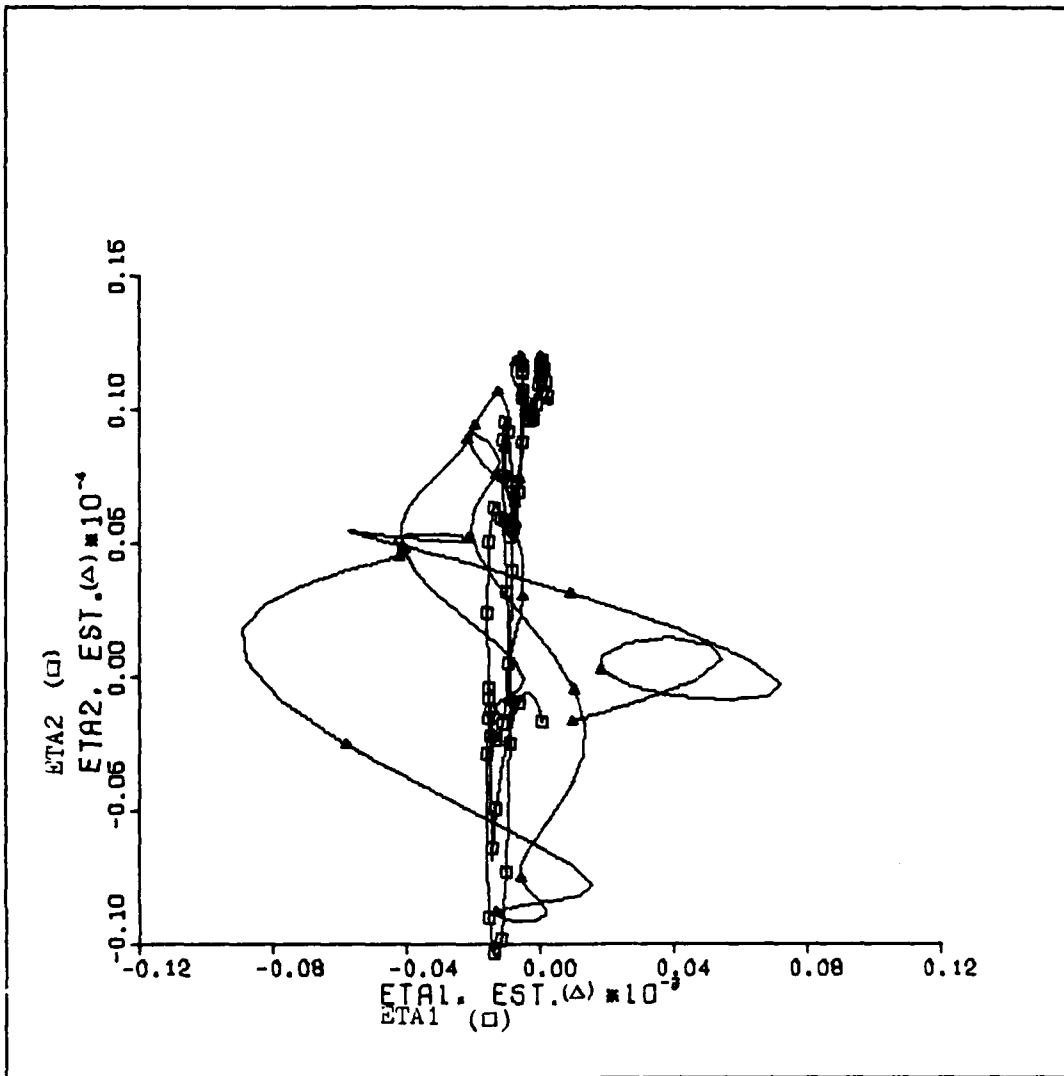


Figure 15a. Phase Portraits: Case C

Controller gain 0.5

Orbit initial conditions

x = 14.96 km
 $P_x = 14.96$ km/sec
 y = 14.96 km
 $P_y = 14.96$ km/sec
 z = 14.96 km
 $P_z = 14.96$ km/sec

Observer initial conditions

$e_{m1} = 14.96$ m
 $e_{m2} = 14.96$ m/sec
 $e_{m3} = 14959.97$ km
 $e_{m4} = 14959.97$ km/sec
 $e_{m5} = 14959.97$ km
 $e_{m6} = 14959.97$ km/sec

Observer gain elements

$K'_{12} = 3.0$
 $K'_{31} = 1500.0$

Five orbits

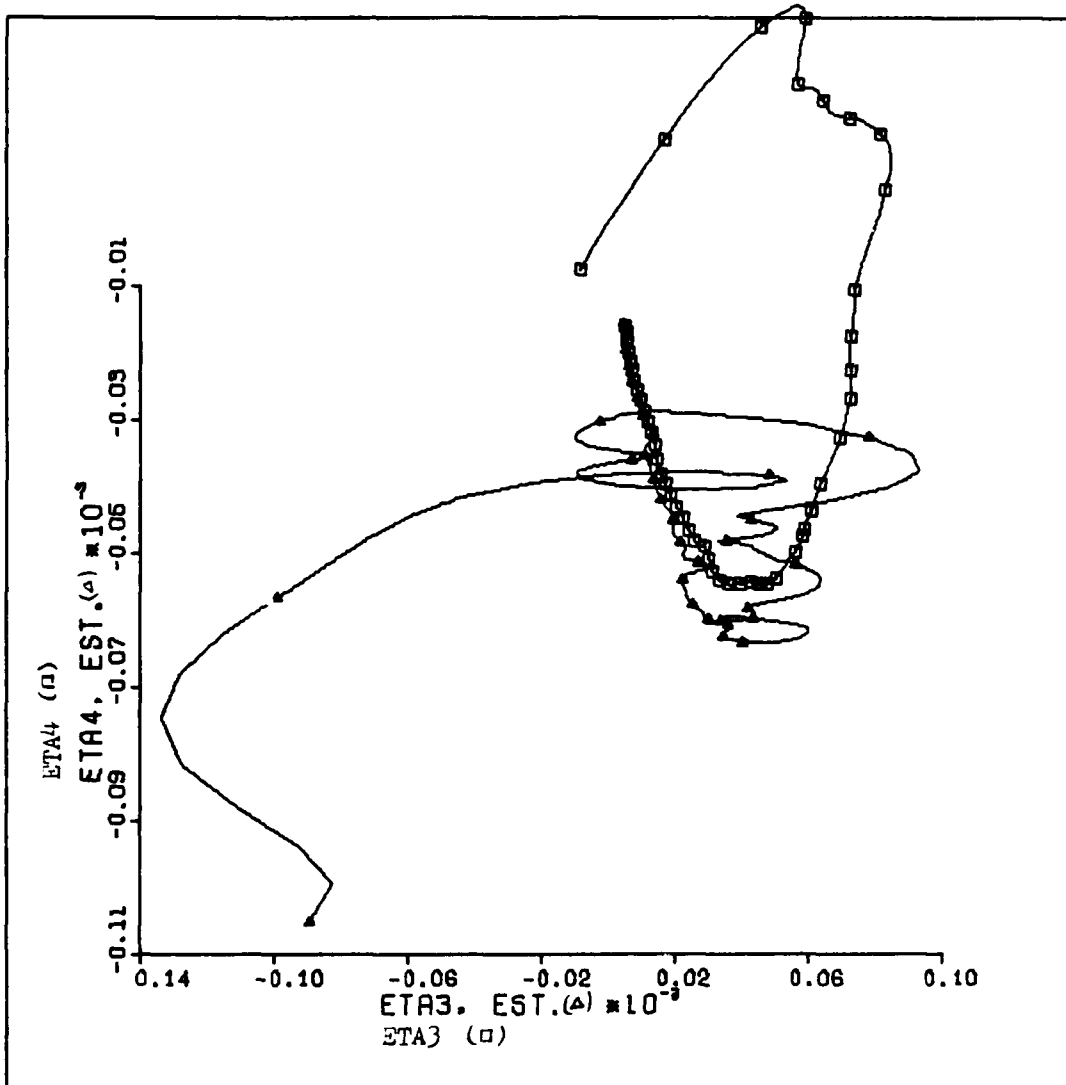


Figure 15b. Third and Fourth States

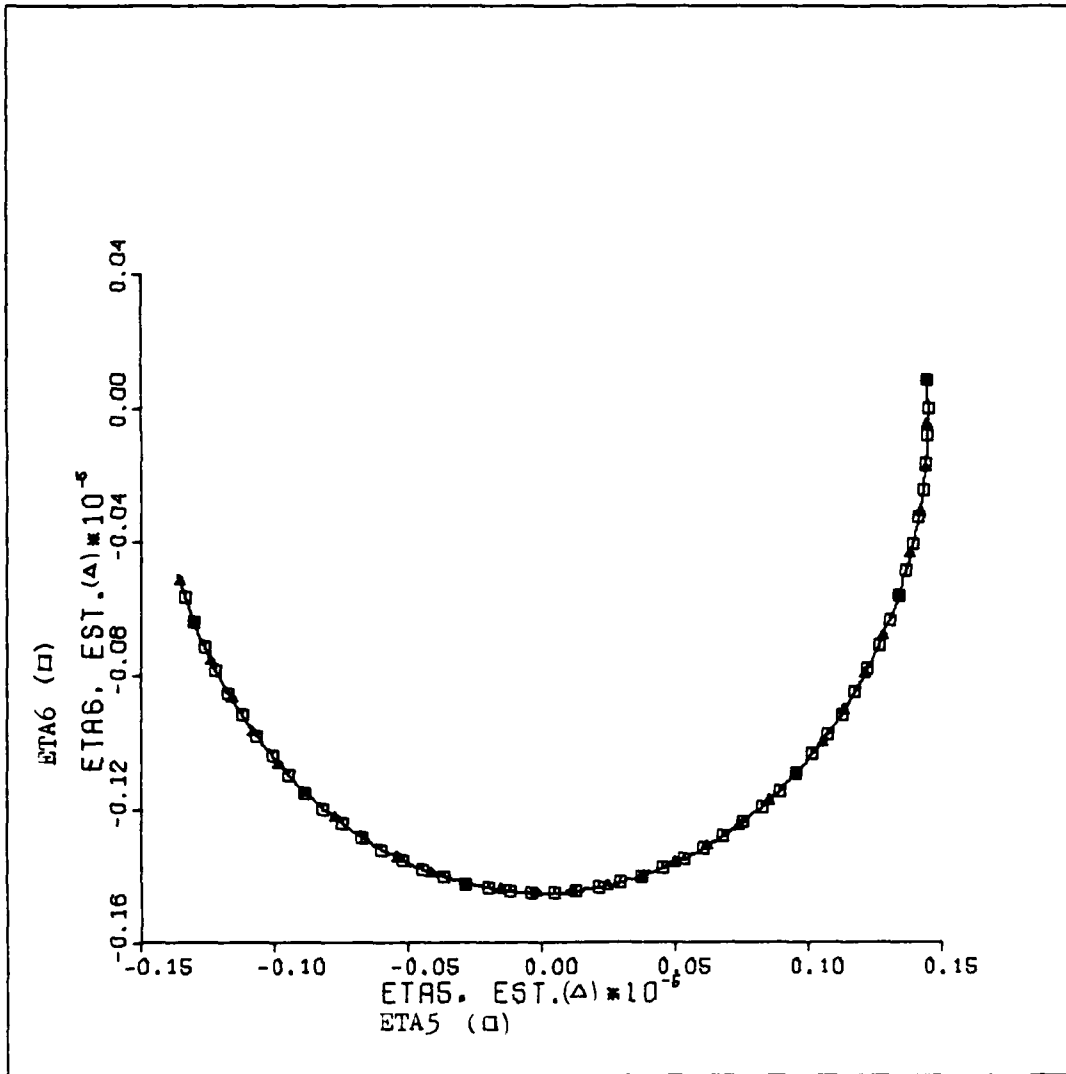


Figure 15c. Fifth and Sixth States

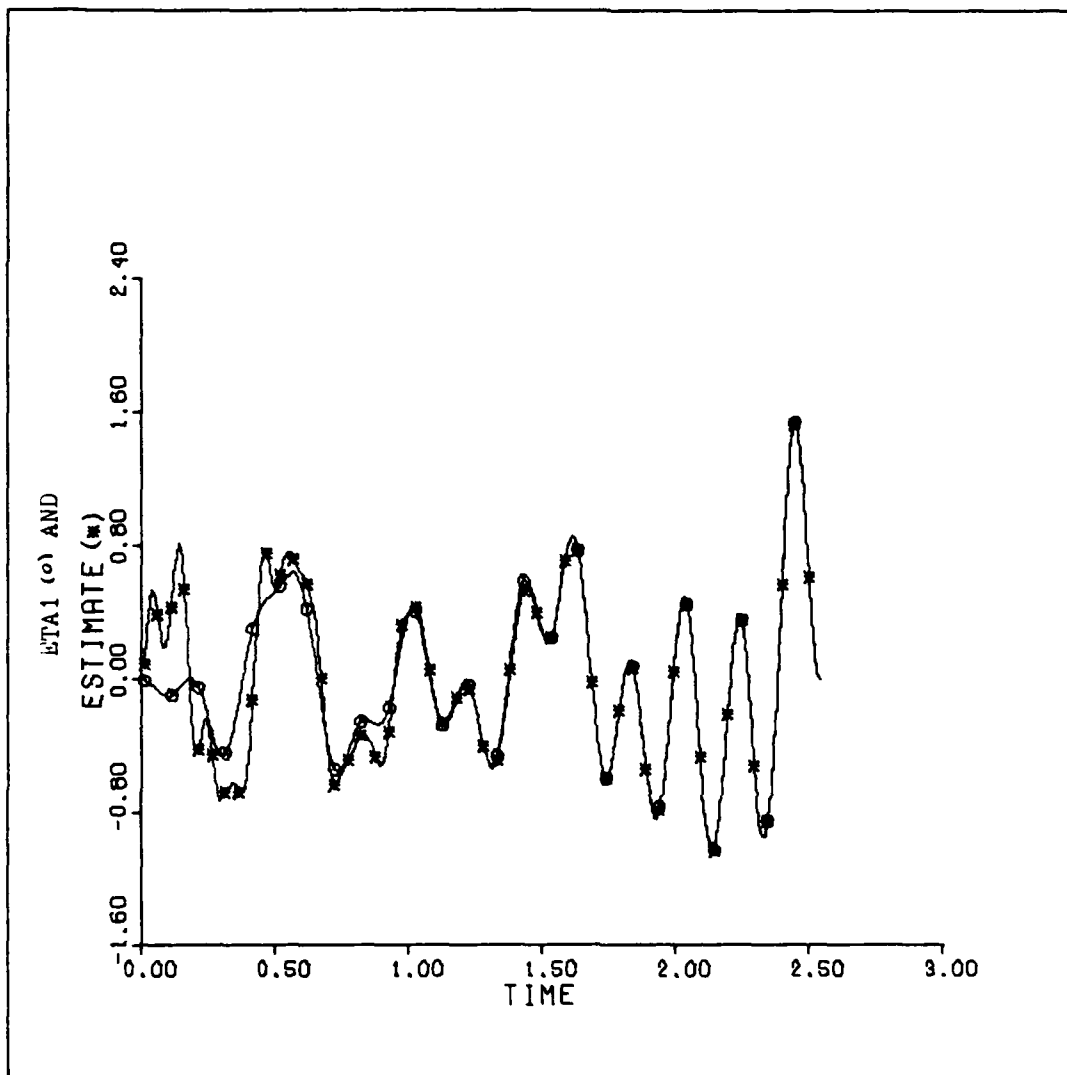


Figure 16a. Effect of Large Observer Initial Conditions

Controller gain 0.5
 Orbit initial conditions
 $x = 4488$ km
 $P_x = 4488$ km/sec
 $y = 4488$ km
 $P_y = 4488$ km/sec
 $z = 0.0$ km
 $P_z = 0.0$ km/sec

Observer initial conditions
 $e_{m1} = 14.96$ m
 $e_{m2} = 14.96$ m/sec
 $e_{m3} = 1.496 \times 10^3$ km
 $e_{m4} = 1.496 \times 10^3$ km/sec
 $e_{m5} = 0.0$ km
 $e_{m6} = 0.0$ km/sec

five orbits

Observer gain elements
 $K'_{12} = 3.0$
 $K'_{31} = 1500.0$

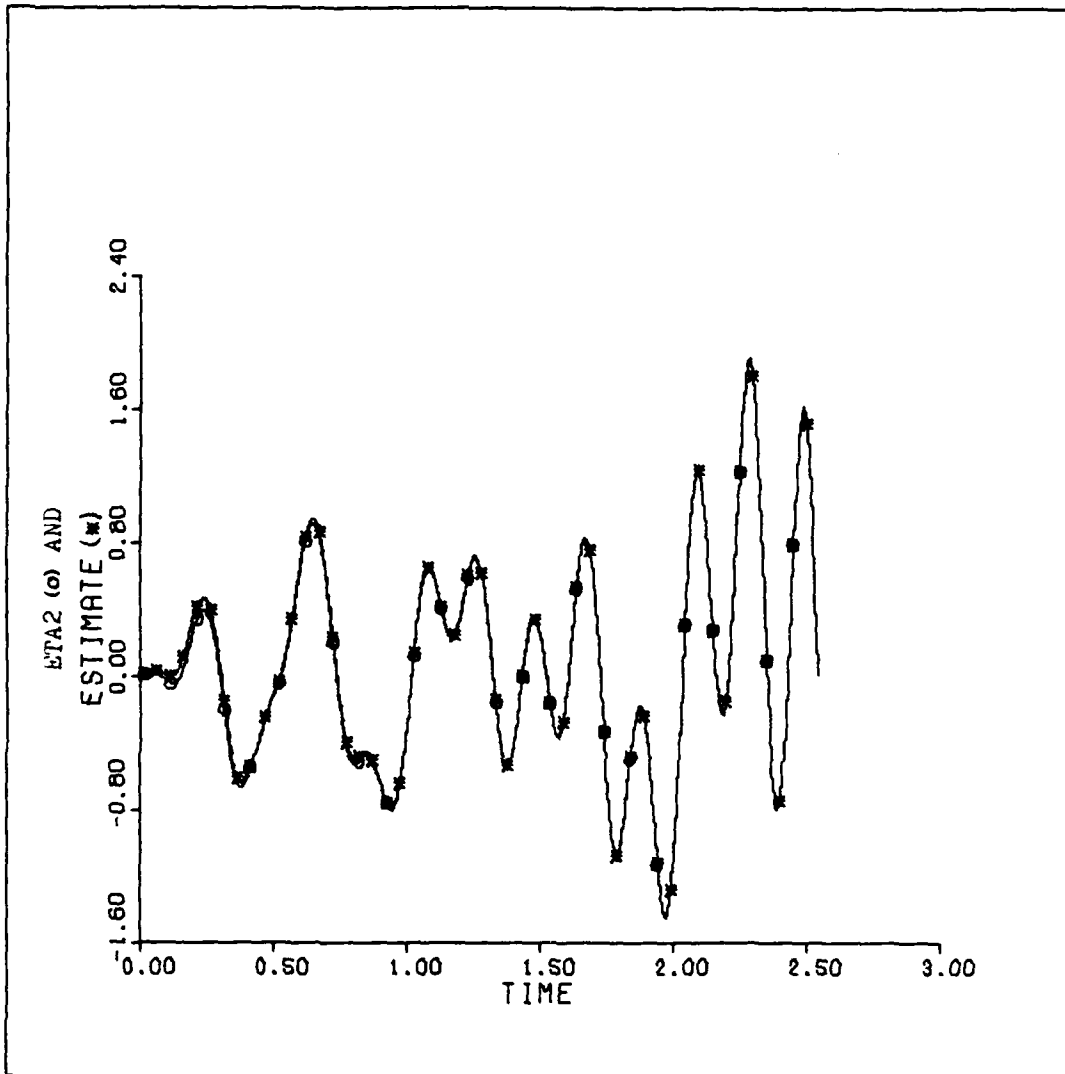


Figure 16b. Second State

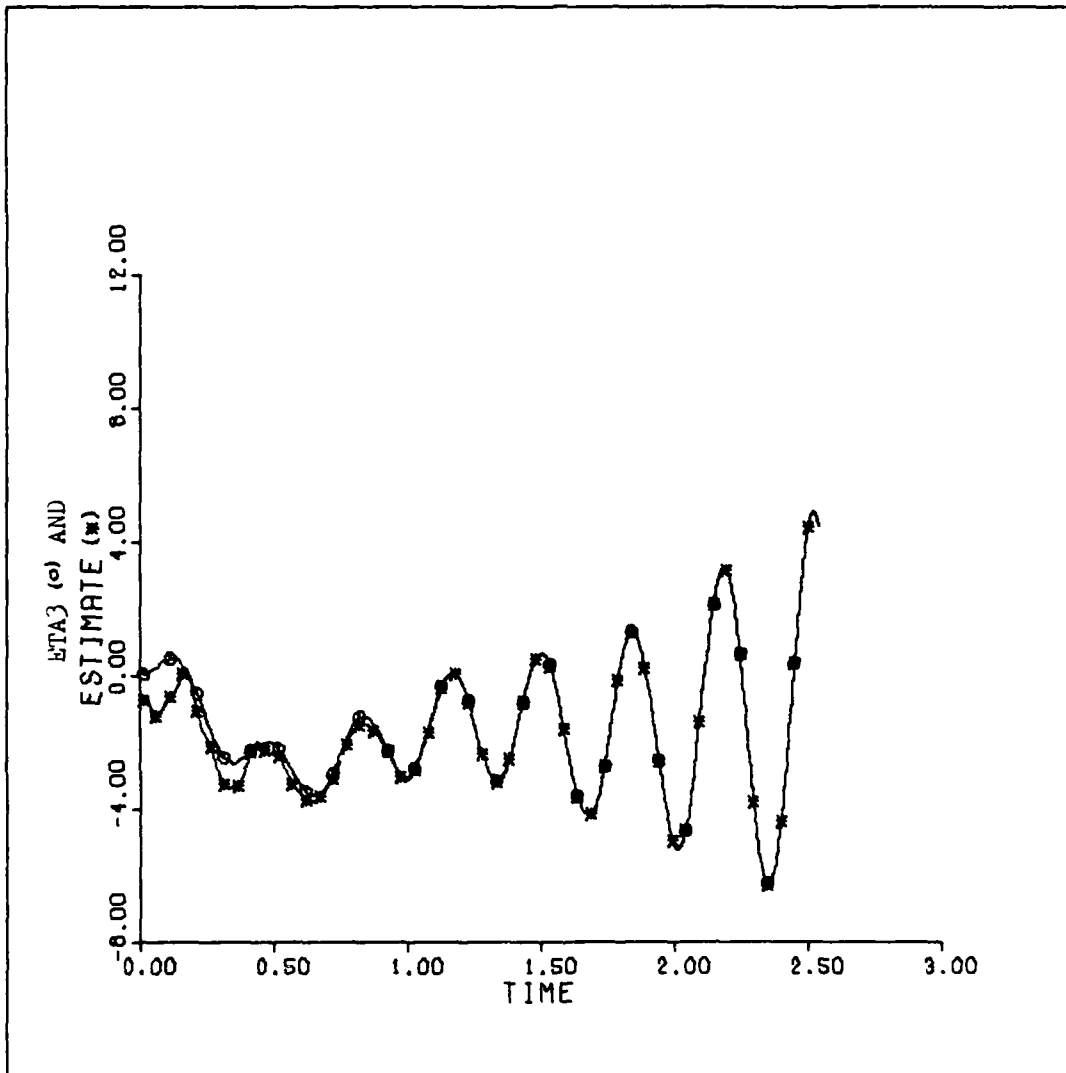


Figure 16c. Third State

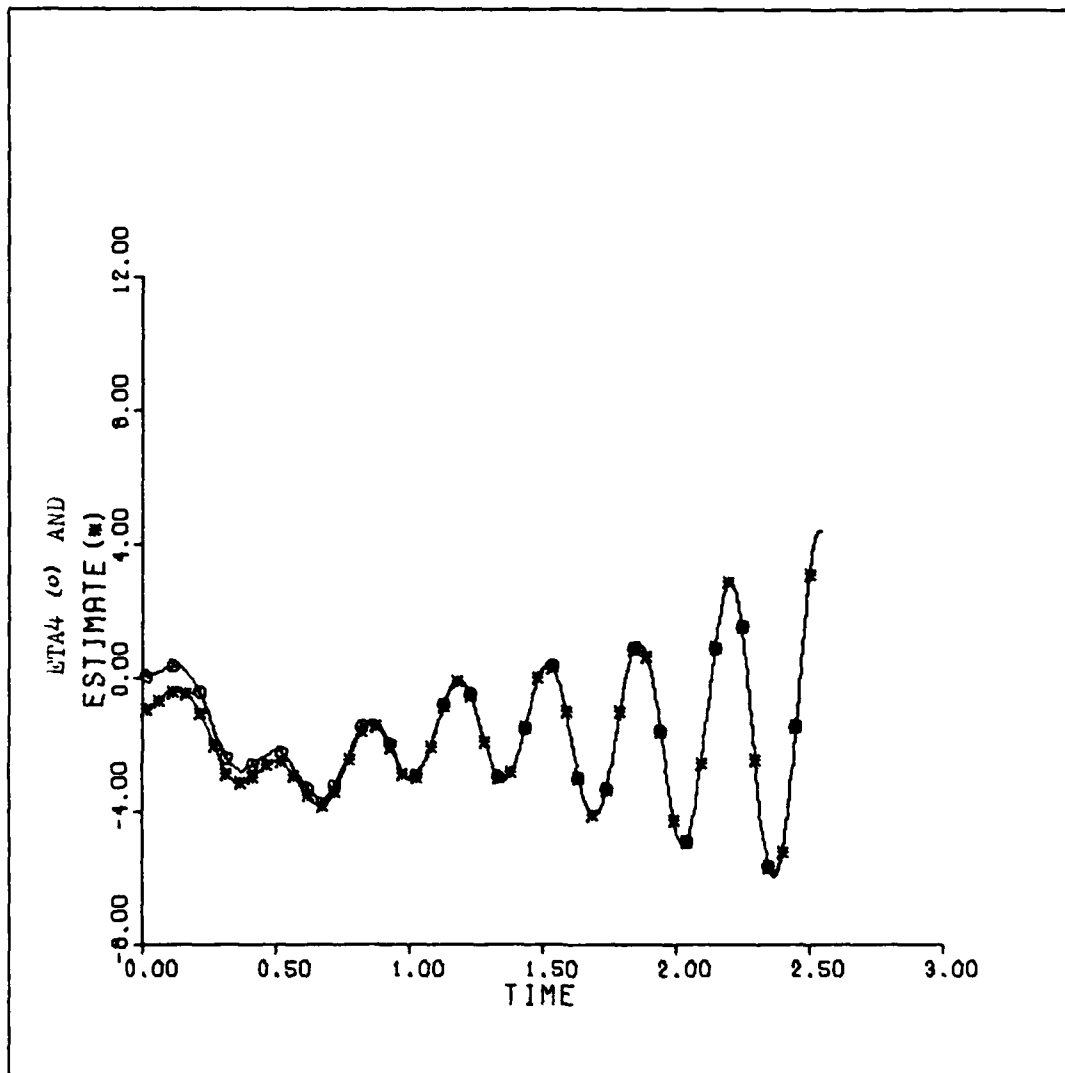


Figure 16d. Fourth State

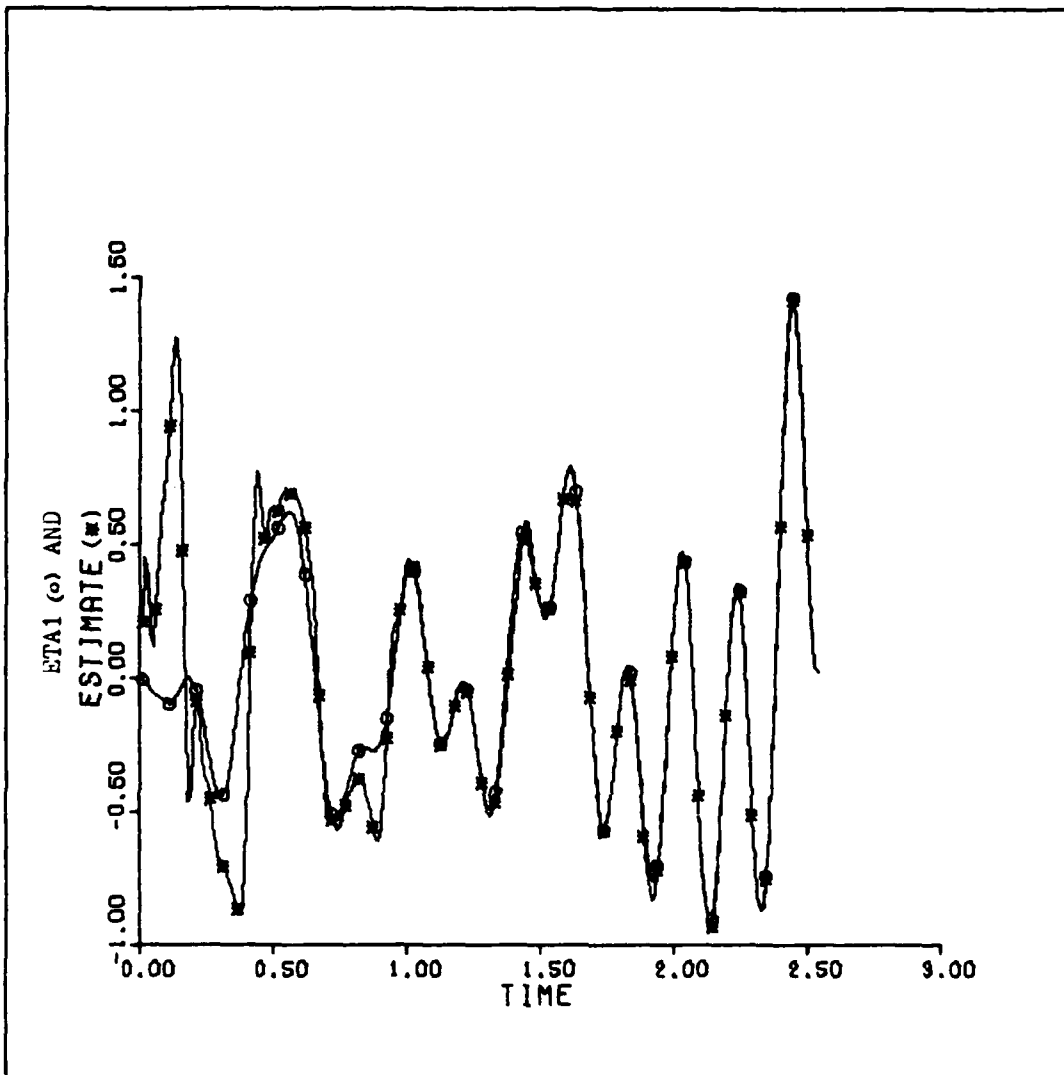


Figure 17a. Case of Figure 16. with Alternate Observer Gain Matrix

Controller gain 0.5
 Orbit initial conditions
 $x = 4488$ km
 $P_x = 4488$ km/sec
 $y = 4488$ km
 $P_y = 4488$ km/sec
 $z = 0.0$ km
 $P_z = 0.0$ km/sec

Observer initial conditions
 $e_{m1} = 14.96$ m
 $e_{m2} = 14.96$ m/sec
 $e_{m3} = 1.496 \times 10^8$ km
 $e_{m4} = 1.496 \times 10^8$ km/sec
 $e_{m5} = 0.0$ km
 $e_{m6} = 0.0$ km/sec

Five orbits

Observer gain elements
 $K'_{12} = 3.0$
 $K'_{31} = 4000.0$

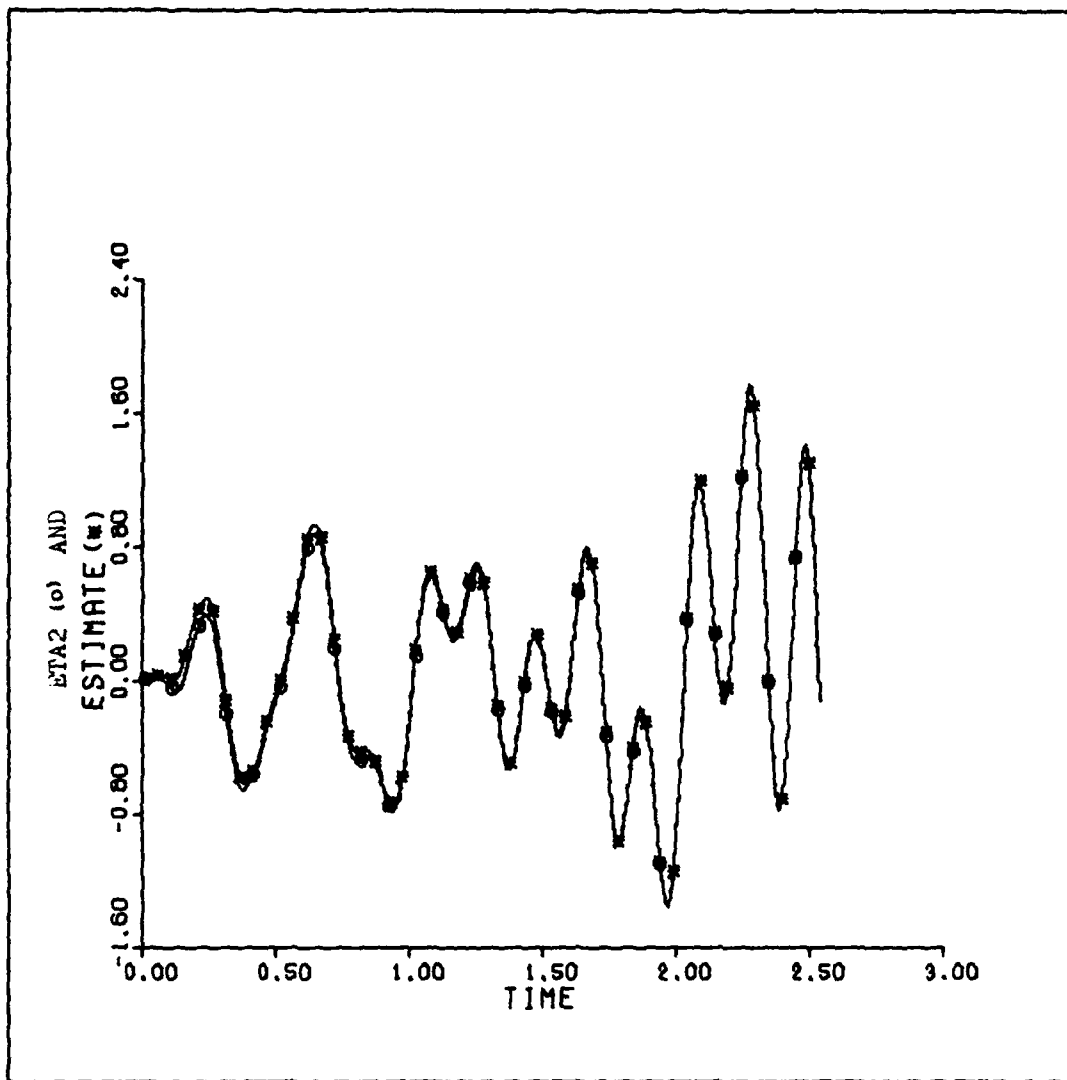


Figure 17b. Second State

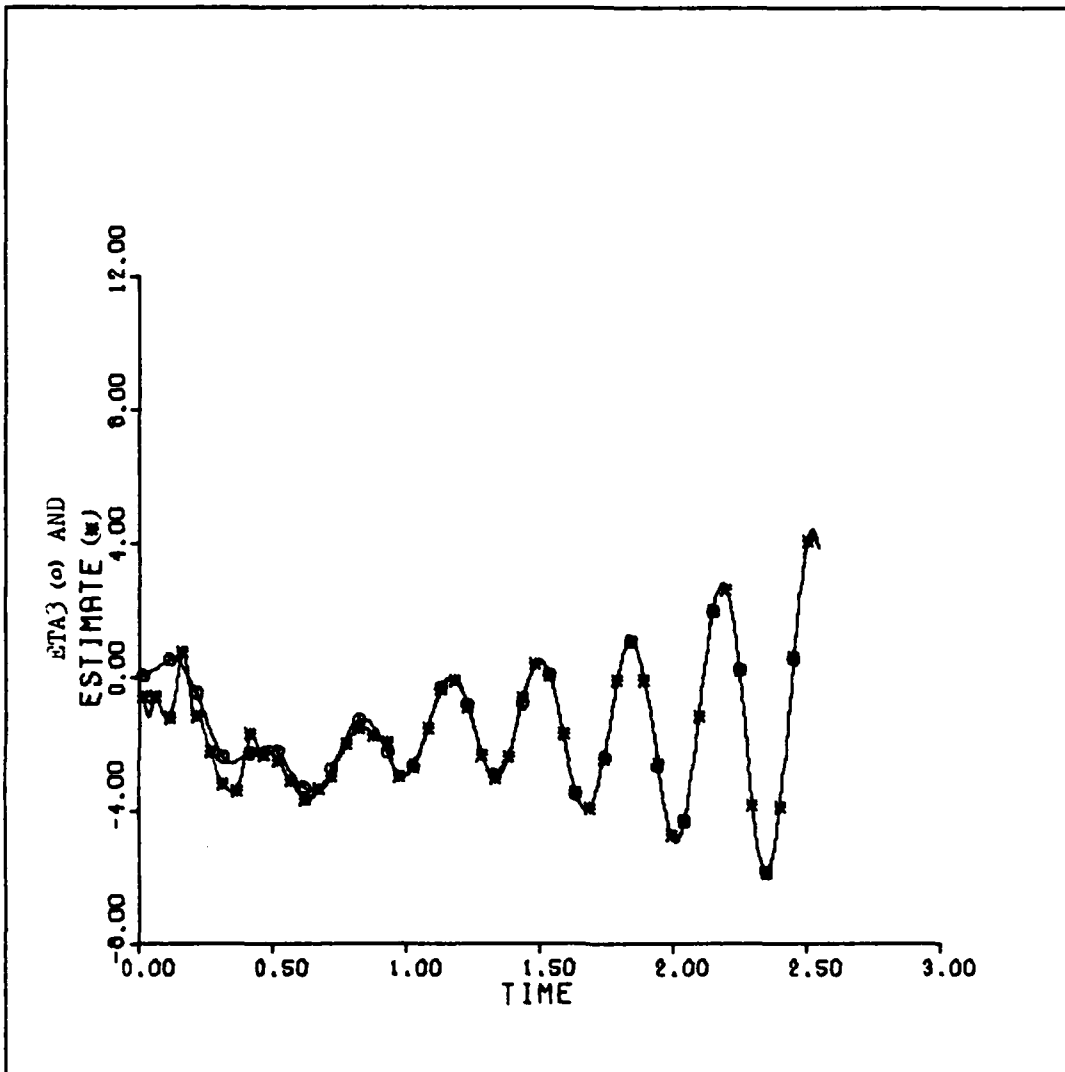


Figure 17c. Third State

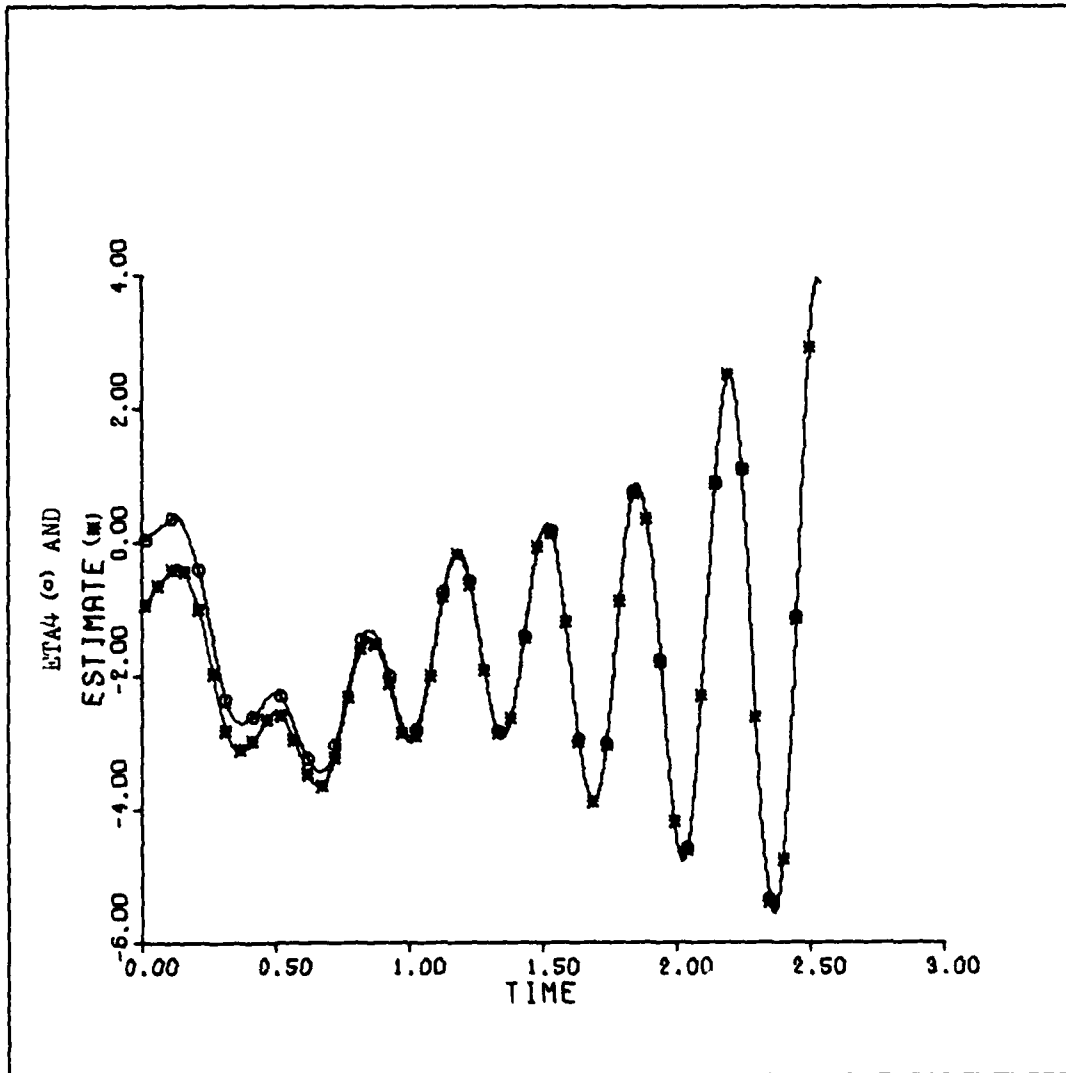


Figure 17d. Fourth State

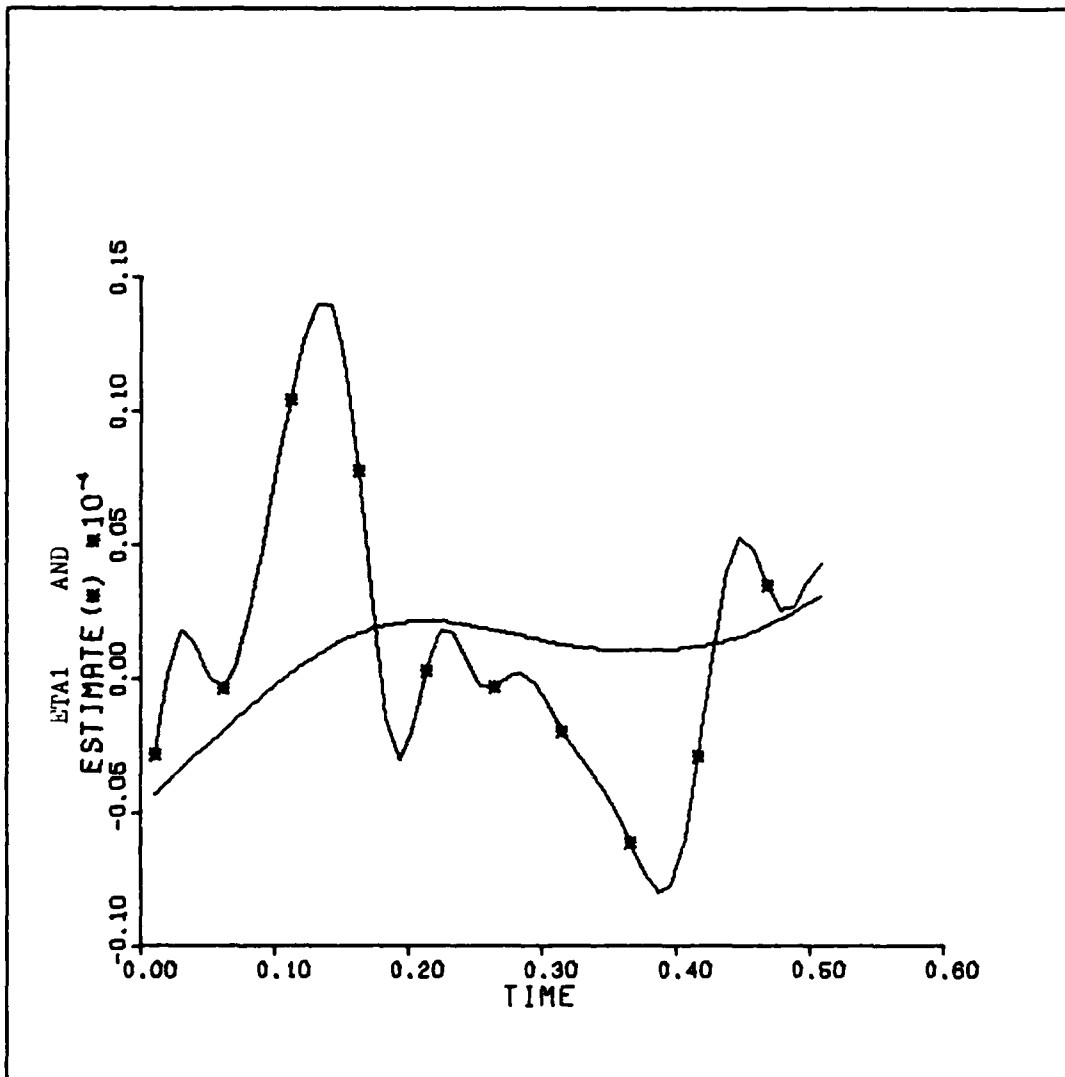


Figure 18a. Additional Example of
a Faster Observer

Controller gain 0.5
Orbit initial conditions
 $x = -50.42$ km
 $P_x = -50.42$ km/sec
 $y = -50.42$ km
 $P_y = -50.42$ km/sec
 $z = 0.0$ km
 $P_z = 0.0$ km/sec

One orbit

Observer initial conditions
 $e_{m1} = 14.96$ m
 $e_{m2} = 14.96$ m/sec
 $e_{m3} = 1496.0$ km
 $e_{m4} = 1496.0$ km/sec
 $e_{m5} = 0.0$ km
 $e_{m6} = 0.0$ km/sec

Observer gain elements
 $K'_{12} = 3.0$
 $K'_{31} = 2500.0$

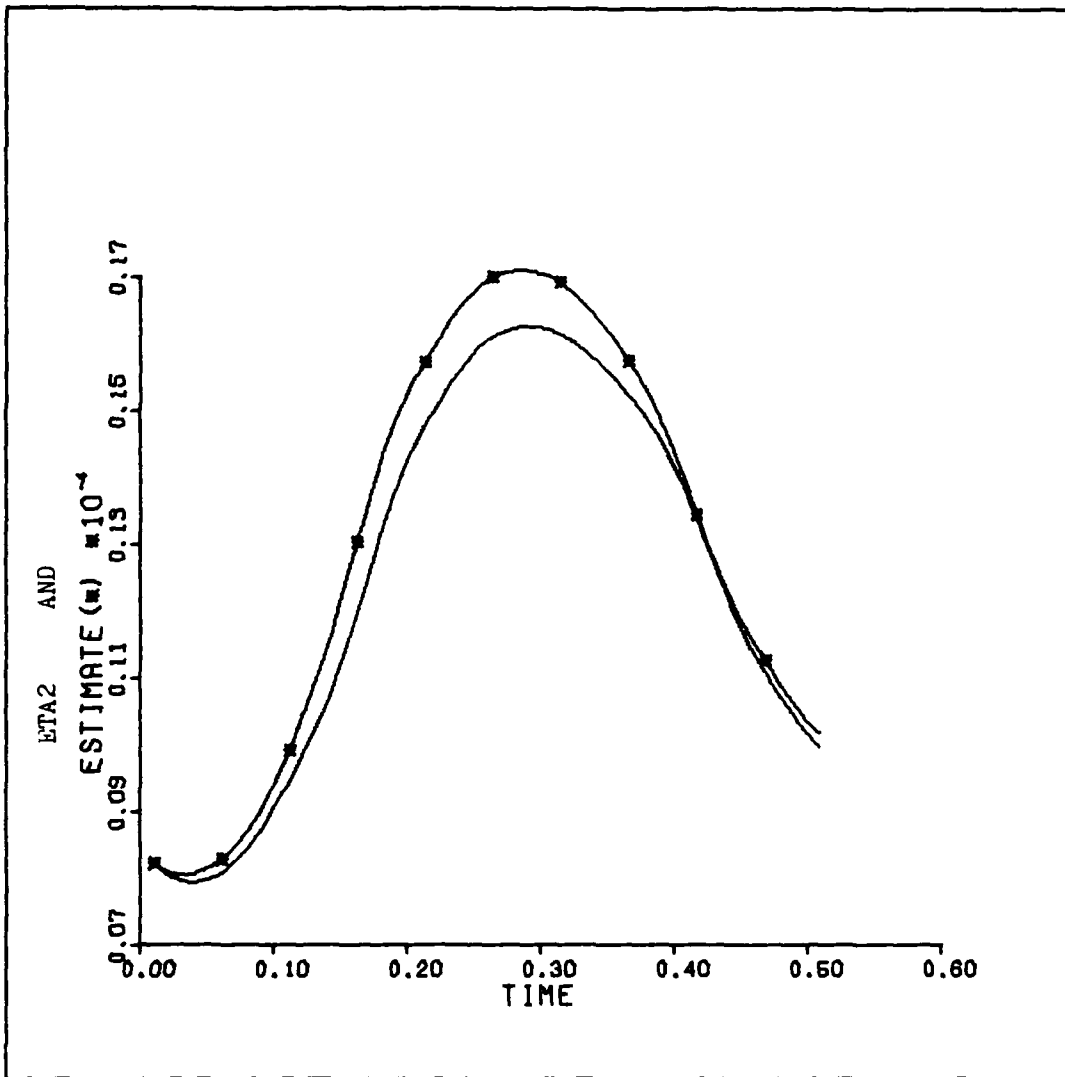


Figure 18b. Second State

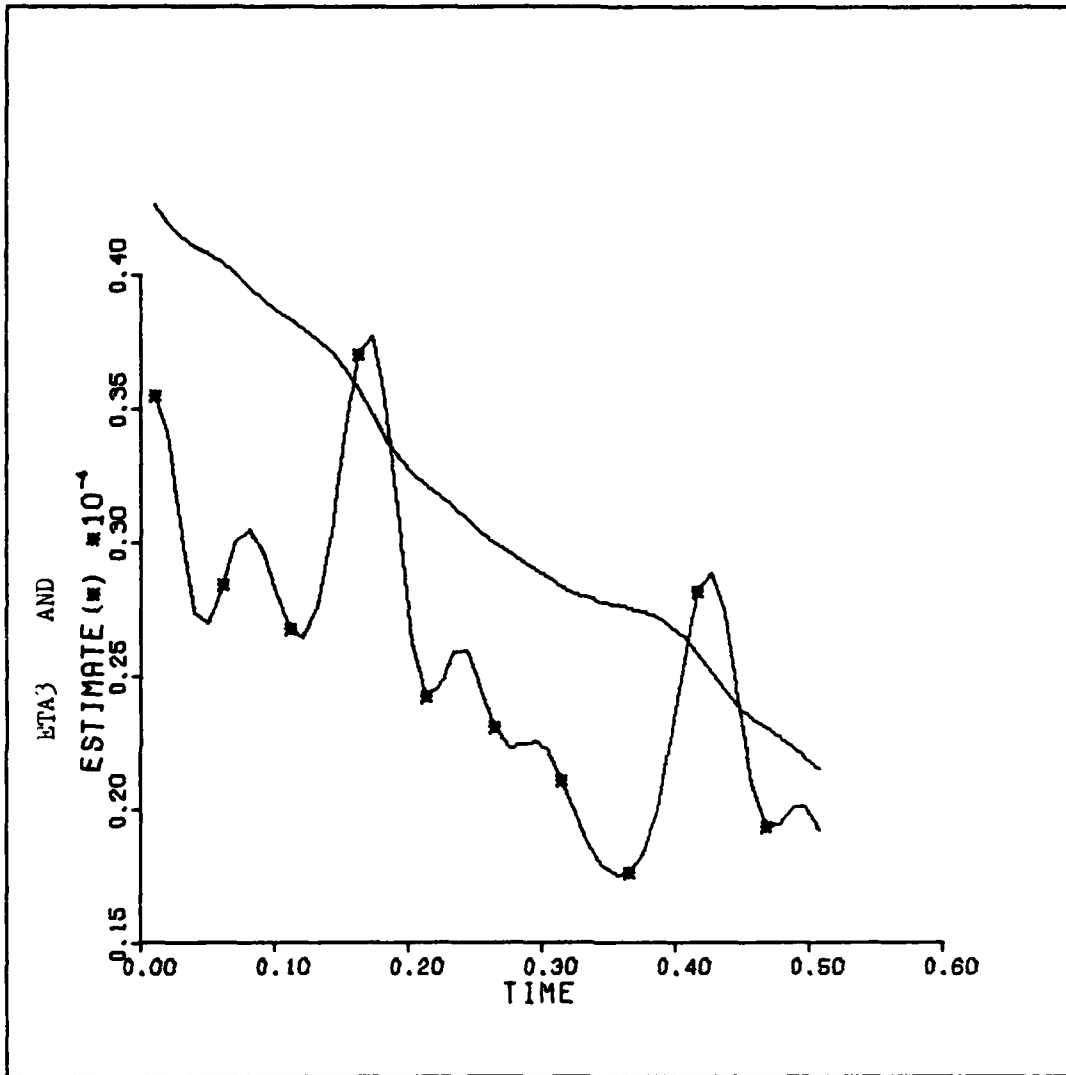


Figure 18c. Third State

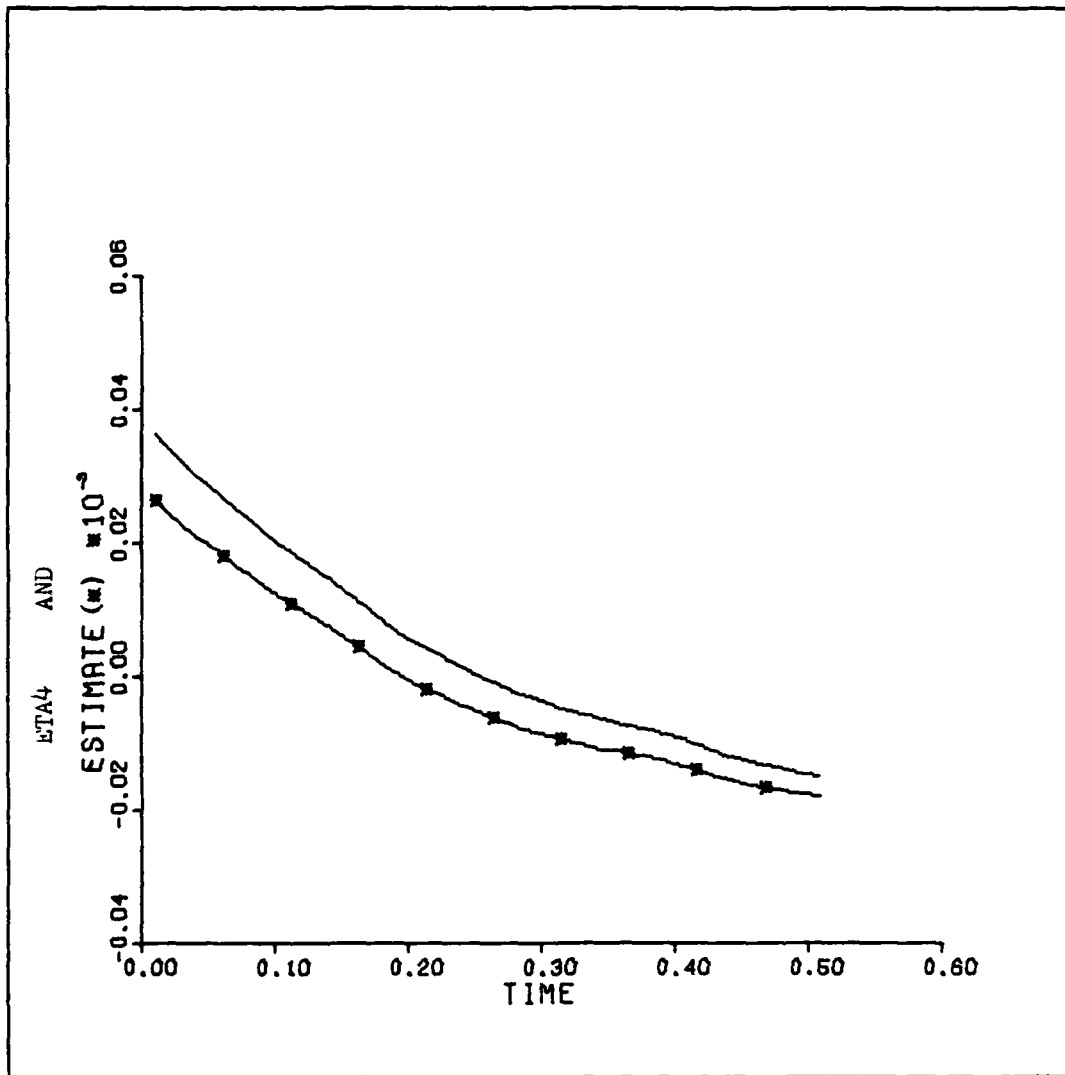


Figure 18d. Fourth State

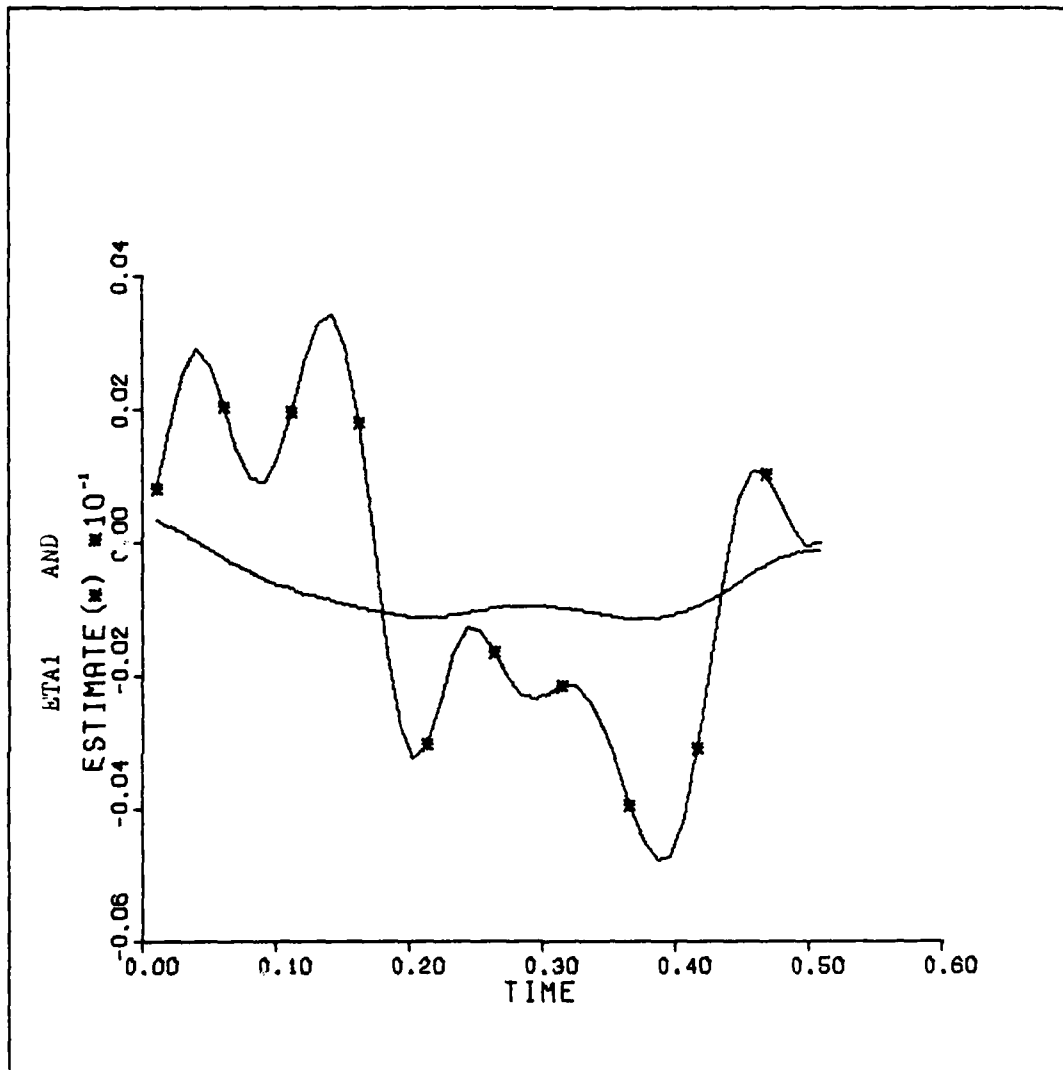


Figure 19a. Behavior With Large Initial Conditions

Controller gain 0.5
 Orbit initial conditions
 $x = 4488$ km
 $P_x = 4488$ km/sec
 $y = 4488$ km
 $P_y = 4488$ km/sec
 $z = 0.0$ km
 $P_z = 0.0$ km/sec

One orbit

Observer initial conditions
 $e_{m1} = 1.5$ km
 $e_{m2} = 1.5$ km/sec
 $e_{m3} = 7.48 \times 10^5$ km
 $e_{m4} = 7.48 \times 10^5$ km/sec
 $e_{m5} = 0.0$ km
 $e_{m6} = 0.0$ km/sec

Observer gain elements
 $K'_{12} = 3.0$
 $K'_{31} = 1500.0$

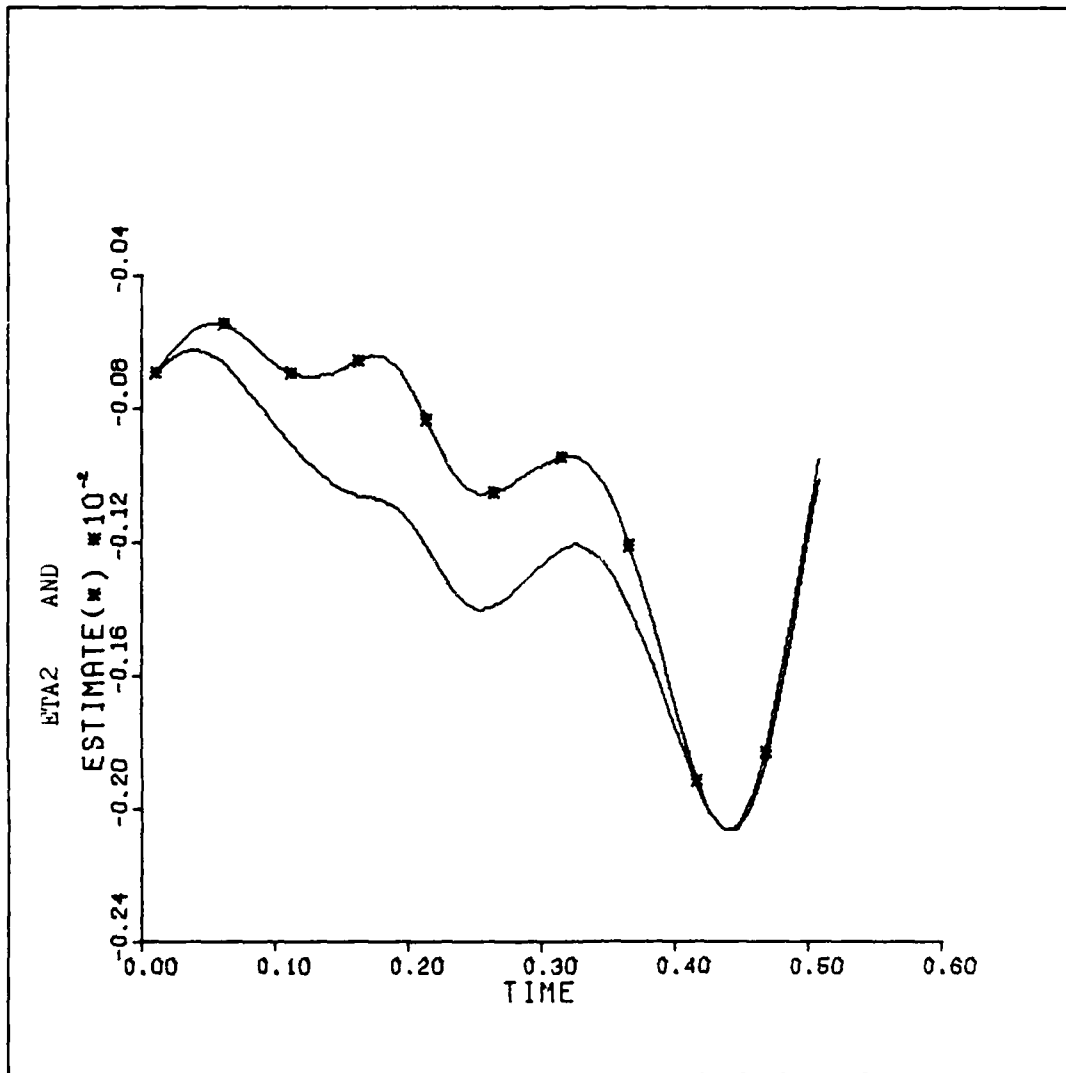


Figure 19b. Second State

AD-A111 147 AIR FORCE INST OF TECH WRIGHT-PATTERSON AFB OH SCHOO--ETC F/G 22/3
CLOSED-LOOP CONTROL OF A SATELLITE IN AN UNSTABLE PERIODIC ORBI--ETC(U)
DEC 81 F C VASS
UNCLASSIFIED AFIT/GA/AA/81D-11 NL

2 of 2

AD A
11/14



END
DATE
FILMED
10-82
DTIC

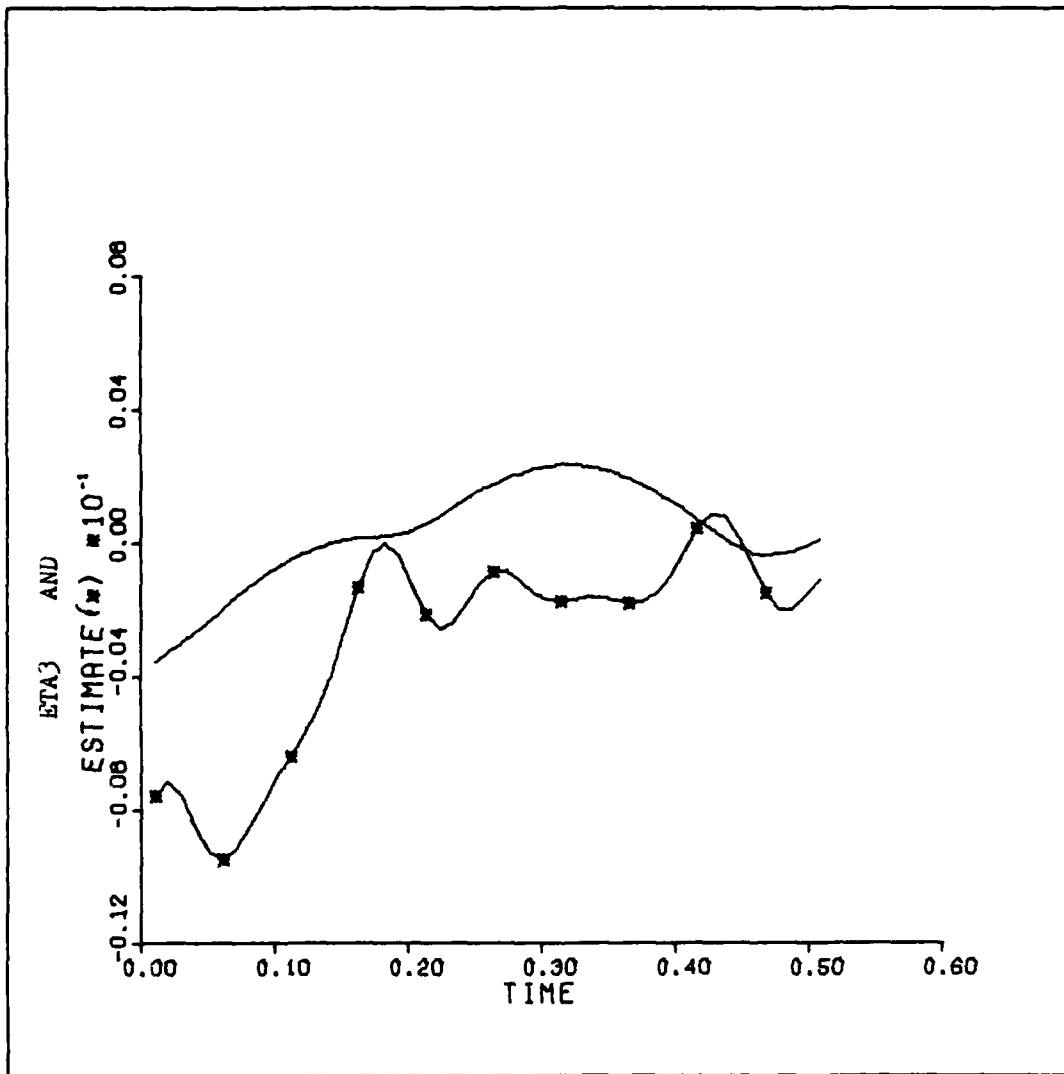


Figure 19c. Third State

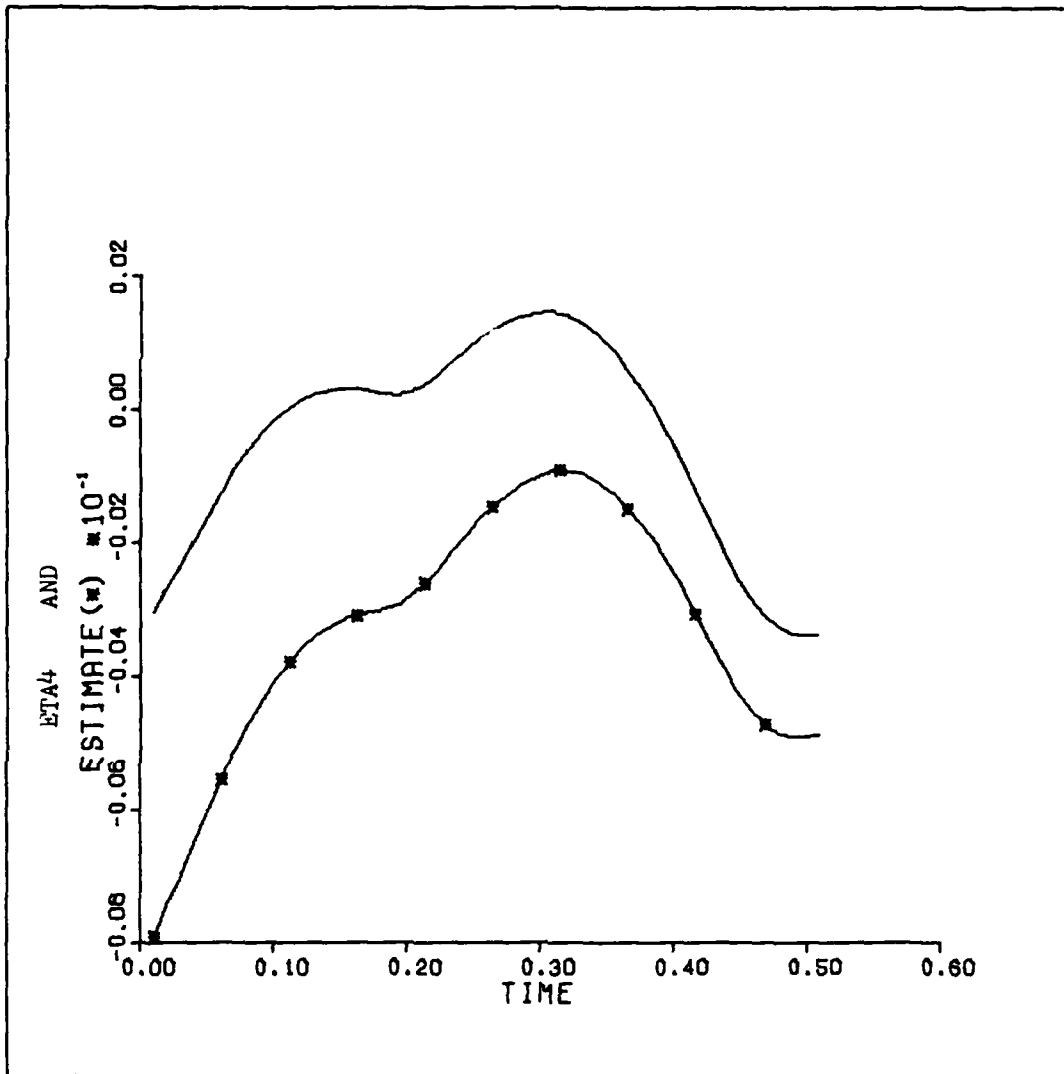


Figure 19d. Fourth State

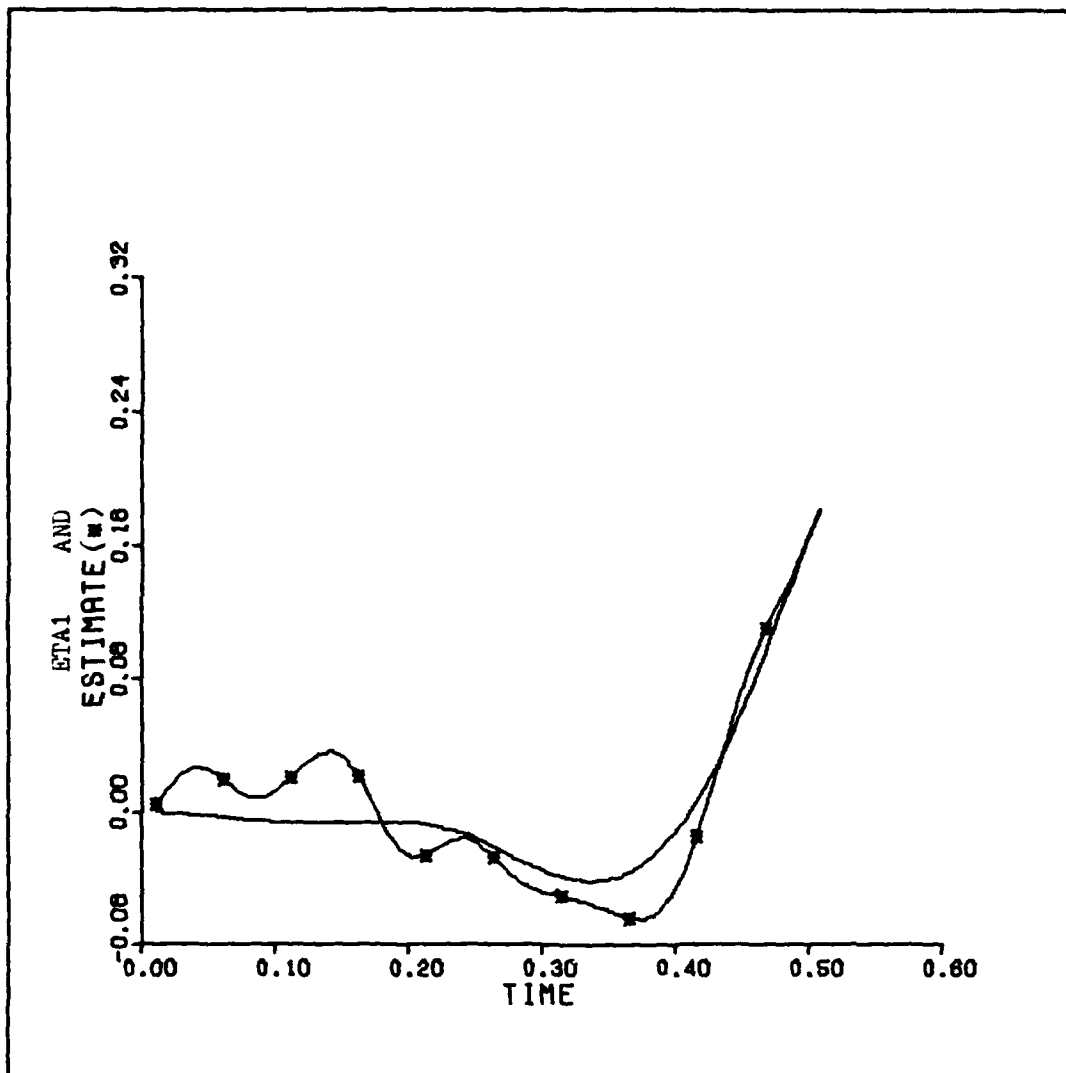


Figure 20a. Case of Figure 19. With Order of Magnitude Difference in Observer Initial Conditions

Observer initial conditions
 $e_{m1} = 1.5 \text{ km}$
 $e_{m2} = 1.5 \text{ km/sec}$
 $e_{m3} = 7.48 \times 10^6 \text{ km}$
 $e_{m4} = 7.48 \times 10^6 \text{ km/sec}$
 $e_{m5} = 0.0 \text{ km}$
 $e_{m6} = 0.0 \text{ km/sec}$

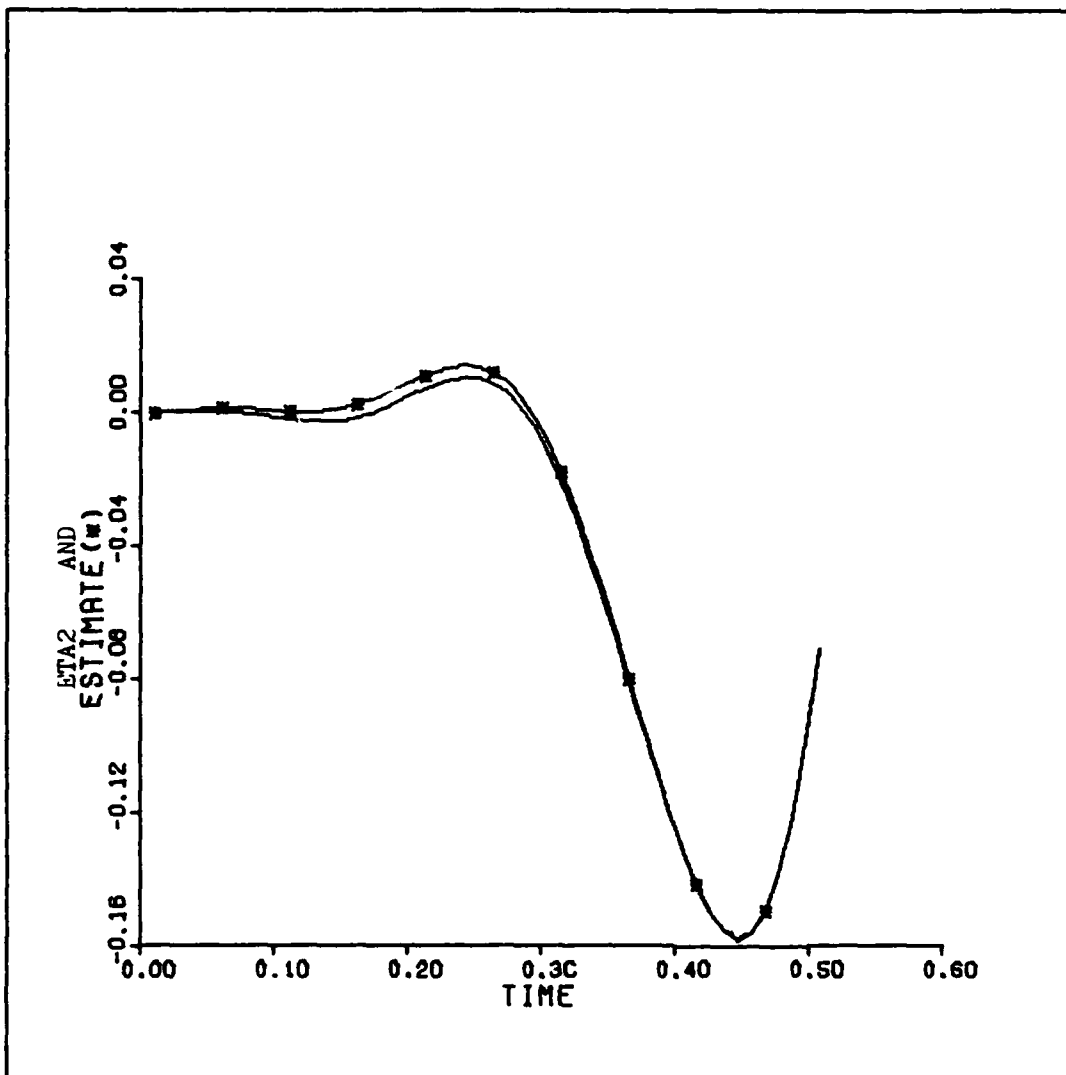


Figure 20b. Second State

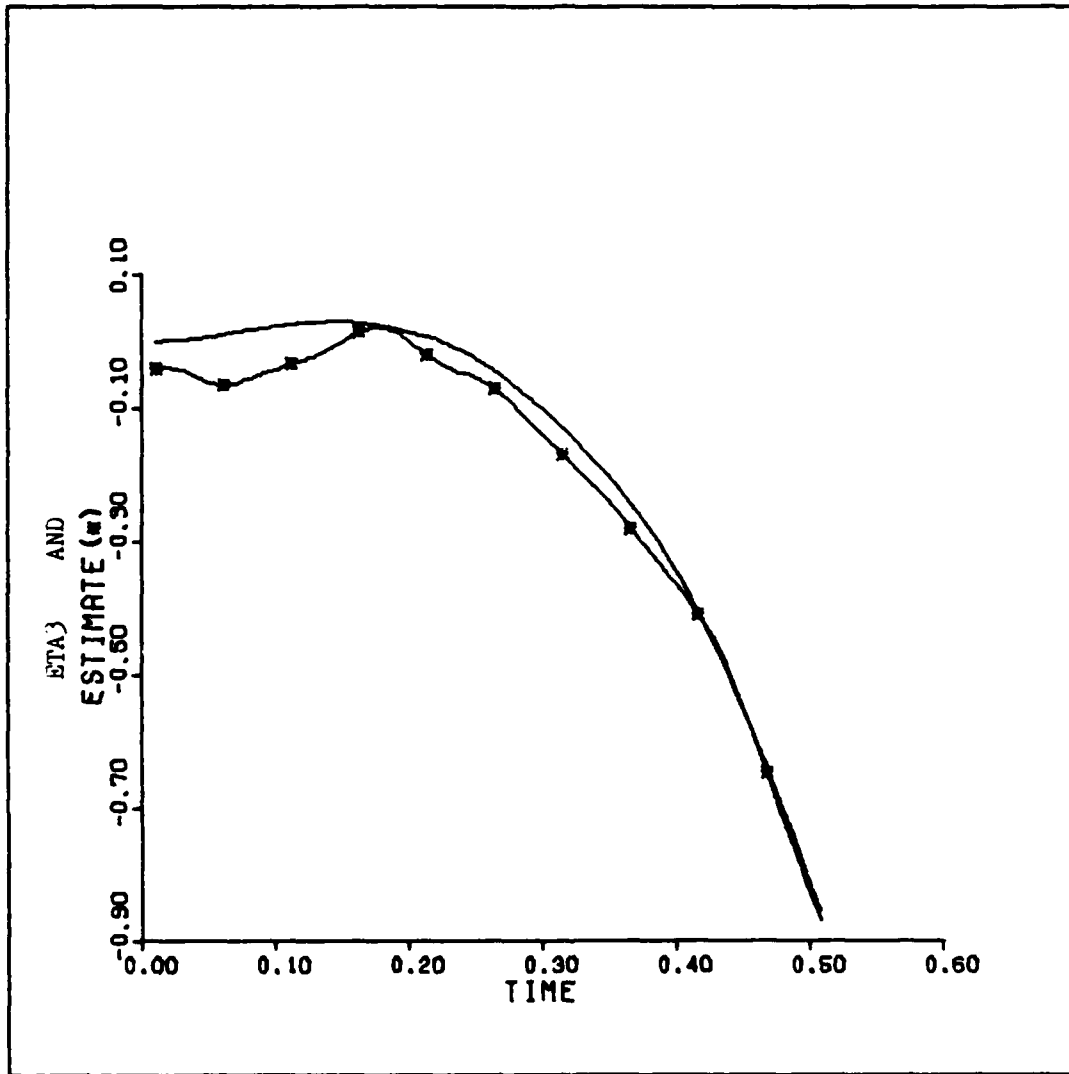


Figure 20c. Third State

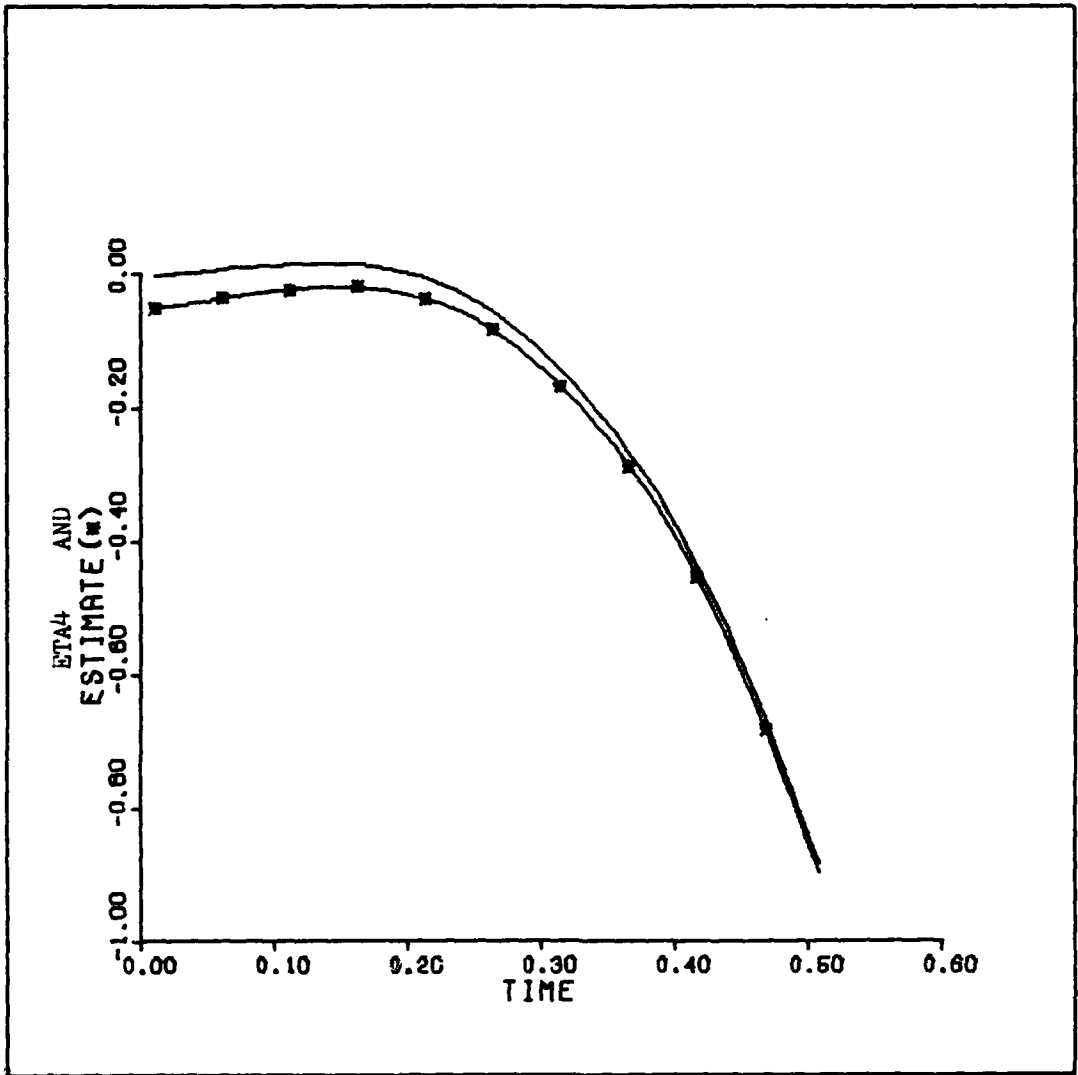


Figure 20d. Fourth State

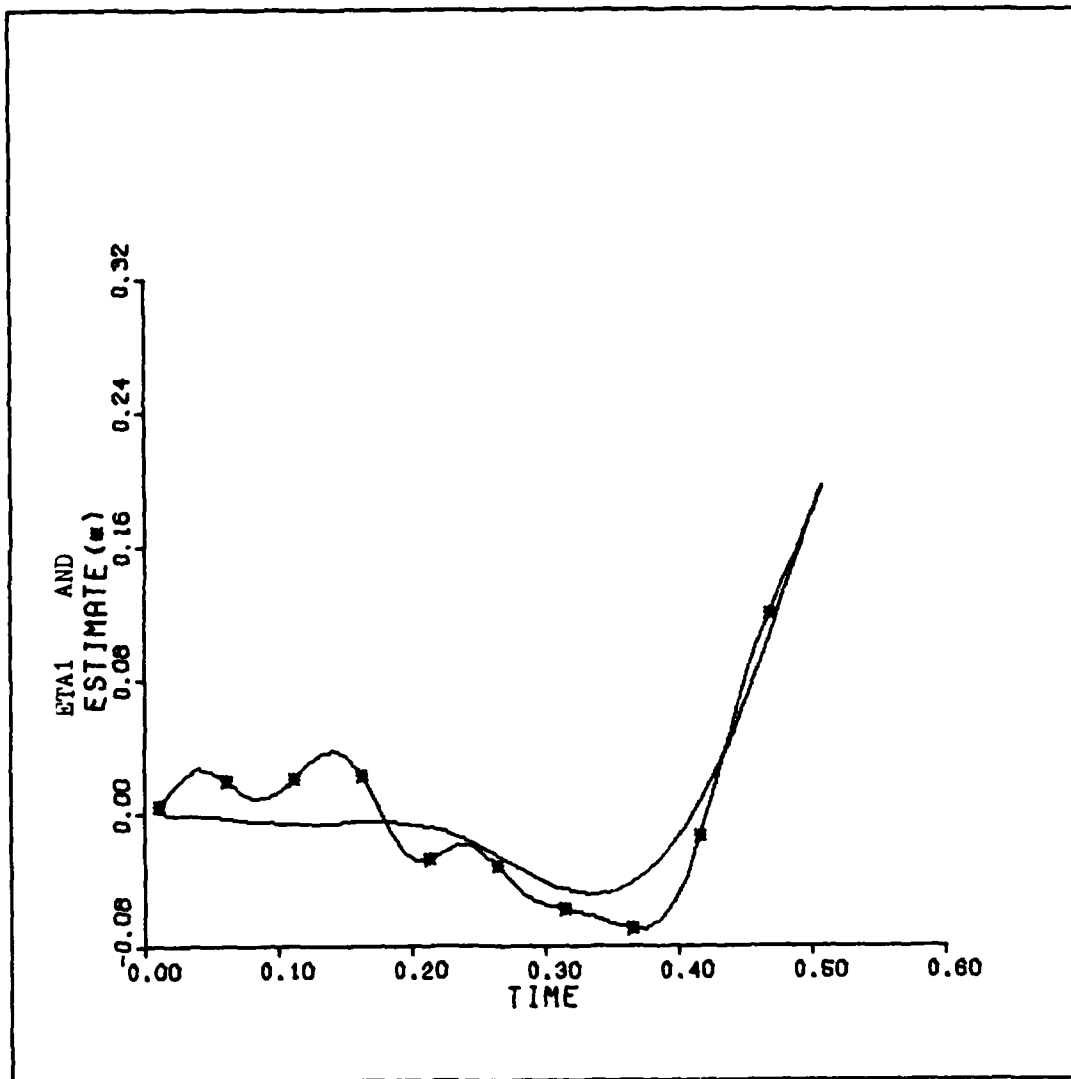


Figure 21a. Case of Figure 20. With Order of Magnitude Difference in Orbit Initial Conditions

Orbit initial conditions

$x = 448.8 \text{ km}$
 $P_x = 448.8 \text{ km/sec}$
 $y = 448.8 \text{ km}$
 $P_y = 448.8 \text{ km/sec}$
 $z = 0.0 \text{ km}$
 $P_z = 0.0 \text{ km/sec}$

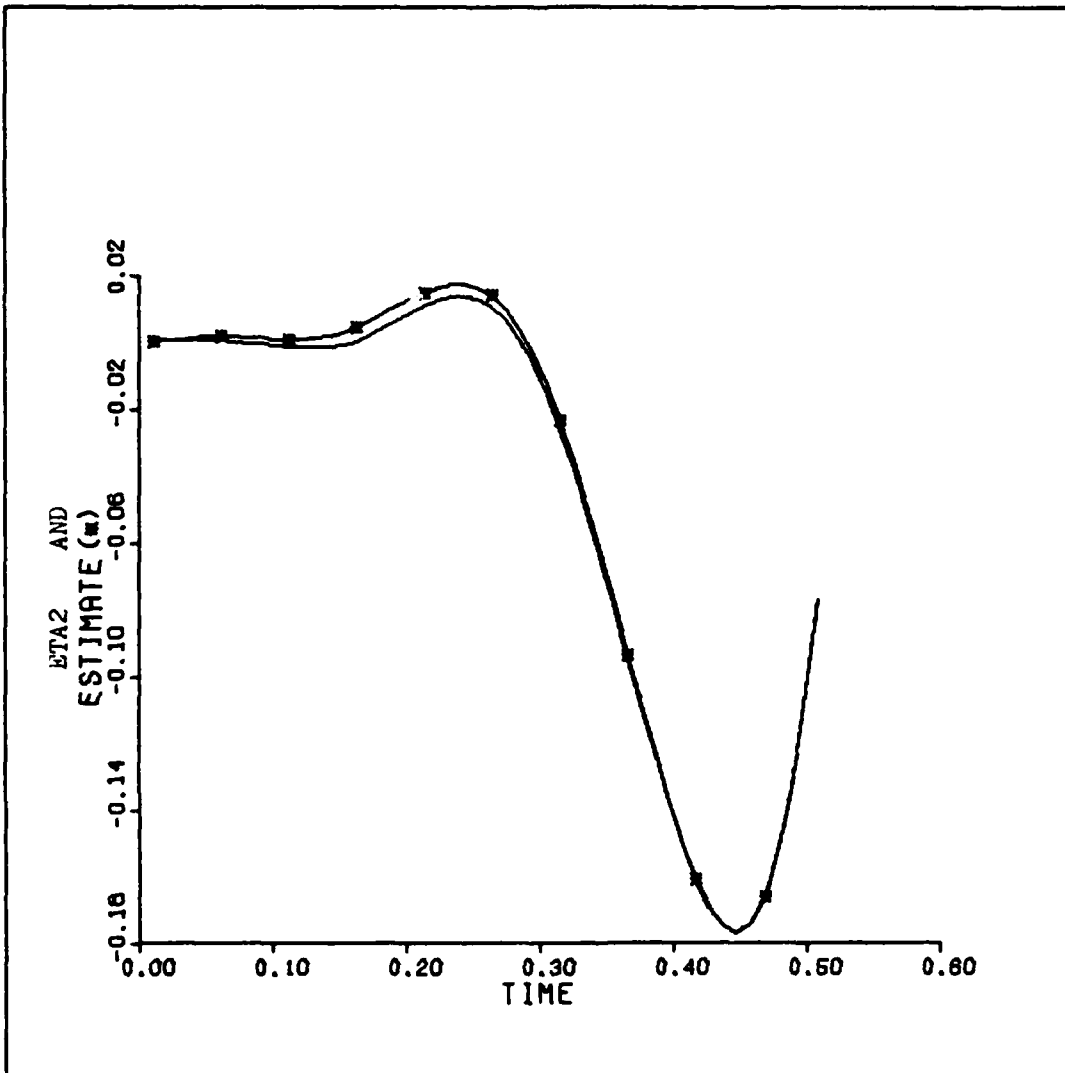


Figure 21b. Second State

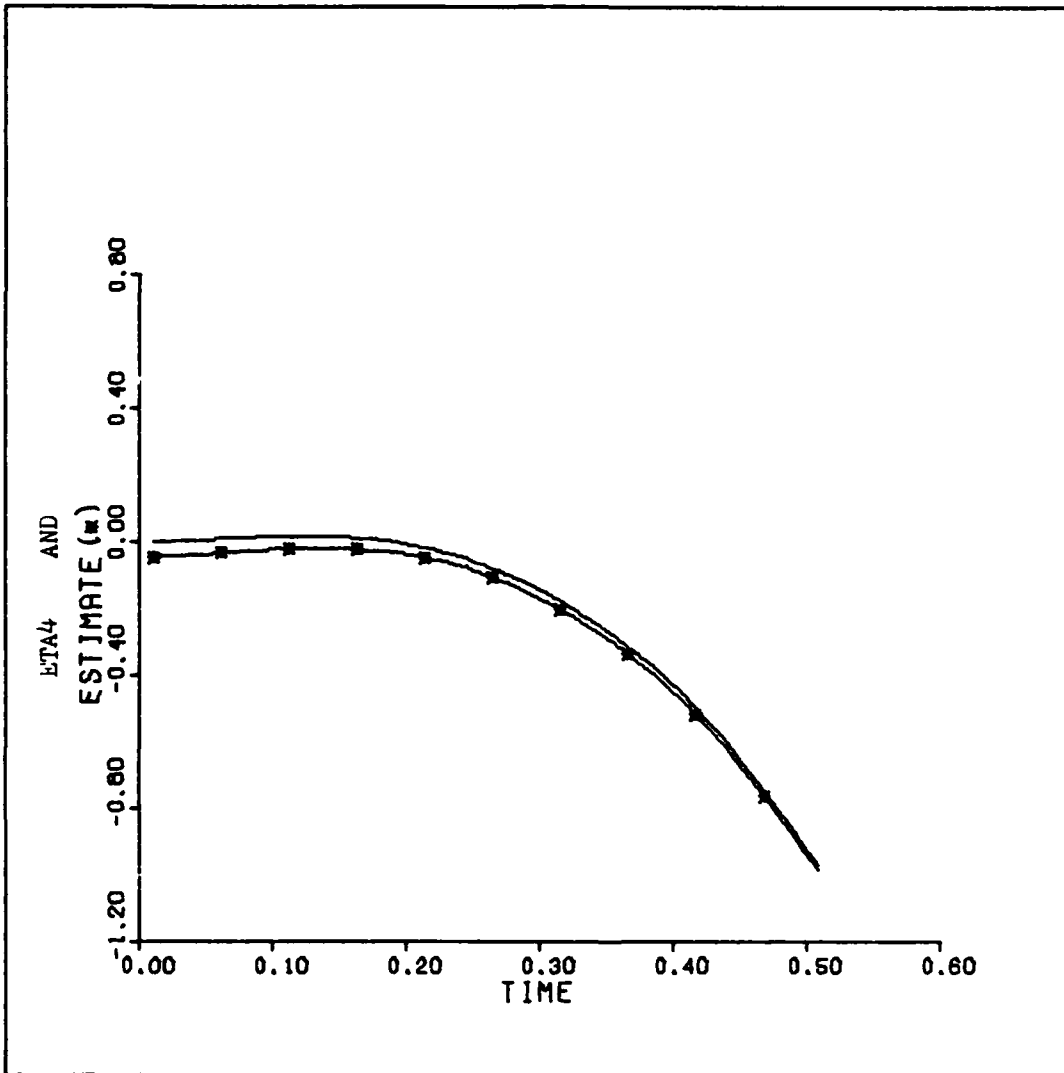


Figure 21d. Fourth State

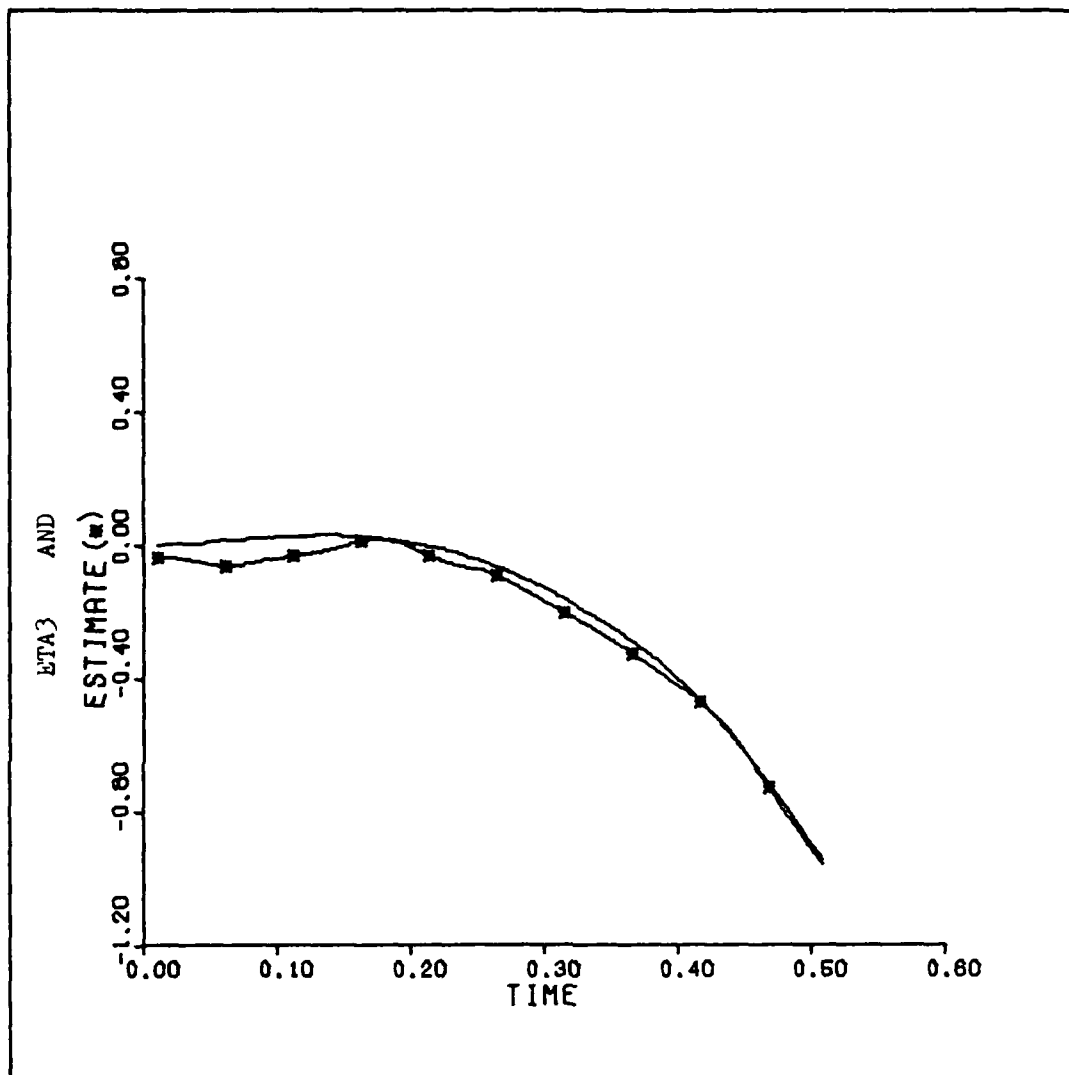


Figure 21c. Third State

Bibliography

1. Balas, M.J. "Observer Stabilization of Singularly Perturbed Systems," Journal of Guidance and Control, 1:93-95 (January 1978).
2. Calico, Robert M. Lecture Notes for MC 8.25, Spacecraft Stability. School of Engineering, Air Force Institute of Technology, Wright-Patterson AFB, 1981.
3. D'Azzo, John J. and Constantine H. Houpis. Linear Control System Analysis and Design; Conventional and Modern (Second edition). New York: McGraw-Hill Book Company, 1981.
4. Ehrler, Dennis W. A Perturbation Analysis of Modal Control of an Unstable Periodic Orbit. MS thesis. Wright-Patterson AFB, Ohio: Air Force Institute of Technology, December 1981.
5. Farquhar, R.W., "The Control and Use of Libration Point Satellites," NASA Technical Report R-346, 1970.
6. Farquhar, R.W., "Future Mission For Libration Point Satellites," Astronautics and Aeronautics, 3:52-56 (May 1969).
7. Farquhar, R.W. and A.A. Kamel. "Quasi-Periodic Orbits About the Translunar Libration Point," Celestial Mechanics, 7:458-473 (June 1973).
8. Farquhar, R.W. et al. "Trajectories and Orbital Maneuvers for the First Libration Point Satellite," Journal of Guidance and Control, 3:549-553 (November 1980).
9. Gelb, A., et al. Applied Optimal Estimation. Cambridge: MIT Press, 1974.
10. Jordan, P.W. and P. Smith. Nonlinear Ordinary Differential Equations. Oxford: Oxford University Press 1977.
11. Kronmiller, G.C. Jr. and Elie J. Baghdady. "The GRARR System: Concept Design, and Performance," Space Science Reviews, 5:265-307 July 1966.
12. Kwakernaak, H. and Raphael Sivan. Linear Optimal Control Systems. New York: John Wiley and Sons Inc., 1972.
13. Luenberger, David G. Introduction to Dynamic Systems: Theory, Models, and Applications. New York: Wiley, 1979.

14. Luenberger, David G., "An Introduction to Observers", IEEE Transactions on Automatic Control, 16:596-602 (December 1971).
15. Luenberger, David G., "Observers for Multivariable Svstems," IEEE Transactions on Automatic Control, 11:190-197 (April 1966).
16. Luenberger, David G., "Observing the State of a Linear Svstem", IEEE Transactions on Military Electronics, 8:74-80 (November 1963).
17. Meirovitch, L. Methods of Analytical Dynamics. New York: McGraw-Hill, 1970.
18. Melbourne, William G., "Navigation Between the Planets," Scientific American, 234:58-74 (June 1976).
19. Reid, Gary, Lecture Notes for EE 5.10, Linear Algebra. School of Engineering, Air Force Institute of Technology, Wright-Patterson AFB, 1980.
20. Shelton, W.S., Modal Control of a Satellite in Orbit About L3. MS thesis. Wright-Patterson AFB, Ohio: Air Force Institute of Technology, December 1980.
21. Smith, D.E., Stabilizing an Unstable Orbit About L3 in the Sun, Earth, Moon System Using Linear Constant Gain Feedback. MS thesis. Wright-Patterson AFB, Ohio: Air Force Institute of Technology, December 1980.
22. Steg, L. and J.P. DeVries, "Earth-Moon Libration Points: Theory Existence and Applications," Space Science Reviews, 5:210-233 (February 1966).
23. Tilton, H.A., Three Dimensional Orbital Stability About the Earth-Moon Equilateral Libration Points. MS thesis. Wright-Patterson AFB, Ohio: Air Force Institute of Technology, December 1980.
24. Wiesel, W.E., "The Restricted Earth-Moon-Sun Problem I: Dvnamics and Libration Point Orbits" 1981.
25. Wiesel, W.E., "Floquet Reference Solutions for the Lunar Theory and Jovian Moon System," American Institute of Aeronautics and Astro-nautics Paper 80-1655.
26. Wiesel, W.E., Lecture Notes for Astrodynamics Sequence, School of Engineering, Air Force Institute of Technology, Wright-Patterson AFB, 1980-1981.

Vita

Felicia C. Vass was born on April 9, 1958, in Flemington, New Jersey. In 1961, her family moved to Arlington, Virginia. She attended Virginia Polytechnic Institute and State University, earning her Bachelor of Science degree in Aerospace and Ocean Engineering in June, 1980. Upon graduation, she received a commission in the USAF through ROTC, and the following day was assigned to Wright-Patterson AFB to begin the Master of Science degree program in Astronautical Engineering, Guidance and Control at the Air Force Institute of Technology.

Permanent address:

2520 N. George Mason Dr.
Arlington, Virginia 22207

REPORT DOCUMENTATION PAGE		READ INSTRUCTIONS BEFORE COMPLETING FORM
1. REPORT NUMBER AFIT/GA/AA/81D-11	2. GOVT ACCESSION NO. AD-A111147	3. RECIPIENT'S CATALOG NUMBER
4. TITLE (and Subtitle) CLOSED-LOOP CONTROL OF A SATELLITE IN AN UNSTABLE PERIODIC ORBIT ABOUT L3	5. TYPE OF REPORT & PERIOD COVERED Ms Thesis	
	6. PERFORMING ORG. REPORT NUMBER	
7. AUTHOR(s) Felicia C. Vass 2Lt, USAF	8. CONTRACT OR GRANT NUMBER(s)	
9. PERFORMING ORGANIZATION NAME AND ADDRESS Air Force Institute of Technology (AFIT-EN) Wright-Patterson AFB, Ohio 45433	10. PROGRAM ELEMENT PROJECT, TASK AREA & WORK UNIT NUMBERS	
11. CONTROLLING OFFICE NAME AND ADDRESS	12. REPORT DATE December, 1981	
	13. NUMBER OF PAGES 109	
14. MONITORING AGENCY NAME & ADDRESS (if different from Controlling Office)	15. SECURITY CLASS. (of this report) Unclassified	
	15a. DECLASSIFICATION DOWNGRADING SCHEDULE	
16. DISTRIBUTION STATEMENT (of this Report) Approved for public release; distribution unlimited		
17. DISTRIBUTION STATEMENT (of the abstract entered in Block 20, if different from Report) 28 JAN 1982		
18. SUPPLEMENTARY NOTES Approved for public release; IAW 190-17 Fredric C. Lynch, Major, USAF Director of Public Affairs		
19. KEY WORDS (Continue on reverse side if necessary and identify by block number) Periodic Orbits Lagrangian Point L3 Modal Control Poincaré Exponents Luenberger Observer		
20. ABSTRACT (Continue on reverse side if necessary and identify by block number) A stable Luenberger Observer was developed to reconstruct the error states in modal coordinates for a satellite in a periodic orbit about the Earth-Moon Lagrangian point, L3. Observer pole placement for the third root was found to be linear with applied gain. Convergence of the observer estimate to the true state vector was rapid in all cases, but depended upon the initial conditions considered. The addition of the observer did not impede the long-term behavior of the controller in stabilizing the orbit.		

SECURITY CLASSIFICATION OF THIS PAGE (When Data Entered)



SECURITY CLASSIFICATION OF THIS PAGE (When Data Entered)

END

DATE
FILMED

03-82

DTIC